Purdue University
Purdue e-Pubs

Open Access Dissertations | Theses and Dissertations

5-2018

Oxidative Transfer Reactions at a Metal-Metal Bond

Heather Rounds
Purdue University

Follow this and additional works at: https://docs.lib.purdue.edu/open_access_dissertations

Recommended Citation

Rounds, Heather, "Oxidative Transfer Reactions at a Metal-Metal Bond" (2018). *Open Access Dissertations*. 1812.
https://docs.lib.purdue.edu/open_access_dissertations/1812

This document has been made available through Purdue e-Pubs, a service of the Purdue University Libraries.
Please contact epubs@purdue.edu for additional information.

OXIDATIVE ADDITION REACTIONS AT A METAL-METAL BOND

by

Heather Rounds

A Dissertation

Submitted to the Faculty of Purdue University

In Partial Fulfillment of the Requirements for the degree of

Doctor of Philosophy

Department of Chemistry

West Lafayette, Indiana

May 2018

THE PURDUE UNIVERSITY GRADUATE SCHOOL
STATEMENT OF COMMITTEE APPROVAL

Dr. Christopher Uyeda, Chair

Department of Chemistry

Dr. Mingji Dai

Department of Chemistry

Dr. Corey Thompson

Department of Chemistry

Dr. Jianguo Mei

Department of Chemistry

Approved by:

Dr. Christine Hrycyna

Head of the Graduate Program

Dedicated to my husband for his encouraging words and support throughout my academic career.

ACKNOWLEDGMENTS

First, I would like to thank my advisor, Dr. Christopher Uyeda, for all of his guidance and support throughout the course of obtaining my PhD. His insight and passion for advancing science has taught me the importance of learning as much as possible. He has also taught me the importance of critically thinking about the science I have been exposed to. I appreciate all the time and resources he has given for me to achieve my goals and I will be forever grateful.

I would also like to thank my colleagues in the Uyeda group, Jake, Mike, Conner, John, Shawn, Annah, Sourish, and Seulah for all their support and willingness to help with any problem at hand. I would also like to thank them for all their advice and support inside and outside of the laboratory.

I would especially like to thank my fellow 5th years, Talia, Ian, Doug, Sudipta, and Colby for all their support throughout our time at Purdue. It was a learning process for all of us in setting up our laboratory and setting the foundation for future members. To all of you, I will miss you when we part ways, but you will always leave a positive mark in my life.

Thanks to the post-docs of our lab, YouYun and Arnab, for their insight. Without your help I would not have learned as much as I have and appreciate the time and resources you have dedicated to help me with my projects. I also am very appreciative of your willingness to drop whatever you are doing to give me advice.

I would also like to thank my fellow colleagues in other research groups, Anthony and Anne for their willingness to help with any problem whether it pertained to research or life. Thank you for being both great colleagues and great friends. I will cherish your friendship forever.

Lastly, I would to thank my parents for always encouraging me to do well in my studies and pushing me to reach my highest potential. Without their love and support I would not have achieved this goal. I also want to thank my grandparents for always being there and understanding that I couldn’t make it to all the family functions but always welcoming me with open arms when I could. And to the rest of my family for always supporting my aspirations in life and giving me the foundations for developing a passion for science. I would especially like to thank my husband for all his encouraging words and sacrifices he has made. Without your unconditional love this journey would have been a lot more difficult.

TABLE OF CONTENTS

LIST OF TABLES vii
LIST OF FIGURES viii
LIST OF ABBREVIATIONS xii
ABSTRACT xiv
CHAPTER 1. CATALYTIC ACTIVATION OF STRAINED RINGS 1
1.1 Background 1
1.1.1 Transition Metal-Mediated Strained Ring Activation 1
1.2 Dinuclear Pathways for the Activation of Strained Three-Membered Rings 2
1.2.1 Introduction 2
1.2.2 Results and Discussion 3
1.2.2.1 Stoichiometric Aziridine Ring Opening 3
1.2.2.2 Catalytic Rearrangement of Vinylcyclopropane 6
1.2.2.3 Catalytic Rearrangements of Heteroatom-Containing Cyclopropanes 11
1.2.3 Experimental Section 12
1.3 Dinuclear Transformations of Vinylaziridines 28
1.3.1 Introduction 28
1.3.2 Results and Discussion 30
1.3.2.1 Formation of δ-lactam through Complex **2**. 30
1.3.2.2 Formation of δ-lactam through Complex **4**. 32
1.3.2.3 Stoichiometric Aziridine Ring Opening. 34
1.3.2.4 Formation of β-lactam through Complex **5**. 35
1.3.3 Experimental 37
CHAPTER 2. DINUCLEAR FACILITATED OXIDATIVE TRANSFER REACTIONS 51
2.1 Heteroatom-Abstraction of Three-Membered Rings 51
2.1.1 Introduction 51
2.1.2 Results and Discussion 53
2.1.3 Experimental 56
2.2 Catalytic Desulfurization 62
2.2.1 Introduction 62

2.2.2 Results and Discussion 63
2.2.3 Experimental 71
APPENDIX A. CRYSTAL STRUCTURE DATA 85
APPENDIX B. DFT CALCULATIONS 98
REFERENCES 117
VITA 122
PUBLICATION 124

LIST OF TABLES

Table 1.1. A comparison of nickel catalysts for the rearrangement of vinylcyclopropane. 7
Table 2.1. Substrate scope for the desulfurization of thiiranes. 64

LIST OF FIGURES

Figure 1.1. Carbon-carbon bond activation of cyclopropanes can be achieved by nickel and iron. 1

Figure 1.2 Design principles for strain-induced oxidative addition reactions of vinyl three-membered ring substrates. (a) C–C oxidative addition using electron-rich, low-coordinate metal complexes. (b) Oxidative addition driven by dinuclear stabilization of allyl groups (X = C, N). 3

Figure 1.3. (a) Oxidative addition of *N*-tosyl-2-vinylaziridine using **1**. (b) Solid-state structure for **2** and select bond metrics. (c) Changes in bond metrics indicative of ligand-centered redox activities. Bond metrics for **2** (black) are shown in Å. Changes relative to complex **1** are shown in red and blue. (d) LUMO for **2**, which shows primarily ligand character. 4

Figure 1.4. (a) Oxidative addition of *N*-tosyl-2-vinylaziridine using **3**. (b) Solid-state structure for **4** and select bond metrics. 5

Figure 1.5. Catalytic rearrangements of vinylcyclopropanes bearing ring substitution. 9

Figure 1.6. Calculated reaction coordinate for the Ni_2-catalyzed vinylcyclopropane rearrangement (M06l/6-31g(d,p) level of DFT). Free energies (ΔG) are in kcal/mol and are relative to **A**. In the model, the catalyst *i*-Pr groups are truncated to Me groups. 10

Figure 1.7. Catalytic rearrangements of cyclopropanes bearing heteroatom-containing substituents. 11

Figure 1.8. ^{1}HNMR spectrum for complex **2** (C_6D_6, room temperature). 13

Figure 1.9. $^{13}C\{^1H\}$ NMR spectrum for complex **2** (C_6D_6, room temperature). 14

Figure 1.10. COSY spectrum for complex **2** (C_6D_6, room temperature). 14

Figure 1.11. HMQC spectrum for complex **2** (C_6D_6, room temperature). 15

Figure 1.12. UV-Vis spectrum for complex **2** (THF, room temperature). 15

Figure 1.13. ATR-IR spectrum for complex **2**. 16

Figure 1.14. ^{1}HNMR spectrum for complex **4** (toluene-d_8, 233K). 17

Figure 1.15. $^{13}C\{^1H\}$ NMR spectrum for complex **4** (C_6D_6, room temperature). 18

Figure 1.16. VT-NMR spectra for complex **4** (toluene-d_8, 213 K to 353 K, bottom to top). 19

Figure 1.17. COSY complex for complex **4** (toluene-d_8, 213K). 20

Figure 1.18. UV-Vis spectrum for complex **4** (THF, room temperature). 20

Figure 1.19. ATR-IR spectrum for complex **4.** 21

Figure 1.20. ^{1}H NMR spectrum for the catalytic rearrangement of cyclopropane to cyclopentene (contains a mesitylene standard). (C_6D_6) 22

Figure 1.21. ^{1}HNMR spectrum for isolated 3-phenylcyclopentene. ($CDCl_3$) 23

Figure 1.22. $^{13}C\{^{1}H\}$ NMR spectrum for isolated 3-phenylcyclopentene. ($CDCl_3$) 23
Figure 1.23. ^{1}HNMR for isolated 3-hexylcyclopentene. ($CDCl_3$) 24
Figure 1.24. $^{13}C\ \{^{1}H\}$ NMR for isolated 3-hexylcyclopentene. ($CDCl_3$) 25
Figure 1.25. ^{1}HNMR spectrum for the catalytic rearrangement of *N*-phenyl cyclopropanecarboxaldimine (contains a mesitylene standard). (C_6D_6) 26
Figure 1.26. ^{1}H NMR spectrum for the catalytic rearrangement of cyclopropanecarboxaldehyde (contains a mesitylene standard). (C_6D_6) 27
Figure 1.27. ^{1}HNMR for isolated 1-phenyl-3-pentanone. ($CDCl_3$) 28
Figure 1.28. Nucleophilic ring opening and 1,3-sigmatropic rearrangment of vinylaziridines.... 29
Figure 1.29. Formation of β-lactams from vinylaziridines and CO. 30
Figure 1.30. Heating complex **2** generates 1,3-butadiene as an organic product. 31
Figure 1.31. Proposed mechanism of CO insertion to give δ-lactam from complex **2**. 32
Figure 1.32. Formation of δ-lactam from complex **4**. 33
Figure 1.33. Proposed mechanism of monometallic formation of the δ-lactam. 34
Figure 1.34. Generation of complex **5** gives dark green crystalline solid. 35
Figure 1.35. Treatment of complex **5** yields 1-phenyl-3-vinylazetidin-2-one. 36
Figure 1.36. ^{1}HNMR for isolated 1-tosyl-3,6-dihydropyridin-2(1H)-one (**23**). ($CDCl_3$) 38
Figure 1.37. $^{13}C\ \{^{1}H\}$ NMR for isolated 1-tosyl-3,6-dihydropyridin-2(1H)-one (**23**). ($CDCl_3$).. 39
Figure 1.38. COSY for isolated 1-tosyl-3,6-dihydropyridin-2(1H)-one (**23**). ($CDCl_3$) 40
Figure 1.39. ^{1}HNMR for complex **25**. (C_6D_6) 42
Figure 1.40 ^{1}HNMR for isolated complex **26**. ($CDCl_3$) 43
Figure 1.41. ^{1}HNMR for isolated 1-phenyl-2,3-dihydro-1H-pyrrole (**27**). ($CDCl_3$) 45
Figure 1.42. COSY for isolated 1-phenyl-2,3-dihydro-1H-pyrrole (**27**). ($CDCl_3$) 46
Figure 1.43. ^{1}HNMR for isolated 1-phenyl-4-vinylazetidin-2-one (**28**). ($CDCl_3$) 47
Figure 1.44. $^{13}C\ \{^{1}H\}$ NMR for isolated 1-phenyl-4-vinylazetidin-2-one (**28**). ($CDCl_3$) 48
Figure 1.45. COSY for isolated 1-phenyl-4-vinylazetidin-2-one (**28**). ($CDCl_3$) 49
Figure 1.46. IR spectrum for isolated 1-phenyl-4-vinylazetidin-2-one (**28**). (THF) 50
Figure 2.1. Oxidative transfer of hetero-atom containing substrates a.) used as transient protecting groups and b.) ring contraction. 51
Figure 2.2. Installing an epoxide prevented the unwanted isomerization of the alkene. 52
Figure 2.3. Ring contraction instead of the cross-coupling reaction occurred with unsaturated thiopyrans. 53
Figure 2.4. Hetero-atom abstraction takes place when heating 1-tosyl-2-vinylaziridine. 54

Figure 2.5. Heating 1-tosylaziridine, 1-tosyl-2-phenylaziridine, and styrene oxide results in hetero-atom abstracted products. 54

Figure 2.6. Hetero-atom abstraction from an epoxide yields styrene and three theoretical complexes. 55

Figure 2.7. ^{1}HNMR spectrum of 1,3-butadiene obtained from heating complex **2**. (C_6D_6)..... 57

Figure 2.8. ^{1}HNMR spectrum of the generation of ethylene (**30**) from 1-tosylaziridine. (C_6D_6)..... 58

Figure 2.9. ^{1}HNMR spectrum of the generation of styrene (**32**) from 1-tosyl-2-phenylaziridine. (C_6D_6)..... 59

Figure 2.10. ^{1}HNMR spectrum of the generation of styrene (**32**) from styrene oxide. (C_6D_6) 60

Figure 2.11. EPR spectrum of complex generated from styrene oxide. (298K, THF) 61

Figure 2.12. EPR spectrum of complex generated from styrene oxide. (125K, THF) 61

Figure 2.13. The Liebenskiend-Srogl cross coupling reaction uses stoichiometric amounts of a copper containing sulfur scavenger. 62

Figure 2.14. Oxidative transfer of the sulfur atom in methyl thiirane transpires to form **33**..... 63

Figure 2.15. Desulfurization attempts with thioureas. 65

Figure 2.16. Heating complex **1** with tetramethylthiourea yields a tetranickel monosulfide complex. 66

Figure 2.17. Activation of tetrahydrothiophenes led to the formation of $[(^{i\text{-}Pr}NDI)Ni_2]_2S$ (**34**)... 67

Figure 2.18. Paramagnetic peaks belonging to **34** can be seen in the ^{1}HNMR (red asterisks)..... 68

Figure 2.19. Cyclic voltammetry diagrams of a.) $[(^{i\text{-}Pr}NDI)Ni_2]_2S_2$ and b.) $[(^{i\text{-}Pr}NDI)Ni_2]_2S$..... 69

Figure 2.20. Proposed mechanism for C-S bond activation of sulfur containing substrates. 70

Figure 2.21. ^{1}HNMR for isolated Complex **33**. (C_6D_6) 72

Figure 2.22. EPR spectrum for isolated Complex **33**. 73

Figure 2.23. UV-Vis spectrum for Complex **33**. 73

Figure 2.24. FT-IR spectrum of Complex **33**. 74

Figure 2.25. ^{1}HNMR for isolated Complex **34**. (C_6D_6) 75

Figure 2.26. EPR spectrum for Complex **34**..... 76

Figure 2.27. UV-Vis spectrum of Complex **34**..... 76

Figure 2.28. FT-IR spectrum of Complex **34**. 77

Figure 2.29. Crude ^{1}HNMR for reaction with methyl thiirane to form propene (**36**). (C_6D_6)..... 78

Figure 2.30. Crude ^{1}HNMR for reaction with phenylthiirane to form styrene (**32**). (C_6D_6) 79

Figure 2.31. Crude ^{1}HNMR for reaction with 2-benzylthiirane to form allylbenzene (**39**). (C_6D_6)..... 80

Figure 2.32. Crude ^{1}HNMR of 3-methylenenon-1-ene (**41**). (C_6D_6)..... 81
Figure 2.33. Crude ^{1}HNMR of 1,3-butadiene. (C_6D_6)..... 82
Figure 2.34. ^{1}HNMR of isolated Complex (**43**). (C_6D_6)..... 83
Figure 2.35. ^{1}HNMR of isolated Complex (**34**). (C_6D_6)..... 84

LIST OF ABBREVIATIONS

Ar	Aryl
ATR-IR	Attenuated total reflectance-infrared spectroscopy
Boc	*tert*-Butyloxycarbonyl
BPY	Bipyridine
°C	Degrees celsius
C	Carbon
$CDCl_3$	Deuterated chloroform
C_6D_6	Deuterated benzene
C_6H_6	Benzene
Cl	Chlorine
cm	Centimeter
CO	Carbon monoxide
COD	Cyclooctadiene
COSY	Correlation spectroscopy
Cu	Copper
d	Doublet
DAD	α-diimine
dba	Dibenzylidene acetone
DCM	Dichloromethane
DFT	Density functional theory
Dipp	Diisopropylphenyl
Equiv.	Equivalents
Et_2O	Ether
H	Hydrogen
Hfacac	Hexafluoroacetylacetone
HOMO	Highest occupied molecular orbital
HMQC	Heteronuclear multiple quantum coherance
IMes	1,3-bis(2,4,6-trimethylphenyl)imidazole
IP	Imine-pyridine

IPr	1,3-bis(diisopropylphenyl)imidazole
i-Pr	Isopropyl
K	Kelvin
L	Liter
LUMO	Lowest unoccupied molecular orbital
M	Metal
N	Nitrogen
NDI	Napthyridine-diimine
NHC	N-heterocyclic carbene
Ni	Nickel
n-Bu	*n*-butyl
n-Hex	*n*-hexyl
Ni	Nickel
NMR	Nuclear Magnetic Spectroscopy
O	Oxygen
PCy_3	Tricyclohexylphosphine
PDI	Pyridine diamine
Pd	Palladium
Ph	Phenyl
PPh_3	Triphenylphosphine
Rh	Rhodium
S	Sulfur
Si	Silicon
THF	Tetrahydrofuran
TMS	Trimethylsilyl
Ts	Tosyl
UV-Vis	Ultraviolt-Visible Spectroscopy
V	Volts
VT	Variable temperature
XRD	X-ray diffraction
Zn	Zinc

ABSTRACT

Author: Rounds, Heather, R. PhD
Institution: Purdue University
Degree Received: May 2018
Title: Oxidative Transfer Reactions at a Metal-Metal Bond
Committee Chair: Christopher Uyeda

Strained, three-membered rings were found to undergo oxidative addition to [^{iPr}NDI]$Ni_2(C_6H_6)$ complex [NDI = napthyridine-diimine). Activation of the C-N bond of 1-tosyl-2-vinylaziridine generates a dinickel metallacyclic product. Based on this reactivity, the [^{iPr}NDI]$Ni_2(C_6H_6)$ complex was shown to be a highly active catalyst for rearranging vinylcyclopropanes to cyclopentenes. Notably, 2-phenyl-1-vinylcyclopropane undergoes regioselective activation at the less hindered C–C bond in contrast to the non-catalytic thermal rearrangement. The dinuclear complex was also found to readily rearrange hetero-atom containing cyclopropanes to their linear products. DFT calculations provide insight into the ability of the Ni–Ni bond to stabilize key intermediates and transition states along the catalytic pathway. Hetero-atom abstraction was also observed in the activation of other strained, three-membered rings with the [^{iPr}NDI]$Ni_2(C_6H_6)$ complex. Crystal structures were obtained from the activation of sulfur containing heterocycles and their characteristics are currently being investigated to design catalytic desulfurization reactions.

CHAPTER 1. CATALYTIC ACTIVATION OF STRAINED RINGS

Reproduced with permission from *Organometallics*, **2018**, *37*, 545-550. Copyright 2018 American Chemical Society.

1.1 Background

1.1.1 Transition Metal-Mediated Strained Ring Activation

Cyclopropanes, aziridines, and epoxides participate in a broad range of strain-induced ring-opening reactions mediated by transition metal catalysts.[1-6] A key step in many of these transformations is a carbon–carbon or carbon–heteroatom oxidative addition that activates the ring and generates a metallacyclic intermediate.[7-8] The driving force for C-C bond activation is the result of two main factors a.) release of ring-strain energy to form more stable organic products or b.) the formation of stable metallacycles.[1]

There are many examples of transition metal-mediated activation of strained rings with late transition metals such as rhodium[9-10], palladium[11-12], and iridium[13-14] dominating the field. Although late transition metals readily activate C-C bonds of cyclopropanes, there has been a lot of work using more abundant and cost-effective metals such as nickel[15-17] and iron.[18-19]

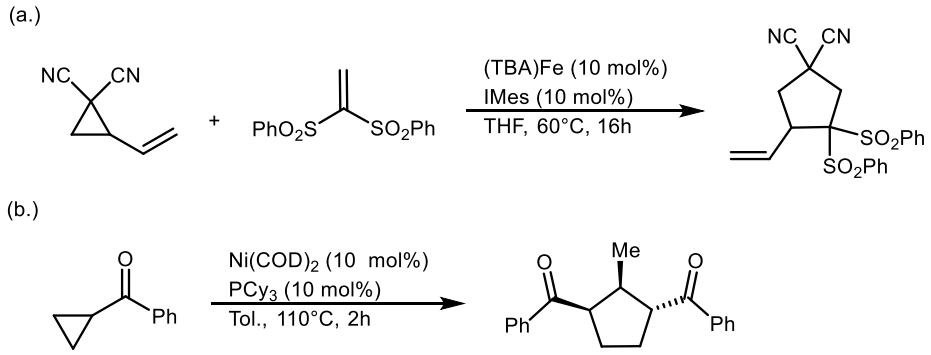

Figure 1.1. Carbon-carbon bond activation of cyclopropanes can be achieved by nickel and iron.

Dieskau et. al. demonstrated the use of a low-valent iron complex for C-C bond activation of various donor-acceptor cyclopropanes and reactions with Michael acceptors (Figure 1.1a).[18] They revealed this system is very selective in that it does not yield any side products such as dimerized starting materials or the formation of seven-membered rings. Another example of C-C bond activation of a hetero-atom containing cyclopropane was reported by Tamaki et. al. where an *in situ* generated $Ni(PCy_3)_2$ complex catalyzes the formation of cyclopentenes (Figure 1.1b).[15] This system could be applied to phenyl-substituted ketones, methyl ketones, and cyclopropanecarboxaldehyde. A nice mechanistic study was also probed to determine the nickel intermediates and the preference in the formation of cyclopentane from two equivalents of the cyclopropyl ketones.

1.2 Dinuclear Pathways for the Activation of Strained Three-Membered Rings

1.2.1 Introduction

In order to facilitate the process of strain-induced reactions with transition metals, catalysts that are effective for ring-opening reactions commonly employ strongly donating and sterically encumbering ligands that support electron-rich metals with low coordination numbers (Figure 1.2).[20-25] For example, Louie demonstrated that $(NHC)_2Ni$ complexes are remarkably active catalysts for the rearrangement of vinylcyclopropanes to form cyclopentenes.[26-27] Computational models suggest that the catalytic intermediates are monoligated Ni species and that C–C oxidative addition is likely rate-determining.[28]

Our group is interested in identifying alternative approaches to promoting bond activation reactions that exploit the cooperative function of multiple metal centers. In this context, we recently described a dinuclear $[^{i\text{-}Pr}NDI]Ni_2(C_6H_6)$ complex that effects the oxidative addition of allyl chloride to form a $Ni_2(\mu\text{-allyl})Cl$ product.[29] A notable feature of this reaction is its unusually low activation barrier (4.1 kcal/mol by DFT), which we attributed to the ability of the dinuclear system to form a stabilizing π-interaction with the incipient allyl system as the C–Cl bond is cleaved. This observation led us to question whether this activation mode could be generalized to other classes of substrates.[30] Here, we report a dinuclear mechanism for the stoichiometric and

catalytic activation of strained three-membered ring substrates, including vinylaziridines and vinylcyclopropanes.

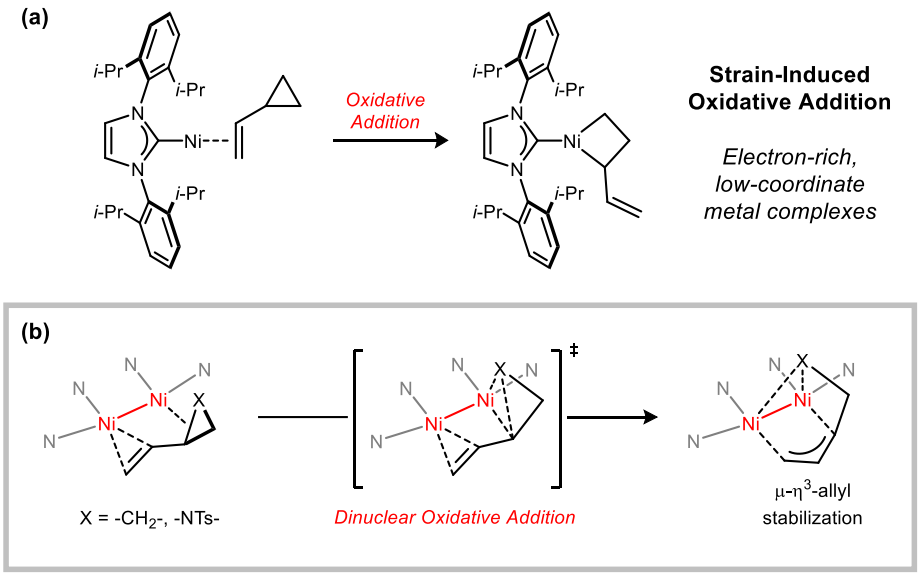

Figure 1.2 Design principles for strain-induced oxidative addition reactions of vinyl three-membered ring substrates. (a) C–C oxidative addition using electron-rich, low-coordinate metal complexes. (b) Oxidative addition driven by dinuclear stabilization of allyl groups (X = C, N).

1.2.2 Results and Discussion

1.2.2.1 Stoichiometric Aziridine Ring Opening

In our initial studies, we examined a stoichiometric oxidative addition reaction of a model strained ring system. Accordingly, the [$^{i\text{-Pr}}$NDI]$Ni_2(C_6H_6)$ complex **1**[31] reacts with *N*-tosyl-2-vinylaziridine over the course of 30 min at room temperature to provide the product of C–N oxidative addition (**2**) in 65% isolated yield as a diamagnetic, crystalline green solid (Figure 1.3a). In a similar fashion to the previously reported [$^{i\text{-Pr}}$NDI]Ni_2(allyl)Cl complex, the solid state structure features a μ-η^3-coordination mode for the allyl fragment and a μ-NTs ligand that symmetrically bridges the two metals (Figure 1.3b). The Ni–Ni bond distance for **2** (2.4600(8) Å) is relatively unchanged from that observed for **1** (2.496(1) Å), suggesting that the electron pair required for the two-electron oxidative addition is being provided by the reduced ligand π-system

rather than from the Ni–Ni bond. This description is supported by distortions in the NDI bond metrics that are characteristic of a change in the ligand charge state from dianionic to neutral (Figure 1.3c). DFT calculations are also consistent with an oxidative addition reaction that involves substantial electronic participation from the redox-active ligand. The calculated LUMO for **2** is predominantly associated with the delocalized NDI π-system with a minor fraction of Ni–Ni π* character (Figure 1.3d). This orbital corresponds to the HOMO for the $Ni_2(C_6H_6)$ complex **1**.

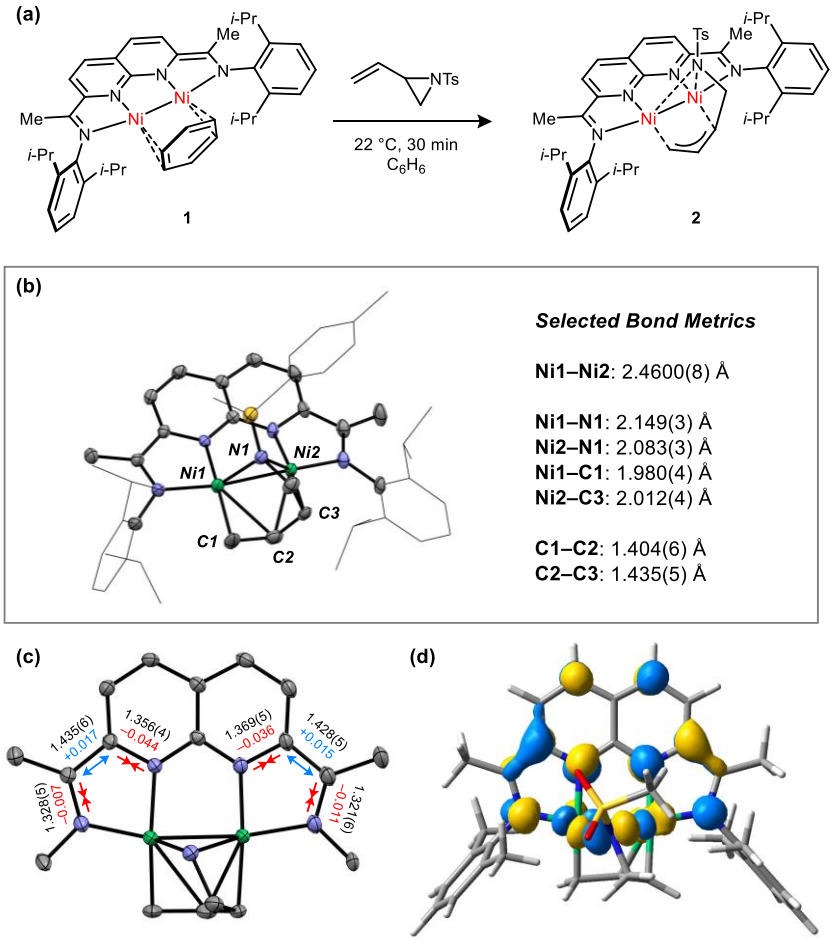

Figure 1.3. (a) Oxidative addition of *N*-tosyl-2-vinylaziridine using **1**. (b) Solid-state structure for **2** and select bond metrics. (c) Changes in bond metrics indicative of ligand-centered redox activities. Bond metrics for **2** (black) are shown in Å. Changes relative to complex **1** are shown in red and blue. (d) LUMO for **2**, which shows primarily ligand character.

The [$^{i\text{-Pr}}$IP]Ni(COD) complex **3** bears a supporting ligand that approximates half of the $^{i\text{-Pr}}$NDI system and thus provided a suitable mononickel analog for **1**. Complex **3** similarly reacts with *N*-tosyl-2-vinylaziridine to yield the blue diamagnetic metallacycle **4** in 66% yield (Figure 1.4a). The ^{1}H NMR resonances for complex **4** are broad at room temperature but sharpen and resolve at lower temperatures, suggestive of a fluxional process that occurs on the ^{1}H NMR chemical shift timescale. The most notable structural difference between the dinuclear and mononuclear oxidative addition products is the orientation of the coordinated allyl group (Figure 1.4b). In **2**, the allyl ligand spans the two Ni centers and is η^3-coordinated with C1–C2 and C2–C3 distances that are nearly equal. By contrast, the allyl ligand in **4** is η^1-coordinated, and the C2–C3 distance is relatively short at 1.337(5) Å, suggesting that it maintains significant double bond character.

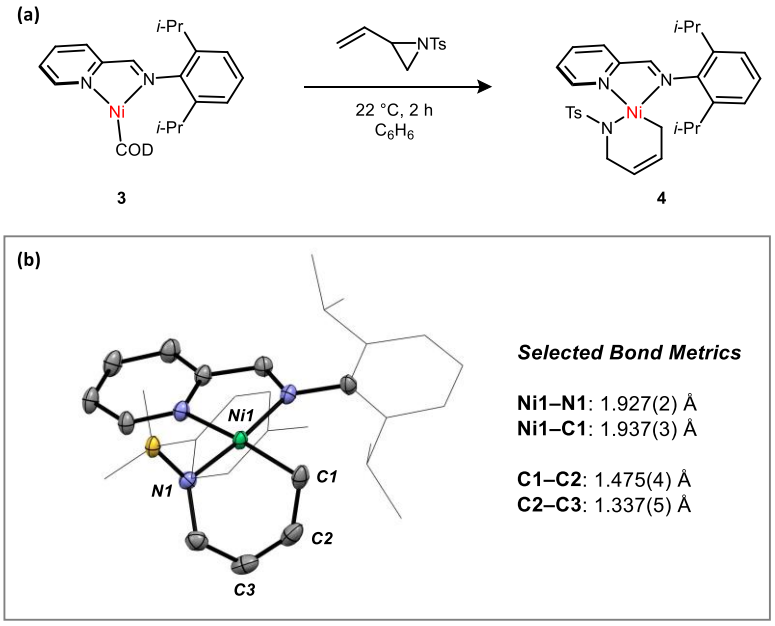

Figure 1.4. (a) Oxidative addition of *N*-tosyl-2-vinylaziridine using **3**. (b) Solid-state structure for **4** and select bond metrics.

1.2.2.2 Catalytic Rearrangement of Vinylcyclopropane

At 1 mol% loading, the [$^{i\text{-Pr}}$NDI]$Ni_2(C_6H_6)$ complex **1** catalyzes the rearrangement of vinylcyclopropane to cyclopentene, reaching full conversion after 24 h at room temperature (Table 1.1). Complex **1** is the only observable catalyst resting state under the reaction conditions. Additionally, in stoichiometric reactions between **1** and vinylcyclopropane (1.0 equiv), no intermediates are observed en route to cyclopentene, indicating that the catalytic intermediates are endothermic relative to the C_6H_6 adduct.

Table 1.1. A comparison of nickel catalysts for the rearrangement of vinylcyclopropane.

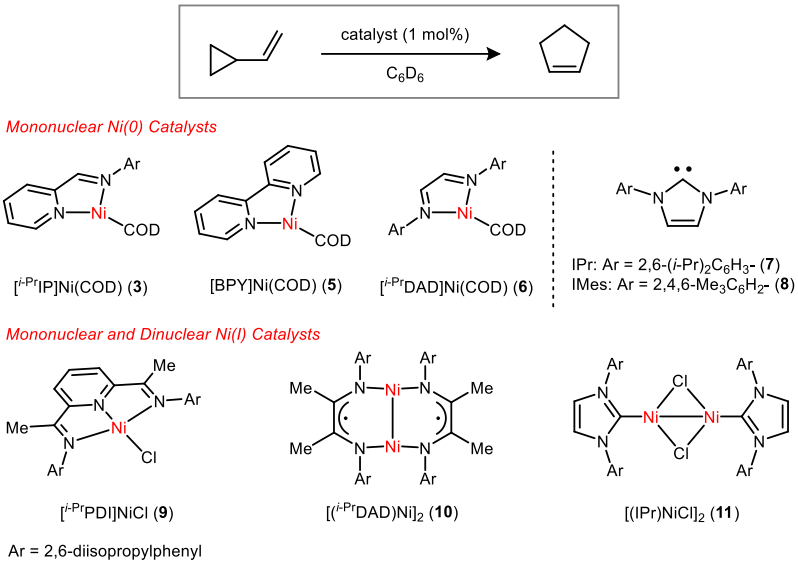

entry	catalyst	time /temp	yield
1	[$^{i\text{-Pr}}$NDI]$Ni_2(C_6H_6)$ (**1**)	24 h / 22 °C	83%
2	[$^{i\text{-Pr}}$IP]Ni(COD) (**3**)	24 h / 60 °C	<1%
3	[BPY]Ni(COD) (**5**)	24 h / 60 °C	<1%
4	[$^{i\text{-Pr}}$DAD]Ni(COD) (**6**)	24 h / 60 °C	<1%
5	$Ni(COD)_2$	24 h / 60 °C	<1%
6	$Ni(COD)_2$ + IPr[b] (**7**)	24 h / 60 °C	8%
7	$Ni(COD)_2$ + IMes[b] (**8**)	24 h / 60 °C	5%
8	[$^{i\text{-Pr}}$PDI]Ni_2Cl (**9**)	24 h / 60 °C	<1%
9	[($^{i\text{-Pr}}$DAD)Ni]$_2$ (**10**)	24 h / 60 °C	<1%
10	[(IPr)NiCl]$_2$ (**11**)	24 h / 22 °C	6%
11	[(IPr)NiCl]$_2$ (**11**)	24 h / 60 °C	50%

[a]Reactions were conducted in a sealed NMR tube, and yields were determined by ^{1}H NMR integration against a mesitylene standard. [b] 1 mol% $Ni(COD)_2$ and 2 mol% NHC.

The mononickel complex **3**, shown above to activate *N*-tosyl-2-vinylaziridine, is not capable of mediating C–C oxidative addition with vinylcyclopropane, providing no detectable conversion of starting material even after 24 h of heating at 60 °C. Related [N,N]Ni(COD)

complexes (**5** and **6**) were similarly unreactive under these conditions, as were the mononuclear and dinuclear Ni(I) complexes: [$^{i\text{-Pr}}$PDI]Ni_2Cl (**9**)[32] and [($^{i\text{-Pr}}$DAD)Ni]$_2$ (**10**).[33] The [NHC]$_2$Ni catalysts, previously studied by Louie,[26] are active for the rearrangement of the parent vinylcyclopropane molecule but require elevated temperatures in order to achieve detectable levels of conversion. For example, the IPr/Ni(COD)$_2$ mixture provides 8% yield of cyclopentene after 24 h of heating at 60 °C. The dimeric [(IPr)NiCl]$_2$ complex (**11**)[34] is more active than its Ni(0) counterpart, though it is unclear whether **11** might disproportionate under the reaction conditions to generate an active Ni(0) species. It is noteworthy that while the [IPr]$_2$Ni catalyst is only modestly active for the rearrangement of vinylcyclopropane, it is substantially more efficient for substrates bearing alkene substituents.[26] On the other hand, the Ni_2 catalyst **1** is only capable of activating substrates with unsubstituted vinyl groups, presumably due to its large steric profile.

For vinylcyclopropane derivatives bearing ring substitutions, the ratio of rearranged cyclopentene isomers is dictated by which of the two cyclopropane C–C bonds is cleaved. In the case of the phenyl-substituted vinylcyclopropane **12**, the catalytic rearrangement with **1** selectively targets the less hindered C–C bond, providing **13** in 93% yield as a single isomer (Figure 1.5). A similar regioselectivity is observed using the alkyl-susbstituted vinylcyclopropane **15**, which forms **16** in 92% yield. It is noteworthy that the thermal rearrangement of **12** proceeds at >200 °C and provides only the alternative product isomer **14**.[35-36] This thermal rearrangement is proposed to occur by C–C bond homolysis to generate a biradical intermediate and is thus governed by the relative stabilities of the benzylic vs. the primary radical.

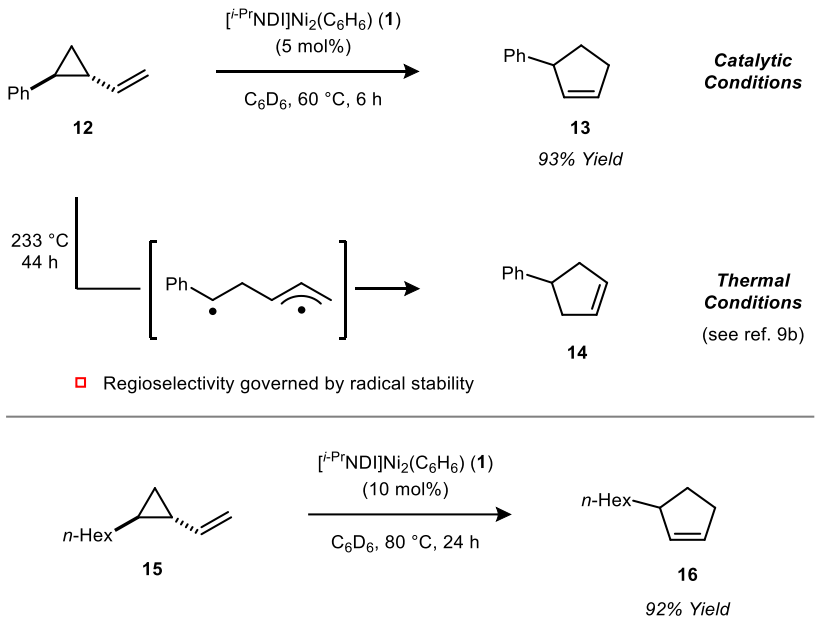

Figure 1.5. Catalytic rearrangements of vinylcyclopropanes bearing ring substitution.

Given the lack of observable intermediates in the Ni_2-catalyzed vinylcyclopropane rearrangement, we turned to DFT models to further probe the mechanism of this reaction (Figure 1.6). As expected based on our experimental results, the exchange of C_6H_6 for vinylcyclopropane is an endothermic process (+13.7 kcal/mol). The vinylcyclopropane adduct (B) exhibits a highly activated C–C bond (1.728 Å), likely due to a strong interaction with the bent C–C σ-bonding orbital of the cyclopropane. Notably, the oxidative addition from B is nearly barrierless (<0.1 kcal/mol), and the C–C distance in the transition state (C) is elongated by only 0.020 Å relative to B. The oxidative addition is highly exothermic and generates a Ni_2 metallacycle (D), which closely resembles the analogous structure that was characterized using *N*-tosyl-2-vinylaziridine (Figure 1.3). From D, reductive elimination is calculated to be rate-determining for the catalytic cycle and has an activation energy of 22.1 kcal/mol. The resulting cyclopentene adduct F is relatively unstable, and ligand exchange with C_6H_6 to generate the free product is favorable.

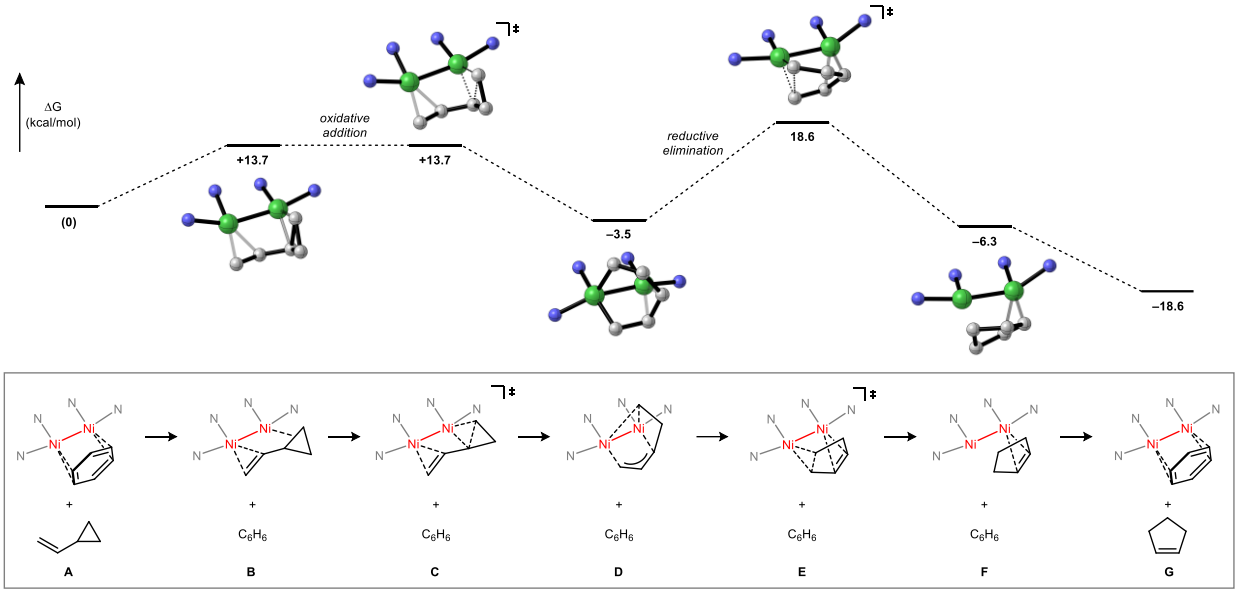

Figure 1.6. Calculated reaction coordinate for the Ni_2-catalyzed vinylcyclopropane rearrangement (M06l/6-31g(d,p) level of DFT). Free energies (ΔG) are in kcal/mol and are relative to **A**. In the model, the catalyst *i*-Pr groups are truncated to Me groups.

It is salient to compare the energetics of the key mechanistic steps using the dinuclear catalyst **1** with those previously calculated for the mononuclear [NHC]Ni catalyst.[28] The most significant consequence of the dinuclear active site is that the oxidative addition transition state and resulting metallacycle intermediate are highly stabilized by the additional π-interactions formed with the second Ni center. The oxidative addition is calculated to be nearly barrierless using **1** but is the rate-determining step for the [NHC]Ni catalyst (approx. 15.6 kcal/mol activation energy).[28] Likewise, the conversion of the [NHC]Ni vinylcyclopropane adduct to the oxidative addition product is thermoneutral, whereas the analogous dinuclear oxidative addition from B to D is exothermic by 17.2 kcal/mol using **1**. In contrast to the oxidative addition steps, the C–C reductive elimination is calculated to be more facile for the [NHC]Ni catalyst (15.5 kcal/mol) as compared to **1** (22.1 kcal/mol). Overall, these results suggest that dinuclear systems may be particularly suited to accelerating challenging oxidative addition reactions of allylic bonds but do so at the expense of stabilizing the resulting metallacycles and slowing down subsequent reductive elimination.

1.2.2.3 Catalytic Rearrangements of Heteroatom-Containing Cyclopropanes

We next turned our attention to exploring activation reactions of cyclopropanes bearing pendant heteroatom-containing substituents. The cyclopropyl imine substrate **17** undergoes a catalytic rearrangement with **1** to form the acyclic α,β-unsaturated product **18** (Figure 1.7).[37] This result suggests that following cyclopropane ring-opening, β-hydride elimination outcompetes the C–N reductive elimination that would lead to 2,5-dihydro-1*H*-pyrrole formation. Similarly, cyclopropylcarboxaldehyde **19** undergoes a catalytic rearrangement to form crotonaldehyde **20** in 80% yield.[38-39] Finally, the cyclopropanol substrate **21** rearranges to the ketone **22** in high yield.[40-41]

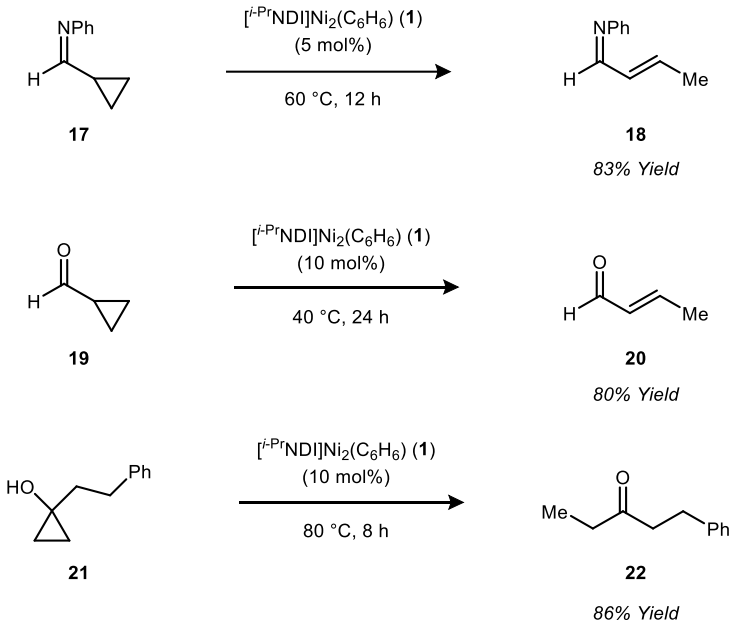

Figure 1.7. Catalytic rearrangements of cyclopropanes bearing heteroatom-containing substituents.

In summary, the dinuclear active site of the [NDI]Ni_2 platform provides a unique electronic environment for the activation of vinyl-substituted strained rings. The presence of an additional metal center enables pre-coordination of the alkene and provides stabilization to the allyl system that results from ring opening. Accordingly, oxidative addition reactions of

substrates such as vinylaziridines and vinylcyclopropanes proceed with remarkably low activation barriers. Ongoing studies are aimed at exploiting these properties for the activation of other strained and unstrained molecules.

1.2.3 Experimental Section

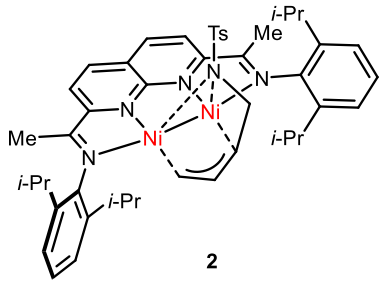

2

In a 20-mL vial, [$^{i\text{-}Pr}$NDI]$Ni_2(C_6H_6)$[42] (30 mg, 0.041 mmol, 1.0 equiv) and 1-tosyl-2-vinylaziridine[43] (9.2 mg, 0.041 mmol, 1.0 equiv) were dissolved in C_6H_6 (5 mL). The solution was observed to undergo an immediate color change from red-brown to green. After stirring at ambient temperature for 30 min, the reaction mixture was filtered through a glass fiber pad, and the filtrate was concentrated to dryness under reduced pressure. The crude residue was washed with pentane (3 x 1 mL) then dried under reduced pressure to give **2** (21 mg, 65% yield) as a dark green powder. Single crystals suitable for XRD were obtained by cooling saturated solutions of **2** in Et_2O to –30 °C in a glovebox freezer. ^{1}HNMR (500 MHz, 295 K, C_6D_6) δ 8.79 (br s, 1H), 7.88 (d, *J* = 7.4 Hz, 2H, Ts H), 7.53 (d, *J* = 7.5 Hz, 1H, Ar H), 7.47 (d, *J* = 7.5 Hz, 1H, Ar H), 7.32 (d, *J* = 7.0 Hz, 1H, Ar H), 7.23 (t, *J* = 7.7 Hz, 1H, Ar H), 6.99 (m, 3H), 6.90 (m, 1H), 6.84 (d, *J* = 7.5 Hz, 2H, Ts H), 6.58 (d, *J* = 8.0 Hz, 1H), 6.27 (d, *J* = 7.9 Hz, 1H), 4.96 (d, *J* = 6.3 Hz, 1H), 4.38 (d, *J* = 7.5 Hz, 1H), 3.86 (sept, *J* = 11.0 Hz, 1H, –$CH(CH_3)_2$), 3.63 (sept, *J* = 7.0 Hz, 1H, –$CH(CH_3)_2$), 3.39 (br s, 1H), 3.35 (d, *J* = 11.0 Hz, 1H), 2.82 (sept, *J* = 6.7 Hz, 1H, –$CH(CH_3)_2$), 2.08 (s, 3H, Ts CH_3), 1.67 (s, 6H, imine CH_3), 1.38 (d, *J* = 6.6 Hz, 3H, –$CH(CH_3)_2$), 1.29 (d, *J* = 6.5 Hz, 3H, –$CH(CH_3)_2$), 1.14 (s, 6H, –$CH(CH_3)_2$), 1.03 (d, *J* = 6.5 Hz, 3H, –$CH(CH_3)_2$), 0.90 (d, *J* = 6.7 Hz, 3H, –$CH(CH_3)_2$), 0.68 (sept, *J* = 6.6 Hz, $_1$H, –$CH(CH_3)_2$), 0.48 (d, *J* = 6.7 Hz, 3H, –$CH(CH_3)_2$), 0.23 (d, *J* = 6.7 Hz, 3H, –$CH(CH_3)_2$). $^{13}C\{^1H\}$NMR (126 MHz, 295 K, C_6D_6) δ 164.9, 164.4, 162.9, 152.9, 149.3, 147.6, 147.3, 147.3, 146.1, 145.9, 143.9,

141.4, 139.6, 128.8, 128.3, 127.9, 127.7, 127.5, 126.7, 125.9, 124.1, 124.0, 124.0, 123.5, 116.9, 112.4, 108.8, 49.3, 44.8, 29.9, 28.2, 28.0, 27.1, 25.6, 24.8, 24.8, 24.6, 24.3, 24.2, 24.0, 23.8, 21.0, 18.3, 14.5. UV–vis (THF) (λ) {ε, cm–1, M–1} 667 {4,500}, 345 {17,000}, 275 {29,000}. Anal. Calc. for (**2**) ($C_{47}H_{57}N_5Ni_2O_2S$): C 64.63%, H 6.58%, N 8.02% found: C 64.85%, H 6.75%, N 7.76%.

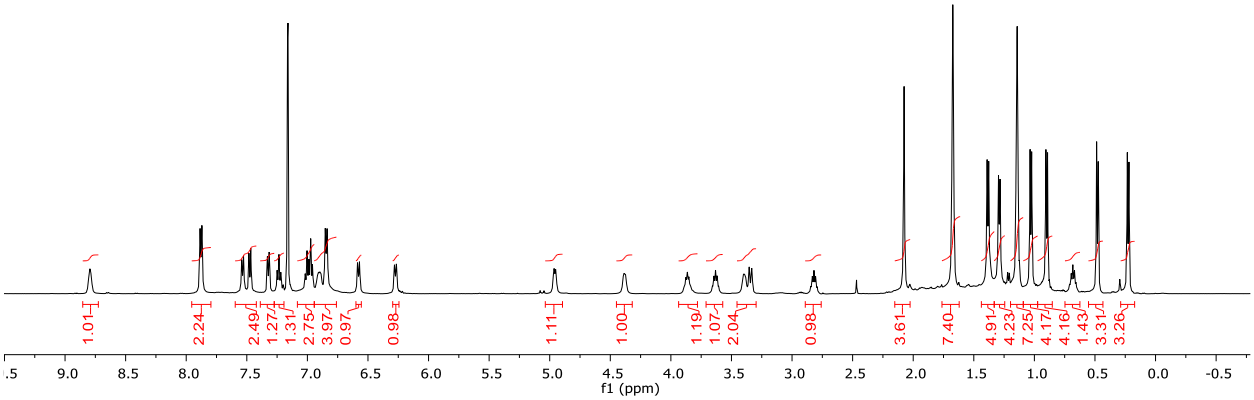

Figure 1.8. ^{1}HNMR spectrum for complex **2** (C_6D_6, room temperature).

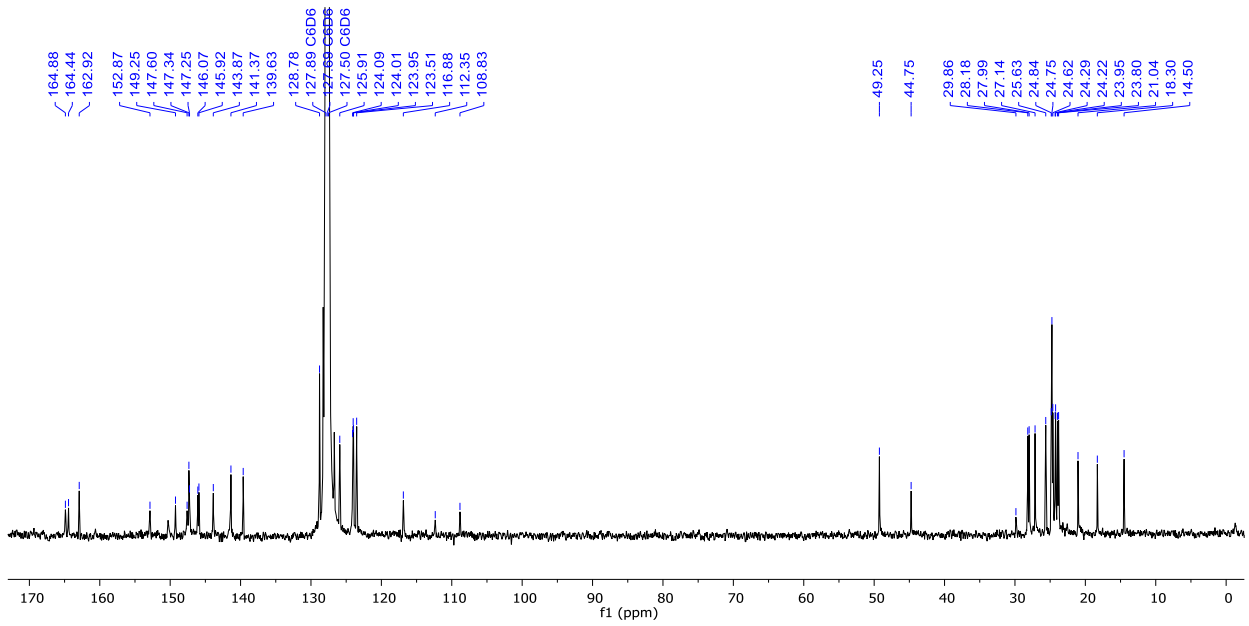

Figure 1.9. $^{13}C\{^{1}H\}$ NMR spectrum for complex **2** (C_6D_6, room temperature).

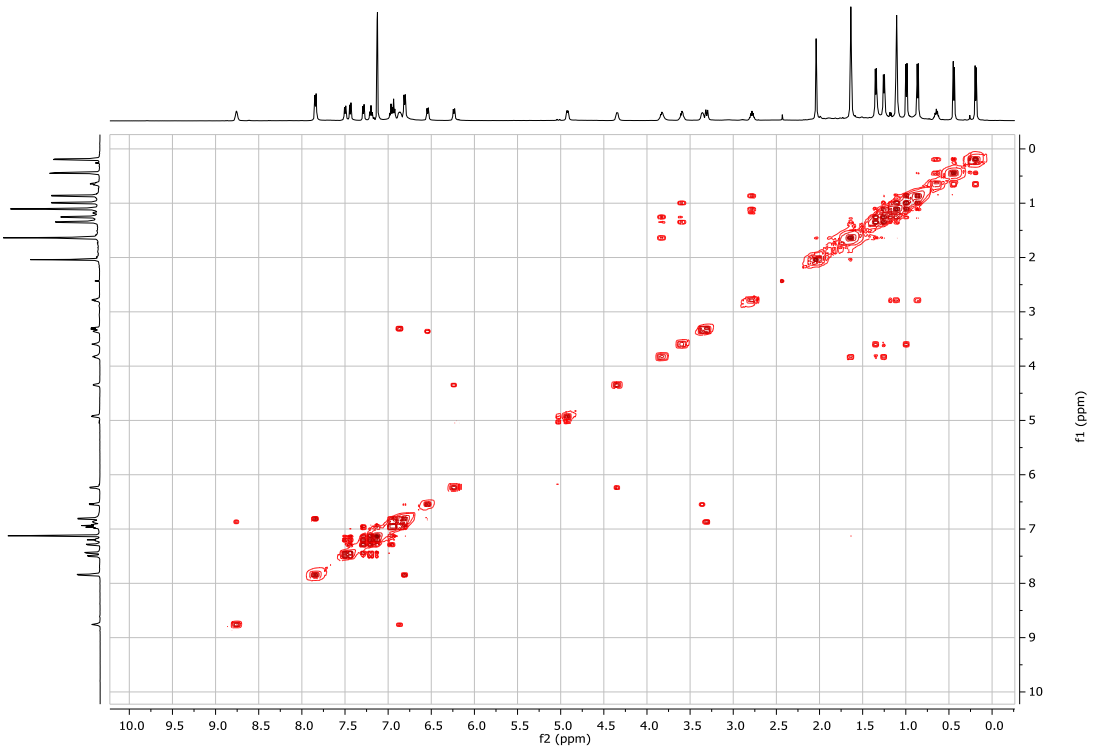

Figure 1.10. COSY spectrum for complex **2** (C_6D_6, room temperature).

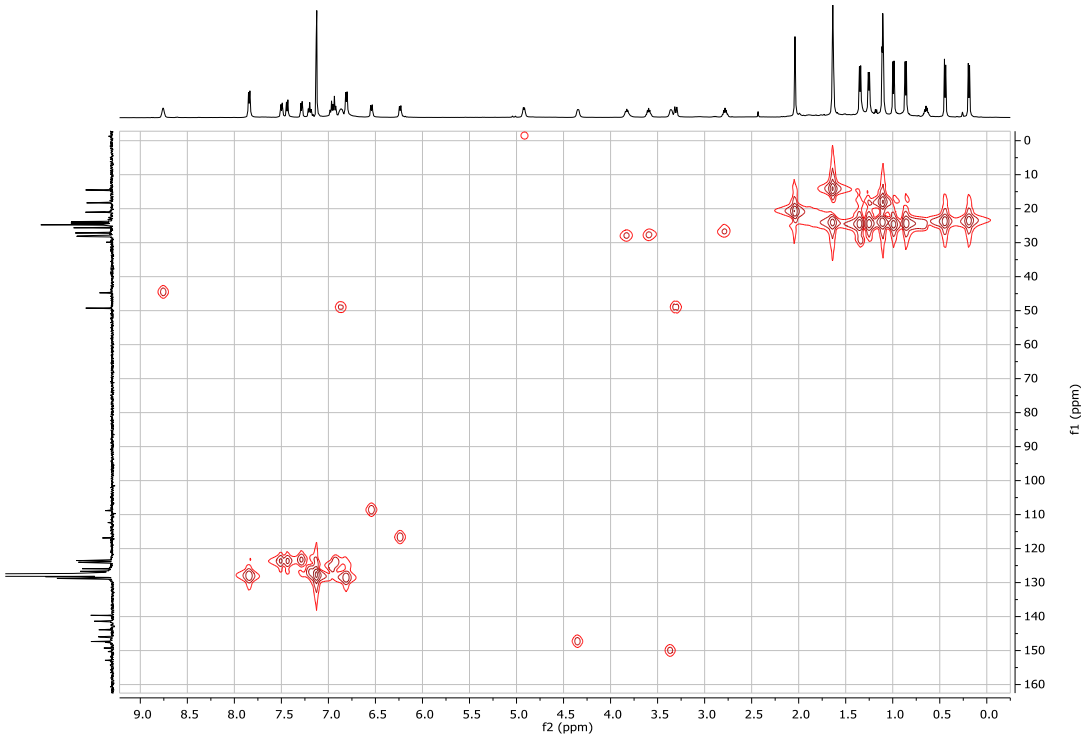

Figure 1.11. HMQC spectrum for complex **2** (C_6D_6, room temperature).

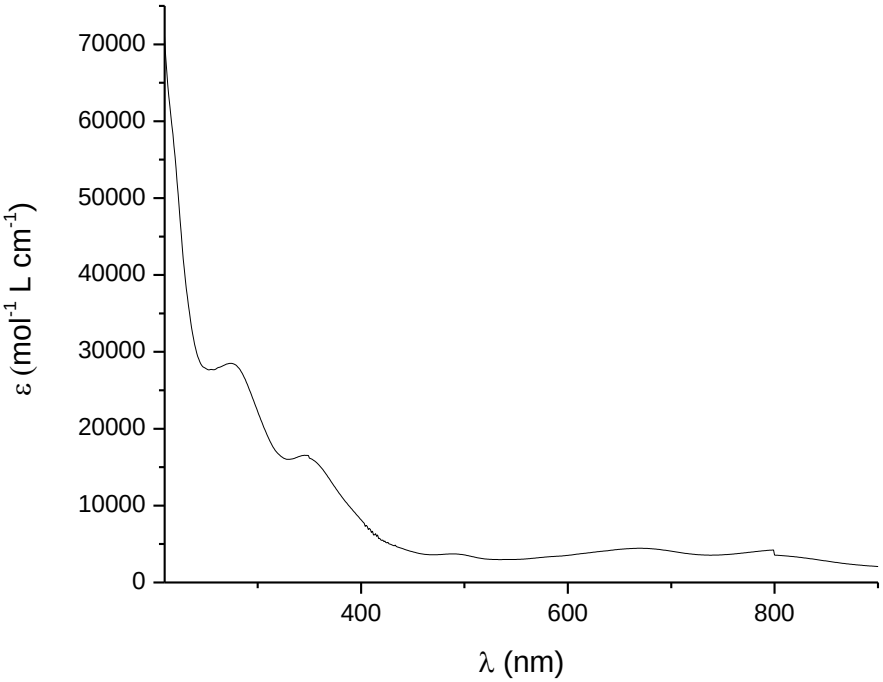

Figure 1.12. UV-Vis spectrum for complex **2** (THF, room temperature).

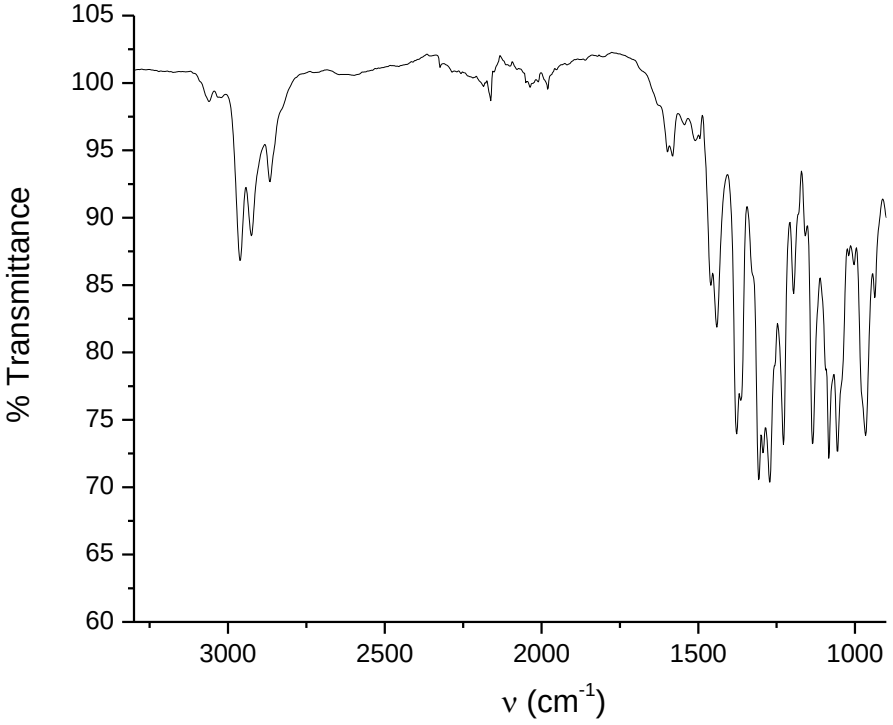

Figure 1.13. ATR-IR spectrum for complex **2**.

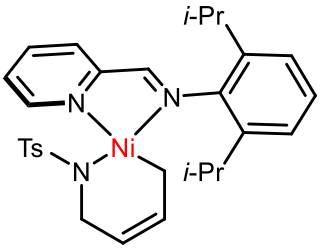

4

In a 20-mL vial, [$^{i\text{-}Pr}$IP]Ni(COD) (**3**)[44] (40 mg, 0.093 mmol, 1.0 equiv) and 1-tosyl-2-vinylaziridine (21 mg, 0.093 mmol, 1.0 equiv) were dissolved in THF (5 mL). The solution was observed to undergo a gradual color change from purple to blue. After 2 h, the reaction mixture was filtered through a glass fiber pad, and the filtrate was concentrated to dryness under reduced pressure. The crude residue was washed with pentane (3 x 1 mL) then dried under reduced pressure to give **4** (33.6 mg, 66%) as a dark blue powder. Single crystals suitable for XRD were obtained by cooling saturated solutions of **4** in Et_2O to –30 °C in a glovebox freezer. ^{1}HNMR

(500 MHz, 233K, toluene-d_8) δ 9.51 (s, 1H, CHNAr), 8.28 (d, 2H, Ar H), 7.61 (s, 1H, Ar H), 6.91 (m, 4H, Ar H), 6.06 (d, *J* = 8.5 Hz , 1H, CH=CH), 5.22 (d, *J* = 8.4 Hz, 1H, CH=CH), 4.21 (s, 1H, –CH(CH_3)$_2$), 3.80 (d, *J* = 16.6 Hz, 1H, –CH(CH_3)$_2$), 3.03 – 2.90 (m, 2H, –CH(CH_3)$_2$), 2.51 (d, *J* = 16.8 Hz, 1H, –CH(CH_3)$_2$), 2.22 – 2.11 (m, 1H), 1.96 (s, 3H, CH_3), 1.58 (d, *J* = 5.6 Hz, 3H, CH(CH_3)$_2$), 1.18 – 1.02 (m, 6H, –CH(CH_3)$_2$), 0.76 (d, *J* = 5.9 Hz, 3H, –CH(CH_3)$_2$). $^{13}C\{^1H\}$ NMR (126 MHz, 295 K, C_6H_6) δ 164.3, 152.2, 145.0, 145.6, 142.2, 140.6, 139.4, 137.2, 131.8, 128.8, 128.6, 128.3, 127.9, 127.7, 127.6, 123.9, 123.4, 47.2, 28.3, 24.5, 22.8, 20.8, 16.8. UV–vis (THF) (λ) {ε, cm–1, M–1} 329 {1800}, 273 {15,000}, 228 {33,000}. Anal. Calc. for (**4**) ($C_{29}H_{35}N_3NiO_2S$): C 63.52%, H 6.43%, N 7.66% found: C 63.48%, H 6.39%, N 7.66%.

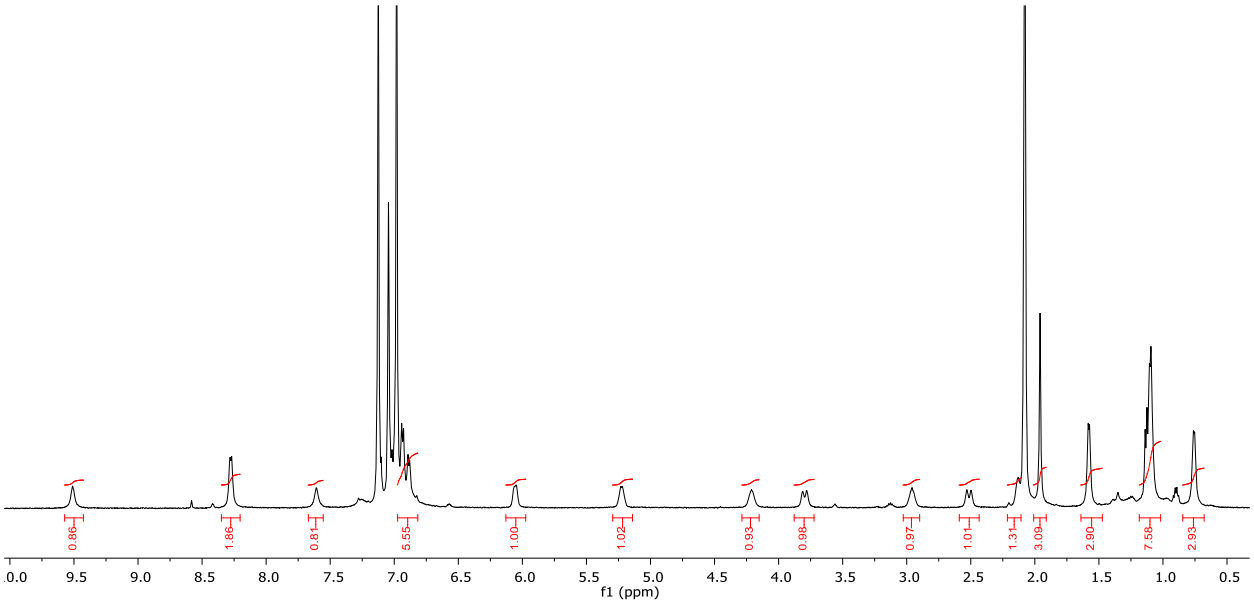

Figure 1.14. ^{1}HNMR spectrum for complex **4** (toluene-d_8, 233K).

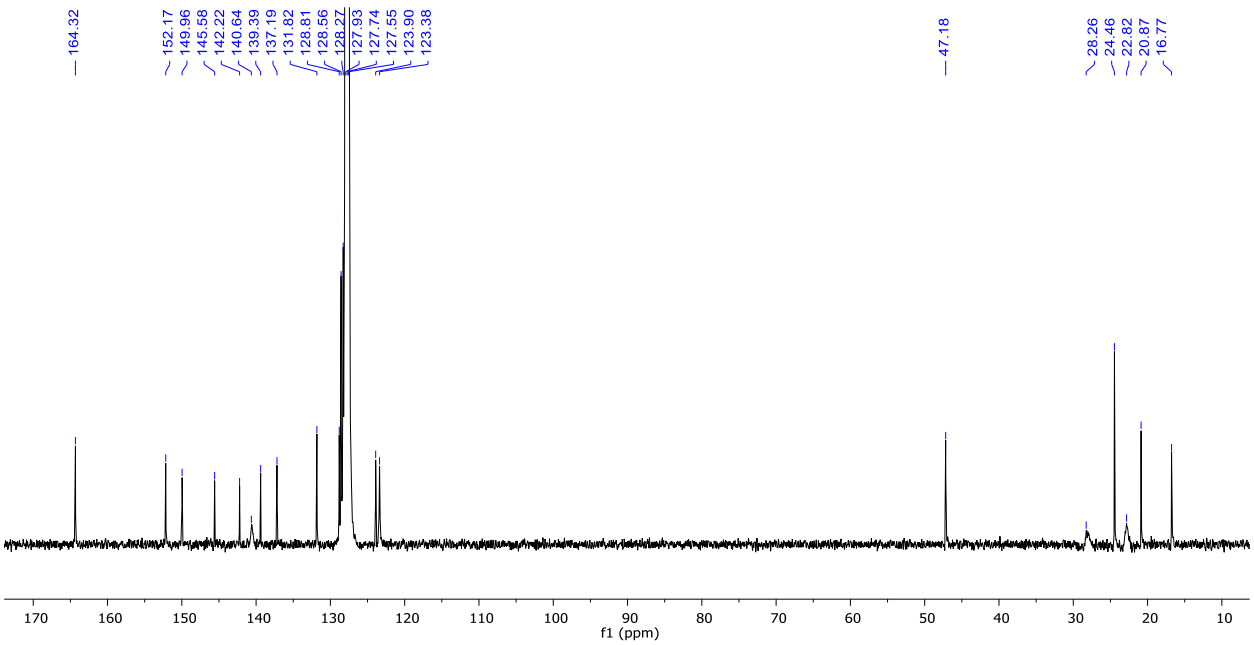

Figure 1.15. $^{13}C\{^{1}H\}$ NMR spectrum for complex **4** (C_6D_6, room temperature).

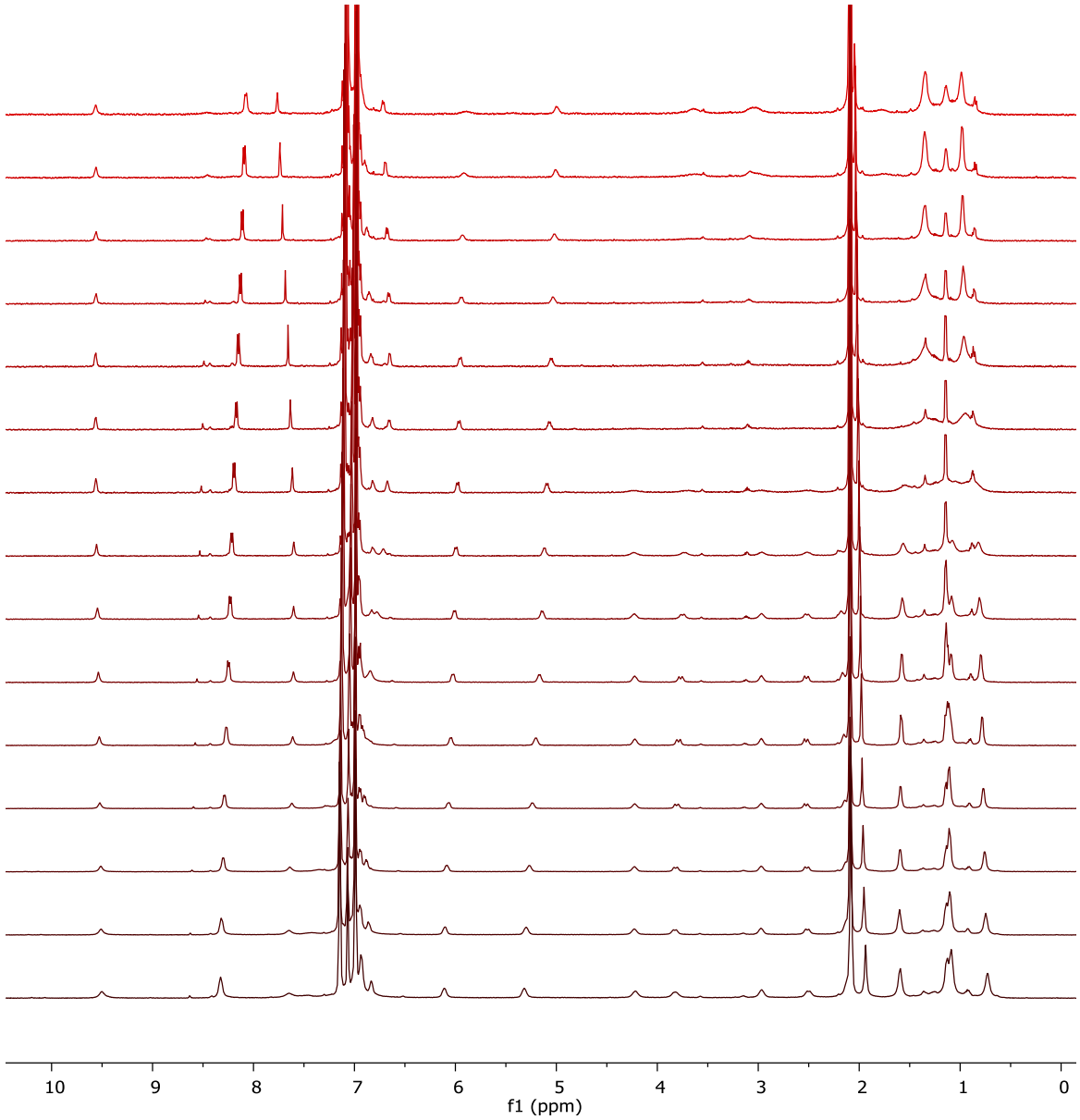

Figure 1.16. VT-NMR spectra for complex **4** (toluene-d_8, 213 K to 353 K, bottom to top).

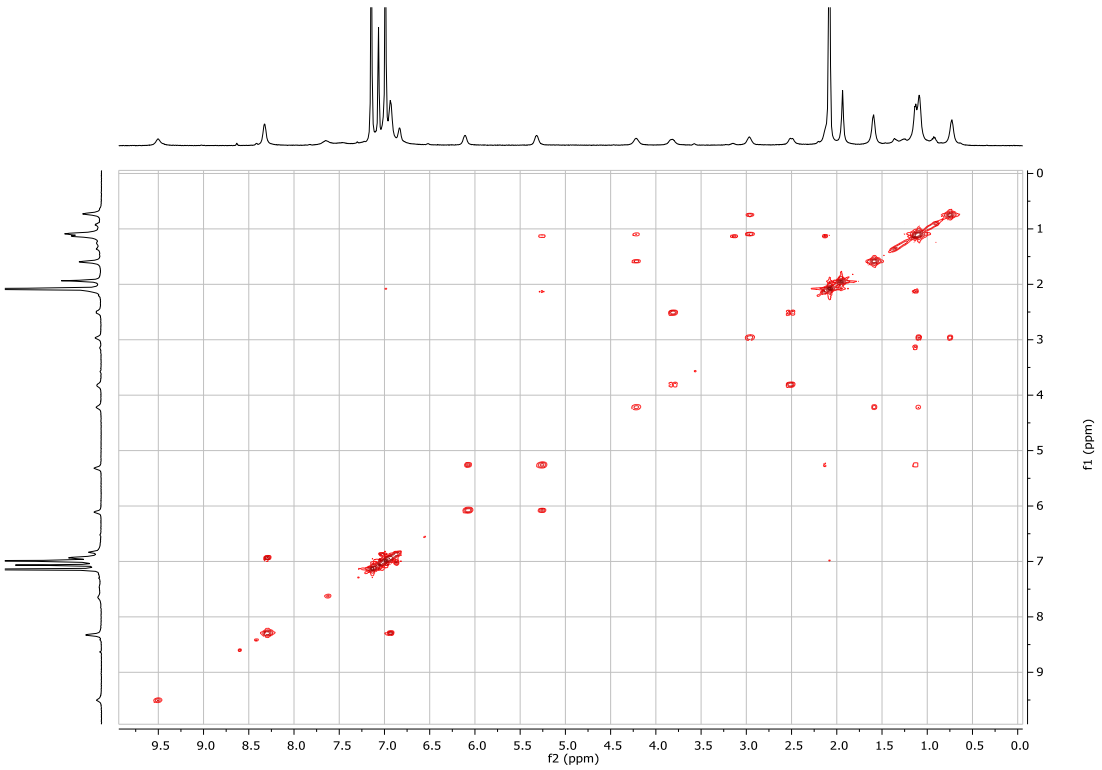

Figure 1.17. COSY complex for complex **4** (toluene-d_8, 213K).

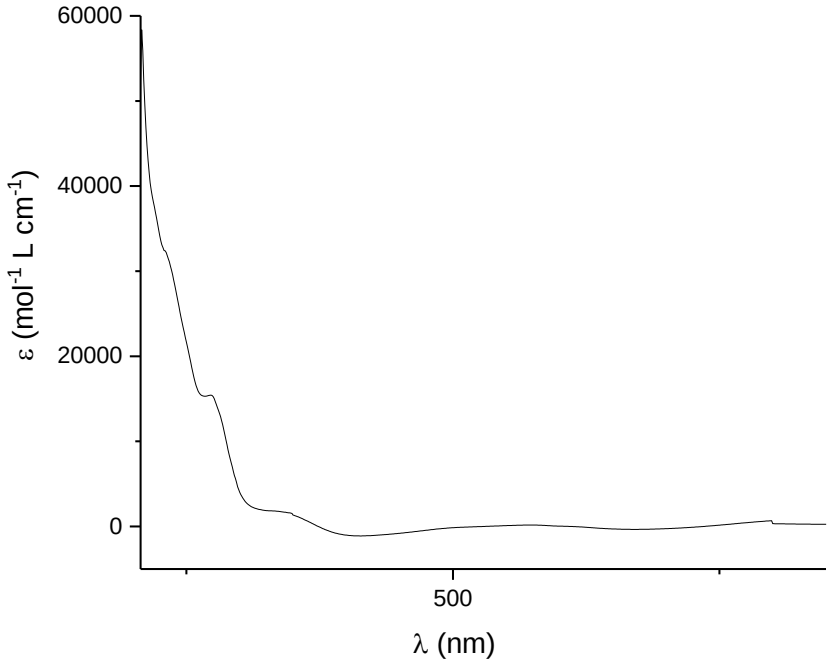

Figure 1.18. UV-Vis spectrum for complex **4** (THF, room temperature).

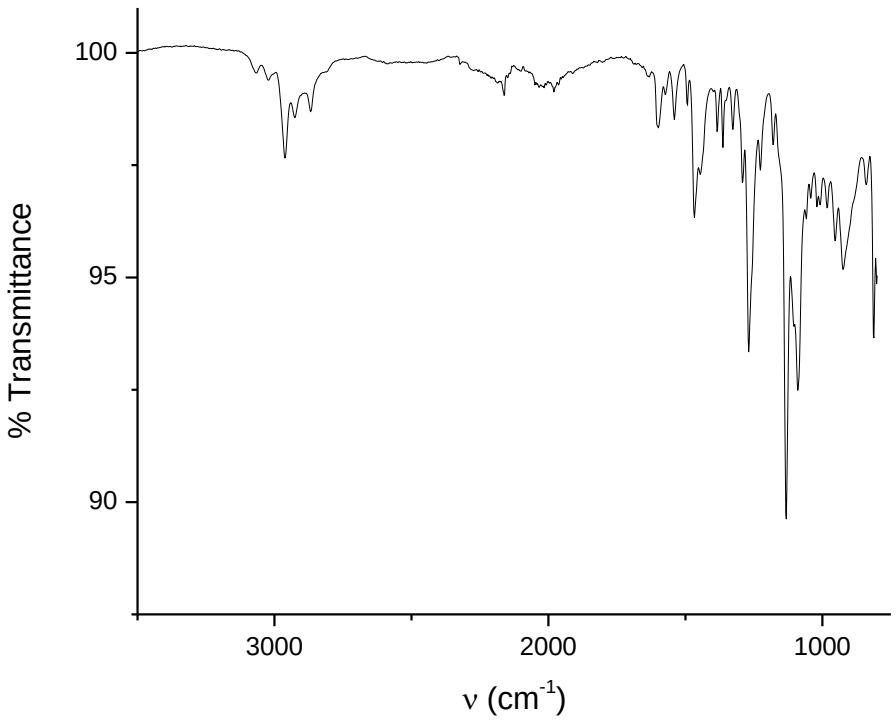

Figure 1.19. ATR-IR spectrum for complex **4.**

General Procedure for the Catalytic Rearrangement of Vinylcyclopropane (Table 1). In an N_2-filled glovebox, vinylcyclopropane[45] (0.14 mmol), mesitylene (0.14 mmol), and the Ni catalyst (0.0014 mmol, 1 mol %) were dissolved in C_6D_6 (0.5 mL), and the solution was loaded into an NMR tube equipped with a J. Young valve. The reaction mixture was allowed to react at ambient temperature or 60 °C for 24 h, and the yield of cyclopentene was determined by ^{1}HNMR integration against the mesitylene standard.

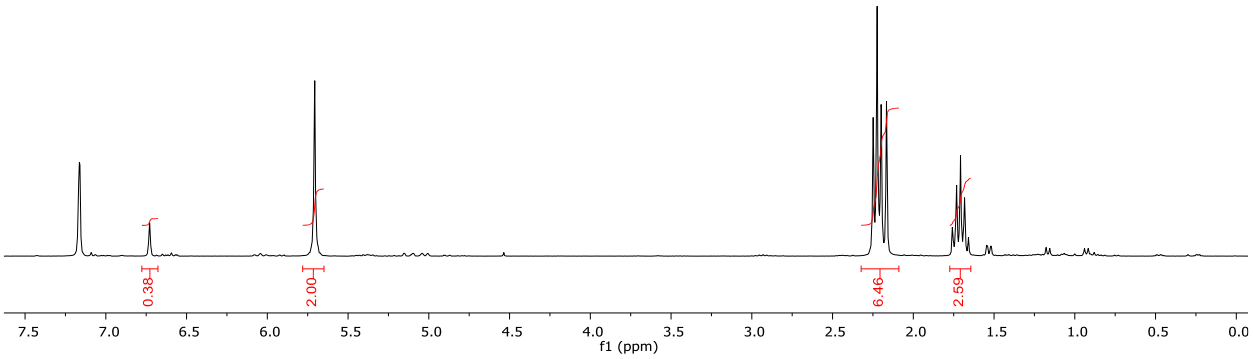

Figure 1.20. ^{1}H NMR spectrum for the catalytic rearrangement of cyclopropane to cyclopentene (contains a mesitylene standard). (C_6D_6)

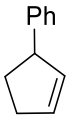

Catalytic Rearrangement of 1-Phenyl-2-vinylcyclopropane (**12**). In an N_2-filled glovebox, 1-phenyl-2-vinylcyclopropane[46] (29 mg, 0.20 mmol), mesitylene (24 mg, 0.20 mmol), and [$^{i\text{-}Pr}$NDI]$Ni_2(C_6H_6)$ (7.3 mg, 0.01 mmol, 5 mol%) were dissolved in C_6D_6 (0.5 mL), and the solution was loaded into an NMR tube equipped with a J. Young valve. The reaction mixture was allowed to react at 60 °C for 6 h, and the yield of 3-phenylcyclopentene[47] was determined by ^{1}H NMR integration against the mesitylene standard (93% yield). The crude mixture was directly loaded on to an SiO_2 column for purification (mobile phase: pentane). 3-Phenylcyclopentene (**13**) was isolated in 52% yield (15 mg) as a colorless oil. ^{1}HNMR (500 MHz, 295 K, $CDCl_3$) δ 7.33 – 7.28 (m, 2H, Ar H), 7.23 – 7.18 (m, 3H, Ar H), 5.96 (dq, *J* = 5.7, 2.3 Hz, 1H, CH=CH), 5.80 (dq, *J* = 5.7, 2.1 Hz, 1H, CH=CH), 3.91 (m, 1H, CH), 2.58 – 2.47 (m, 1H, CH_2), 2.47 – 2.37 (m, 2H, CH_2), 1.79 – 1.69 (m, 1H, CH_2). ^{13}C{^{1}H} NMR (126 MHz, 295 K, $CDCl_3$) δ 146.5, 134.3, 131.9, 128.4, 127.2, 126.0, 51.4, 33.9, 32.5.

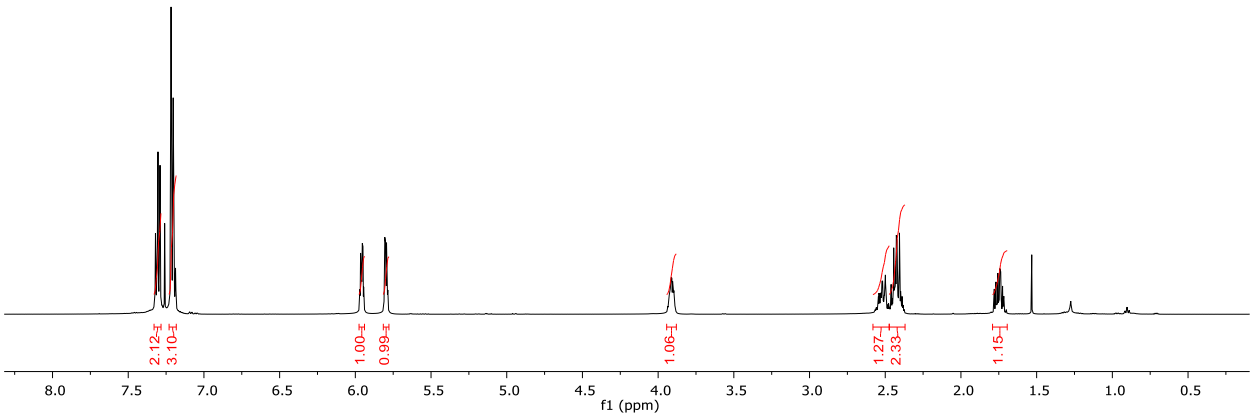

Figure 1.21. ^{1}HNMR spectrum for isolated 3-phenylcyclopentene. ($CDCl_3$)

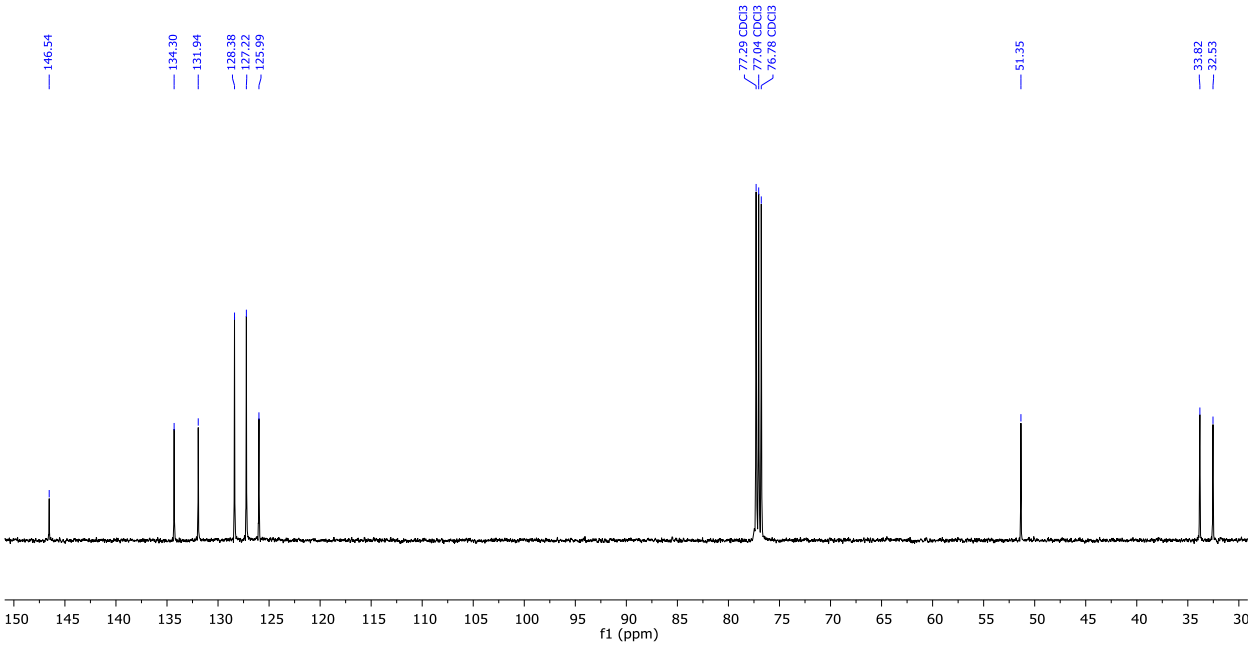

Figure 1.22. $^{13}C\{^{1}H\}$ NMR spectrum for isolated 3-phenylcyclopentene. ($CDCl_3$)

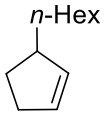

Catalytic Rearrangement of 1-Hexyl-2-vinylcyclopropane (**15**). In an N_2-filled glovebox, 1-hexyl-2-vinylcyclopropane (15.2 mg, 0.10 mmol), mesitylene (12 mg, 0.10 mmol), and [$^{i\text{-}Pr}$NDI]$Ni_2(C_6H_6)$ (7.3 mg, 0.01 mmol, 10 mol%) were dissolved in C_6D_6 (0.5 mL), and the solution was loaded into an NMR tube equipped with a J. Young valve. The reaction mixture was allowed to react at 80 °C for 24 h, and the yield of 3-hexylcyclopentene[48] was determined by ^{1}HNMR integration against the mesitylene standard (92% yield). The crude mixture was directly loaded on to a SiO_2 column for purification (mobile phase: pentane). 3-Hexylcyclopentene (**16**) was isolated in 58% yield (9 mg) as a colorless oil. ^{1}H NMR (500 MHz, 295 K, $CDCl_3$) δ 5.69 (m, 2H, CH=CH), 2.63 (bs, 1H), 2.30 (m, 2H), 2.03 (m, 1H), 1.35 (m, 11H, CH_2), 0.89 (t, J = 6.6 MHz, 3H, CH_3). ^{13}C{^{1}H} NMR (126 MHz, 295 K, C_6D_6) δ 135.5, 123.0, 45.6, 36.2, 32.0, 31.9, 29.9, 29.6, 28.0, 22.7, 14.1.

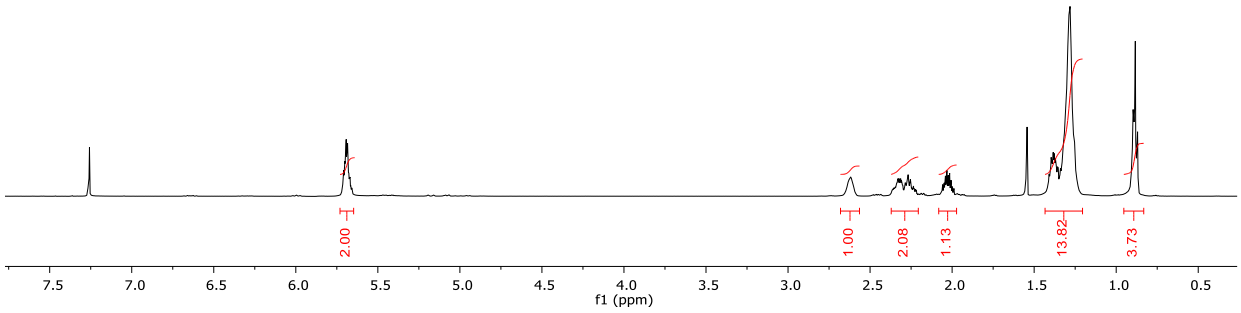

Figure 1.23. ^{1}HNMR for isolated 3-hexylcyclopentene. ($CDCl_3$)

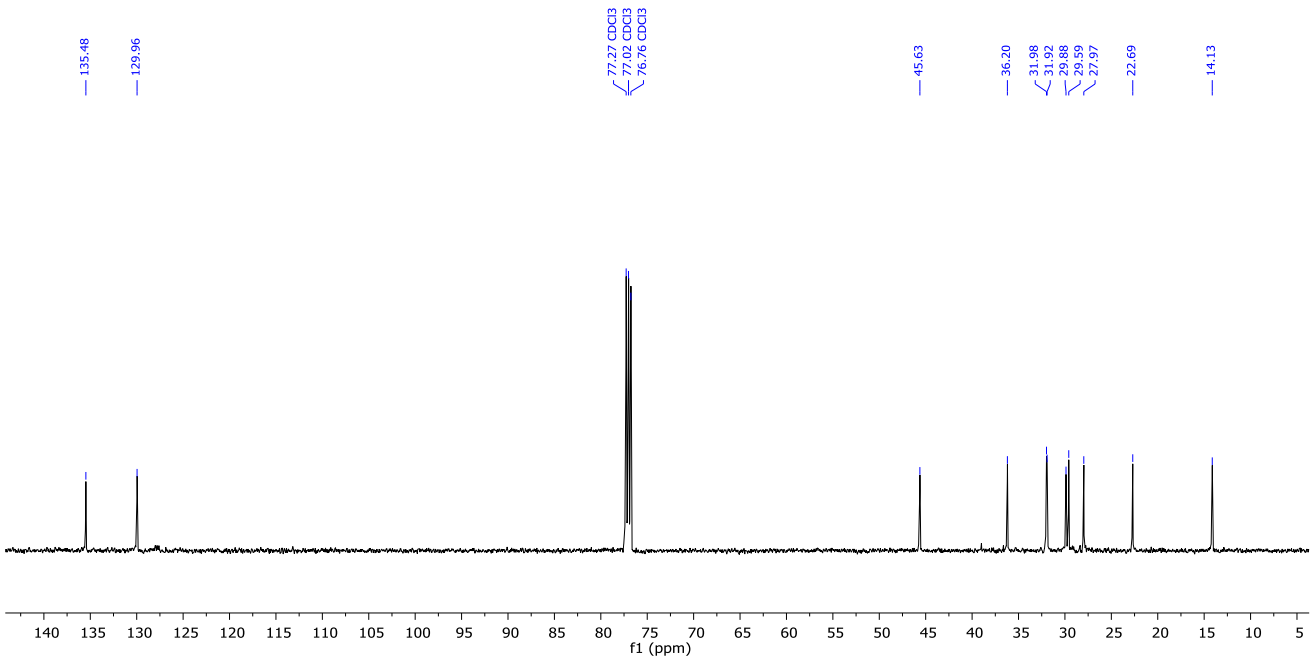

Figure 1.24. ^{13}C {^{1}H} NMR for isolated 3-hexylcyclopentene. ($CDCl_3$)

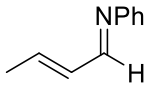

Catalytic Rearrangement of **17**. In an N_2-filled glove-box, **17**[49] (8.0 mg, 0.054 mmol), mesitylene (6.6 mg, 0.054 mmol), and [$^{i\text{-}Pr}$NDI]$Ni_2(C_6H_6)$ (2 mg, 0.0027 mmol, 5 mol%) were dissolved in C_6D_6 (0.5 mL), and the solution was loaded into an NMR tube equipped with a J. Young valve. The reaction mixture was allowed to react at 60 °C for 12 h, and the yield of **18** was determined by ^{1}HNMR integration against the mesitylene standard (83% yield). ^{1}HNMR (300 MHz, 295 K, C_6D_6) δ 7.87 (d, *J* = 8.8 Hz, 1H, –CHNPh), 7.25 – 6.98 (m, 5H, Ar H), 6.64 – 6.45 (m, 1H, –CH=CHCH$_3$), 5.87 (m, 1H, –CH=CHCH$_3$), 1.49 (d, *J* = 6.8 Hz, 3H, CH$_3$).

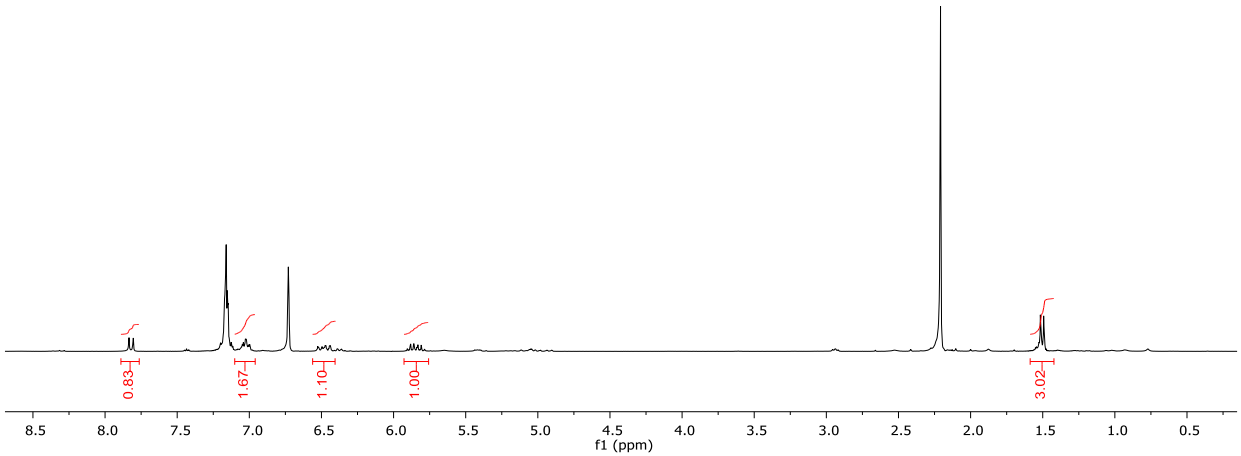

Figure 1.25. ^{1}HNMR spectrum for the catalytic rearrangement of *N*-phenyl cyclopropanecarboxaldimine (contains a mesitylene standard). (C_6D_6)

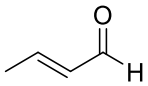

Catalytic Rearrangement of **19**. In an N_2-filled glove-box, cyclopropanecarboxaldehyde **19** (4.4 mg, 0.063 mmol), mesitylene (7.6 mg, 0.063 mmol), and [$^{i\text{-}Pr}$NDI]$Ni_2(C_6H_6)$ (5 mg, 0.0063 mmol, 10 mol%) were dissolved in C_6D_6 (0.5 mL), and the solution was loaded into an NMR tube equipped with a J. Young valve. The reaction mixture was allowed to react at 40 °C for 24 h, and the yield of **20** was determined by ^{1}HNMR integration against the mesitylene standard (80% yield). ^{1}HNMR (300 MHz, 295 K, $CDCl_3$) δ 9.27 (d, *J* = 6.7 Hz, 1H, –CHO), 6.03 – 5.77 (m, 2H, CH=CH), 1.30 (d, *J* = 5.4 Hz, 3H, CH_3).

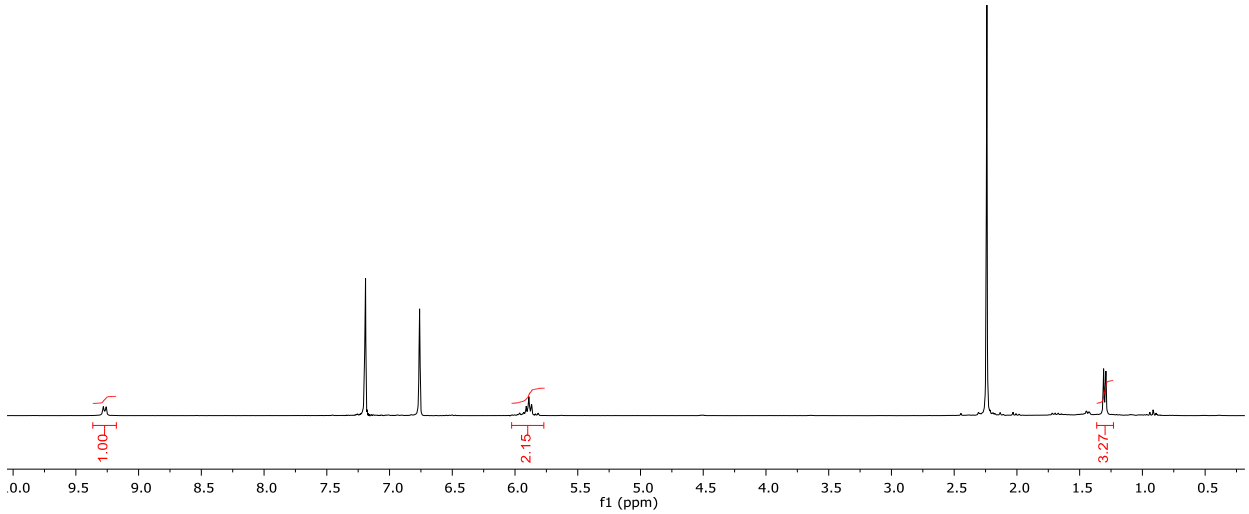

Figure 1.26. ^{1}H NMR spectrum for the catalytic rearrangement of cyclopropanecarboxaldehyde (contains a mesitylene standard). (C_6D_6)

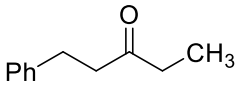

Catalytic Rearrangement of **21**. In an N_2-filled glove-box, 1-phenethylcyclopropan-1-ol[50] (**21**) (4.4 mg, 0.027 mmol), mesitylene (3.3 mg, 0.027 mmol), and [$^{i\text{-}Pr}$NDI]$Ni_2(C_6H_6)$ (2 mg, 0.0027 mmol, 10 mol%) were dissolved in C_6D_6 (0.5 mL), and the solution was loaded into an NMR tube equipped with a J. Young valve. The reaction mixture was allowed to react at 80 °C for 8 h, and the yield of **22**[51] was determined by ^{1}HNMR integration against the mesitylene standard (86% yield). ^{1}HNMR (400 MHz, 295 K, $CDCl_3$) δ 7.32 – 7.24 (m, 2H, Ar H), 7.19 (m, 3H, Ar H), 2.90 (t, *J* = 7.6 Hz, 2H, CH_2), 2.74 (t, *J* = 7.7 Hz, 2H, CH_2), 2.40 (q, *J* = 7.3 Hz, 2H, –CH_2CH_3), 1.04 (t, *J* = 7.3 Hz, 3H, –CH_2CH_3).

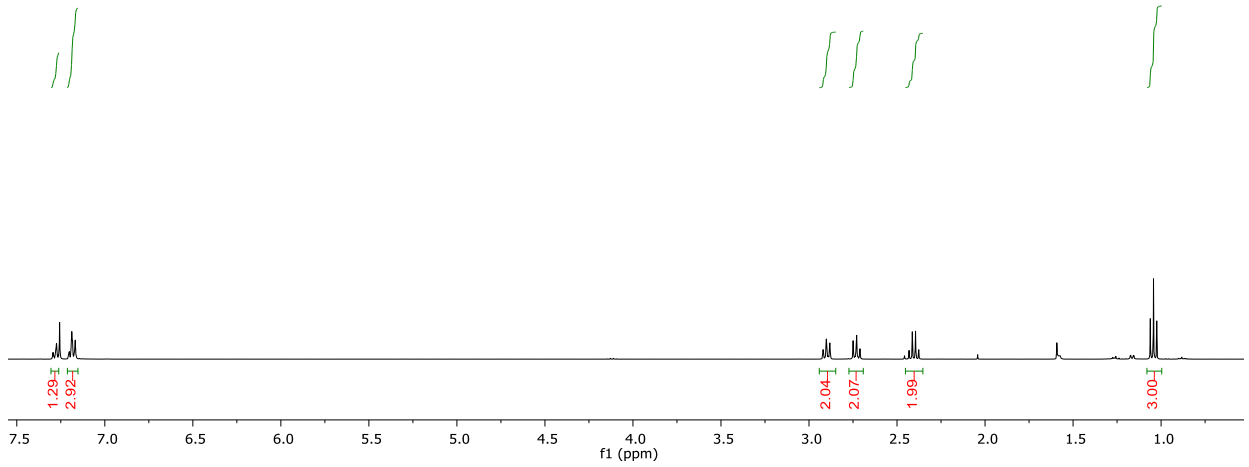

Figure 1.27. ^{1}HNMR for isolated 1-phenyl-3-pentanone. ($CDCl_3$)

1.3 Dinuclear Transformations of Vinylaziridines

1.3.1 Introduction

Aziridines are heterocyclic, strained, three-membered rings that are known to undergo a variety of useful transformation in organic synthesis. They are commonly used in installing nitrogen-containing heterocycles in natural product synthesis because of their ability to exhibit rapid ring-opening. Remarkably, aziridines have a ring strain (27 kcal/mol) close to that of cyclopropanes (29 kcal/mol).[7, 52]

More specifically, vinylaziridines can take part in various transformations incuding nucleophilic ring opening, 1,3-sigmatropic rearrangements, and cycloadditions.[2, 53-54] Cunha et. al. examined the effects of using different *n*-butyl organometallic reagents to mechanistically probe the product selectivity for nucleophilic ring-opening of acyclic and cyclic vinylaziridines (Figure 1.28a).[43] Formation of the 1,3-sigmatropic rearrangement product, pyrroline, was exhibited by Mack and Njardarson when subjecting 1-tosyl-2-vinylaziridine to catalytic amounts of $Cu(hfacac)_2$ and $Zn(hfacac)_2$ when heating at 80°C (Figure 1.28b).[55]

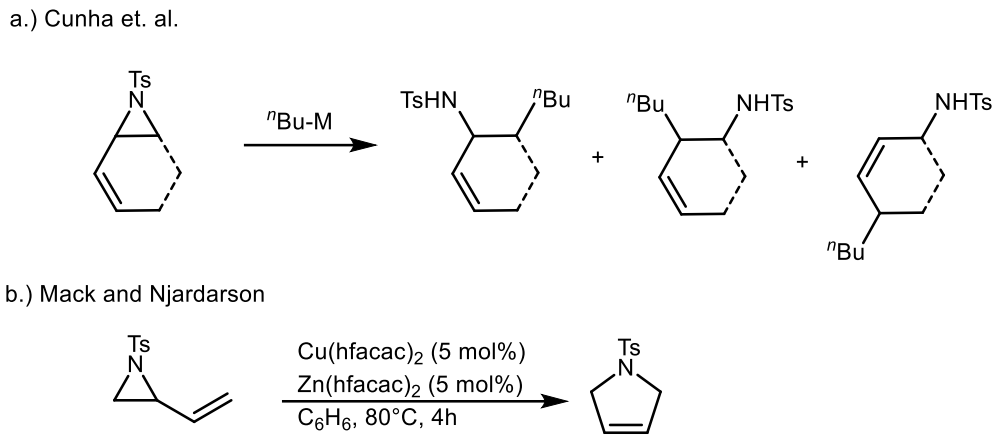

Figure 1.28. Nucleophilic ring opening and 1,3-sigmatropic rearrangment of vinylaziridines.

Many examples of cycloaddition reactions of vinylaziridines with isocyanates, nitriles, and carbon dioxide are present in the literature.[52] Among the most intriguing are reactions between carbon monoxide and vinylaziridines to form lactams. Carbon monoxide insertion into aziridines has been studied intensely with various transition metals.[2, 56] Using catalytic amounts of $[Rh(CO)_2Cl]_2$, Alper's group was able to form β-lactams from vinylaziridines and CO. Ohfune's group demonstrated CO insertion can take place into substituted vinylaziridines in the presence of $Pd_2(dba)_3$•$CHCl_3$ (Figure 1.29a).[57] A very intriguing example was reported by Aggarwal et. al. in which the selectivity of β-lactam formation over δ-lactam formation was governed by two factors: 1.) Higher pressures of CO were selective for the formation of the β-lactam, while lower pressures favored δ-lactam formation, and 2.) in the presence of the -TMS group, CO insertion preferentially took place adjacent to Si (Figure 1.29b).[58-59]

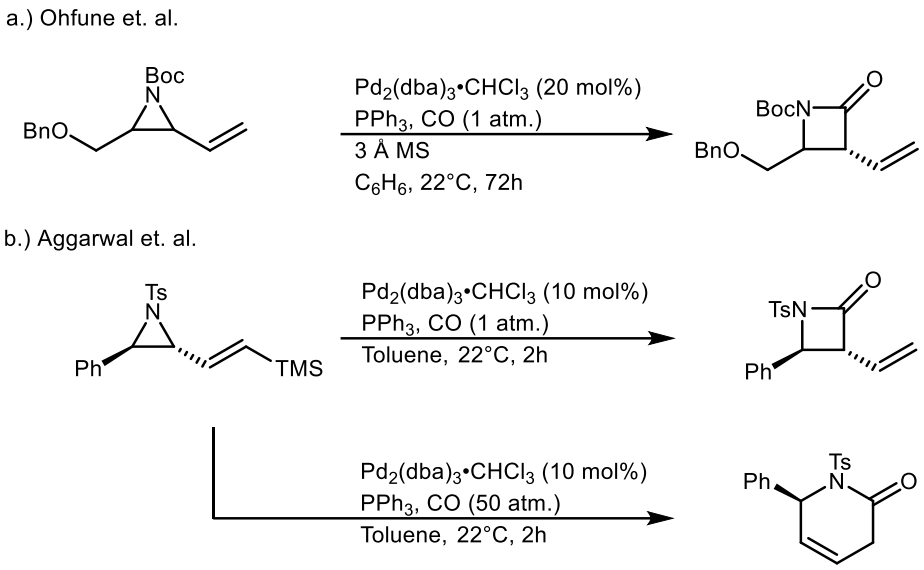

Figure 1.29. Formation of β-lactams from vinylaziridines and CO.

1.3.2 Results and Discussion

1.3.2.1 Formation of δ-lactam through Complex **2**.

We previously observed that an oxidative addition reaction occurs between 1-tosyl-2-vinylaziridine with the dinuclear complex [$^{i\text{-}Pr}$NDI]$Ni_2(C_6H_6)$.We started our investigation with heating complex **2** at 40°C for 12 hours in which the reaction mixture changes from a dark green to dark purple. We expected to form the rearranged pyrroline product but interestingly an oxidative transfer reaction takes place to form 1,3-butadiene and a new bimetallic nickel complex that contains the hetero-atom abstracted portion of vinylaziridine (Figure 1.30).

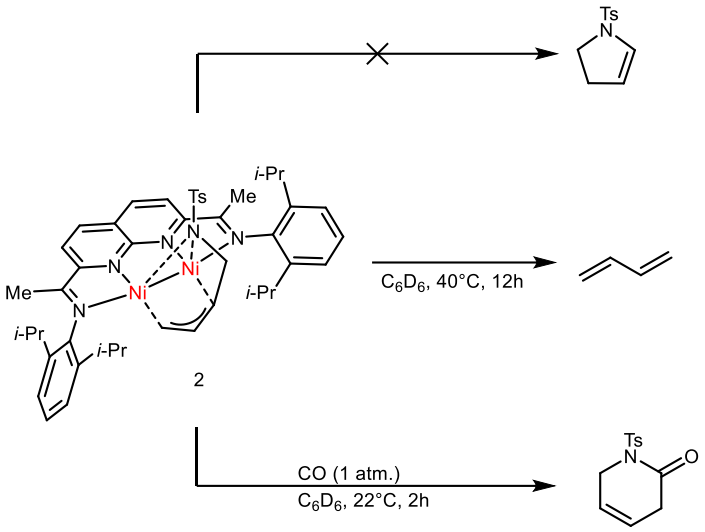

Figure 1.30. Heating complex **2** generates 1,3-butadiene as an organic product.

Focusing efforts toward the reductive elimination of the organic fragment from vinylaziridine we decided to start with carbon monoxide. Insertion of carbon monoxide into vinylaziridines to form ring-expanded β- and δ-lactams are known to form in the presence of various transition metals.[58, 60-64] In the presence of CO (1 atm) complex **2** immediately starts to decompose and change color from dark green to light brown. This indicates the decomposition of complex **2** to form $Ni(CO)_4$, free $^{i\text{-}Pr}$NDI, and a reductively eliminated product, 1-tosyl-3,6-dihydropyridin-2(1H)-one (Figure 1.30).

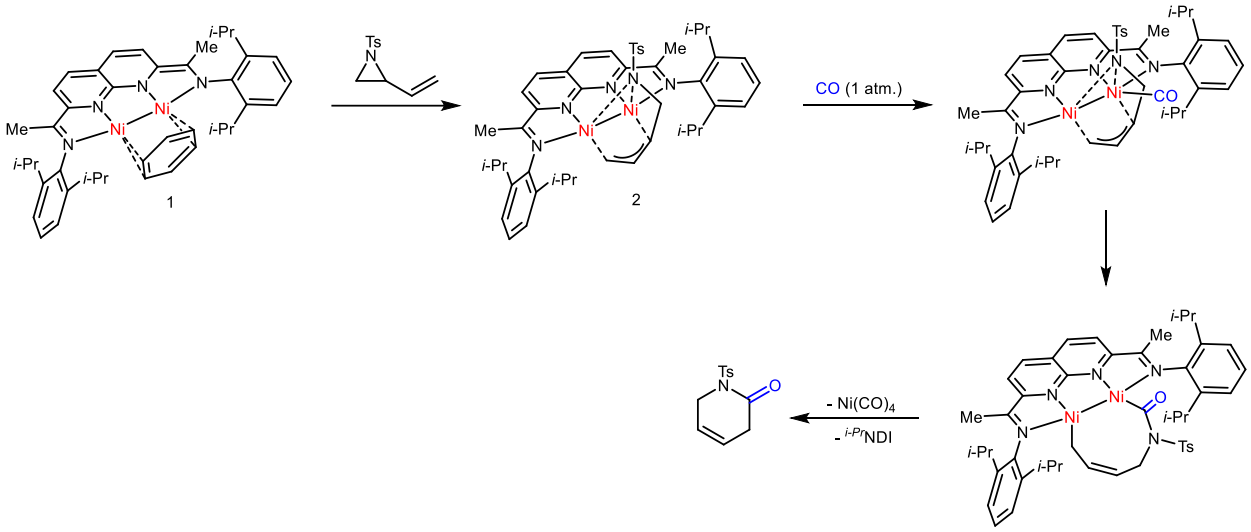

Figure 1.31. Proposed mechanism of CO insertion to give δ-lactam from complex **2**.

A proposed mechanism towards the formation of 1-tosyl-3,6-dihydropyridin-2(1H)-one from complex **2** is described (Figure 1.31). The oxidative addition of vinylaziridine to complex **1** forms the isolated complex **2** which was previously characterized by XRD. In the presence of 1 atm. of CO, it is probable that a molecule of CO will first bond to one of the Ni centers and then insert into the Ni-N bond to form a transient intermediate. Next, due to the excess CO and the low thermodynamic barrier to form $Ni(CO)_4$, reductive elimination takes place to form the δ-lactam and free ligand ($^{i\text{-}Pr}$NDI).

1.3.2.2 Formation of δ-lactam through Complex **4**.

We previously described the formation of the oxidative addition product between complex **3** and 1-tosyl-2-vinylaziridine to form complex **4**. Similar to the reaction studies with the dinuclear complex **2** we wanted to explore reactivity. However, there is some difference in reactivity between the mononuclear system complex **4** and the dinuclear C-N oxidative addition complex **2**. Unlike complex **2** which gave 1,3-butadiene as a product from an oxidative transfer reaction, the same set of conditions gave no reaction with complex **4**. Increasing the heating from 40°C to 80°C also gave no product.

Using our previous strategy, we decided to use CO to reductively eliminate the organic fragment from the complex. Interestingly, we observed very similar reactivity in the mononuclear system compared to the dinuclear system. Reaction of complex **3** with 1-tosyl-2-vinylaziridine gave an immediate color change from dark purple to blue. Subsequent treatment with CO causes the color to change from blue to light brown which indicates decomposition of complex **4** to form δ-lactam 1-tosyl-3,6-dihydropyridin-2(1H)-one, $Ni(CO)_4$, and free $^{i\text{-}Pr}$IP (Figure 1.32).

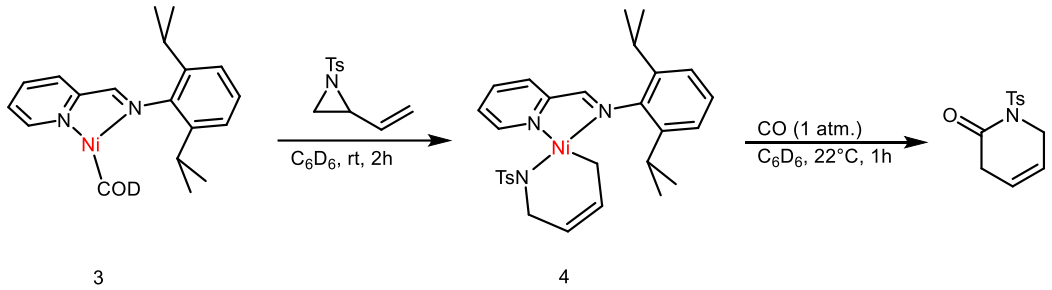

Figure 1.32. Formation of δ-lactam from complex **4**.

The mechanism for the synthesis of 1-tosyl-3,6-dihydropyridin-2(1H)-one with [$^{i\text{-}Pr}$IP]Ni(COD) most likely proceeds in a similar manner to the dinuclear proposed pathway (Figure 1.33). Complex **4** is formed from oxidative addition of 1-tosyl-2-vinylaziridine to complex **3**. Carbon monoxide is introduced to complex **4** in which an Ni-CO bond is formed, and migratory insertion of CO into the Ni-N bond takes place. Subsequent reductive elimination proceeds to form δ-lactam 1-tosyl-3,6-dihydropyridin-2(1H)-one as the only product.

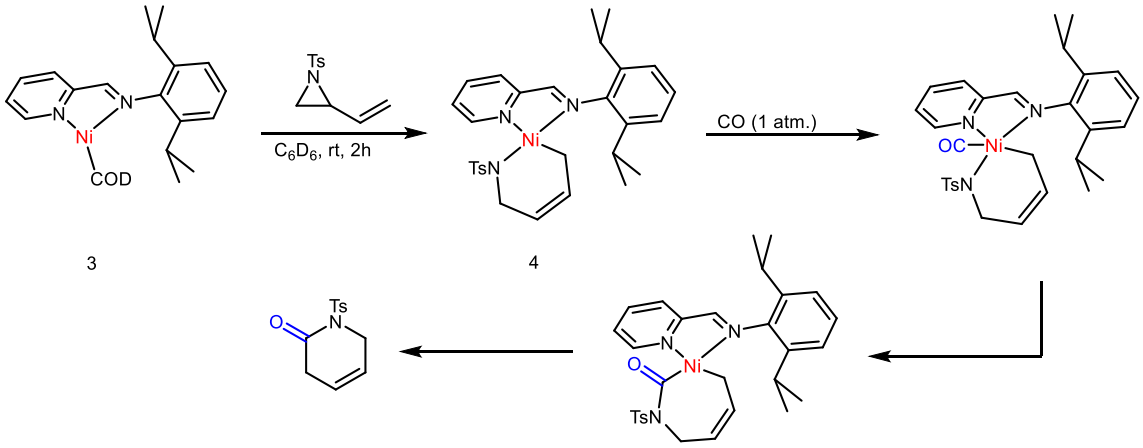

Figure 1.33. Proposed mechanism of monometallic formation of the δ-lactam.

1.3.2.3 Stoichiometric Aziridine Ring Opening

Observing oxidative addition and breaking of the C-N bond of vinylaziridines we wanted to explore the effects of changing the protecting group on the nitrogen. We started our exploration by synthesizing 1-phenyl-2-vinylaziridine and reacting with complex **1** at room temperature for 30 minutes to give a diamagnetic, dark green complex (Figure 1.34). The Ni-Ni bond distance of complex **5** is relatively unchanged from that of complex **1**, 2.496(1) Å, and very similar to that of complex **2**, 2.4600(8) Å. Due to the similarity of the bond metrics of complex **5** to complex **2** we can conclude that the electrons required for oxidative addition are coming from the π-system of the ligand and not from the Ni metal pair. One major difference between complex **5** and complex **2** are the Ni-N bond distances. The two Ni-N bonds of complex **5** are about equal at 2.046(2) Å and 2.052(2) Å while in complex **2** Ni-N bond is shorter than the other at 2.149(3) Å and 2.083(3) Å.

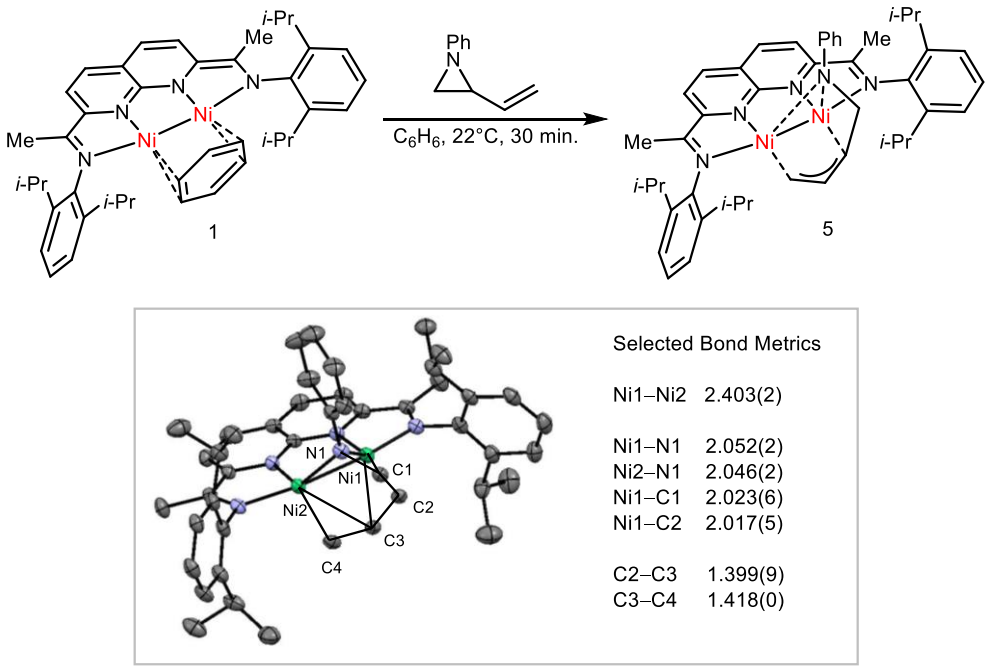

Figure 1.34. Generation of complex **5** gives dark green crystalline solid.

1.3.2.4 Formation of β-lactam through Complex **5**.

Due to the similar mode of binding of 1-phenyl-2-vinylaziridine to [$^{i\text{-}Pr}$NDI]$Ni_2(C_6H_6)$ as 1-tosyl-2-vinylaziridine, we wanted to explore the reactivity profile of complex **5**. More specifically, we wanted to determine if there was a difference in reactivity when substituting the protecting group on the nitrogen from a tosyl group to a phenyl substituent. Complex **5** was generated *in situ* at room temperature for 30 minutes after which an atmosphere of carbon monoxide was introduced. Immediate decomposition of the complex took place in which the dark green solution turned dark brown. A reductive elimination took place in which the CO inserted product was released from the metal fragment and identified as 1-phenyl-3-vinylazetidin-2-one (Figure 1.35).

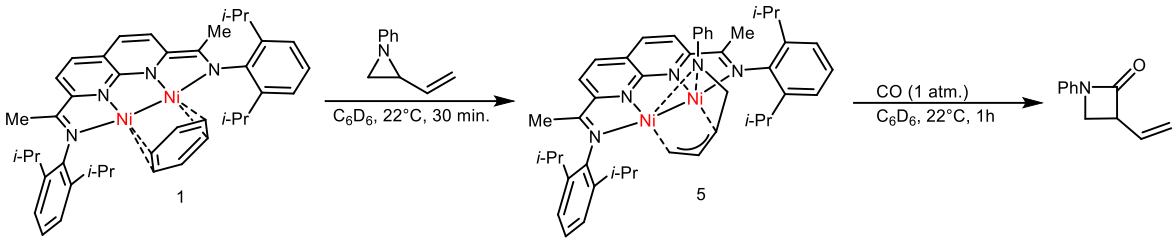

Figure 1.35. Treatment of complex **5** yields 1-phenyl-3-vinylazetidin-2-one.

It is noteworthy to address the reactivity differences between vinylaziridines bearing a tosyl or phenyl group off the nitrogen. One obvious difference is the change in electronics. Tosyl groups are electron-withdrawing groups while phenyl substituents are electron-donating. Heating complex **2** at 40°C results in the formation of hetero-atom abstraction and the production of butadiene. In contrast, heating complex **5** to 40°C results in no reaction and higher temperatures are required for a reaction to take place. This suggests the energy required for reductive elimination to form pyrroline or the β-hydride eliminated product is higher than that to abstract -NTs.

The energy barrier of product formation could be used to explain the differences in complex stability and the reasoning behind the formation of the δ-lactam versus the β-lactam. The δ-lactam could form from a simple decomposition of complex **2** in which CO binds to Ni and migration of CO from one of the Ni centers into the aziridine fragment. Lastly, reductive elimination takes place to form the thermodynamically favorable product. In contrast, reductive elimination of the aziridine fragment from complex **5** can be achieved by heating at 80°C for 24 hours. We can infer the energy barrier for hetero-atom abstraction is too high, so formation of pyrroline takes place.

The difference in activity between 1-tosyl-2-vinylaziridine and 1-phenyl-2-vinylaziridine is intriguing and would be worth investigating by DFT calculations. Other experiments that could be useful in determining the mechanistic difference are to change the protecting group on the nitrogen and expanding the substrate scope to include more substitutions on vinylaziridine. Efforts were made in trying to turn over the CO insertion reactions with both tosyl- and phenyl-substituted aziridines but no promising results were obtained. The CO sources used were phenylformate and $M_x(CO)_y$ where M = iron, cobalt, manganese, chromium, and molybdenum.

1.3.3 Experimental

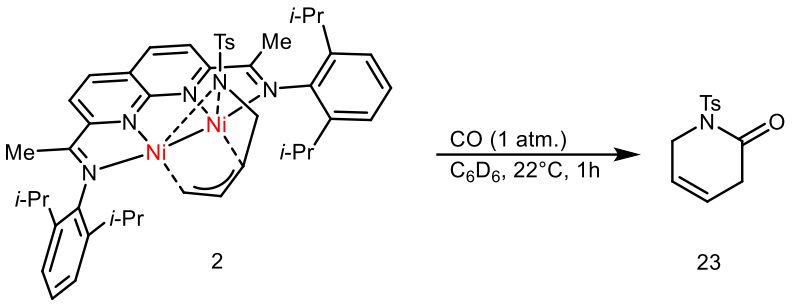

Stoichiometric generation of 1-tosyl-3,6-dihydropyridin-2(1H)-one (**23**) by [$^{i\text{-}Pr}$NDI]$Ni_2(C_6H_6)$. In an N_2-filled glove-box, 1-tosyl-2-vinylaziridine (3.1 mg, 0.014 mmol, 1 equiv.) and [$^{i\text{-}Pr}$NDI]$Ni_2(C_6H_6)$ (10 mg, 0.0014 mmol, 1 equiv.) were dissolved in C_6D_6 (0.5 mL), and the solution was loaded into an NMR tube equipped with a J. Young valve. The reaction mixture was allowed to react at 22 °C for 1 h and allowed to react for 30 minutes. At this time, the tube was placed under an atmosphere of CO (1 atm.) and allowed to react for 1 hour. The yield of **23** was determined by ^{1}HNMR integration against the mesitylene standard (98% yield). ^{1}H NMR (300 MHz, $CDCl_3$) δ 7.94 (d, *J* = 8.3 Hz, 1H), 7.32 (d, *J* = 8.1 Hz, 2H), 5.94 – 5.80 (m, 1H), 5.80 – 5.67 (m, 1H), 4.62 – 4.45 (m, 2H), 3.01 (tq, *J* = 3.8, 1.7 Hz, 2H), 2.44 (d, *J* = 7.1 Hz, 4H). ^{13}C NMR (126 MHz, $CDCl_3$) δ 167.29, 145.03, 135.74, 129.31, 128.86, 127.37, 121.44, 120.94, 77.26, 77.01, 76.75, 47.54, 34.09, 29.70, 21.69.

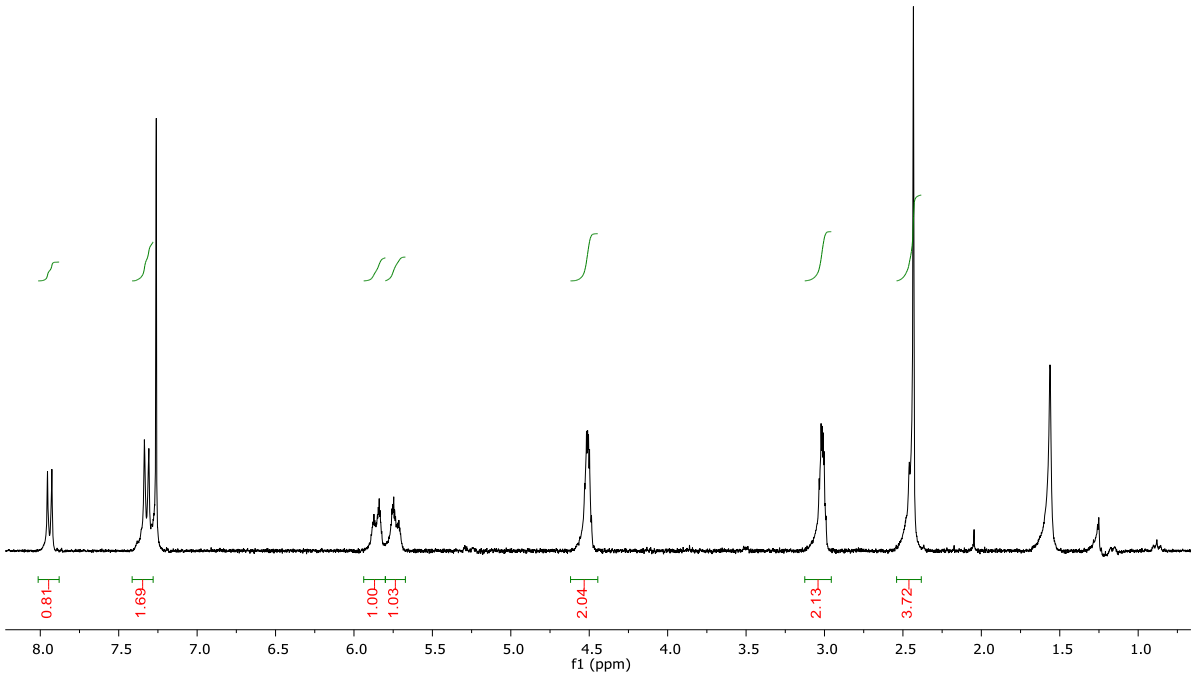

Figure 1.36. ^{1}HNMR for isolated 1-tosyl-3,6-dihydropyridin-2(1H)-one (**23**). ($CDCl_3$)

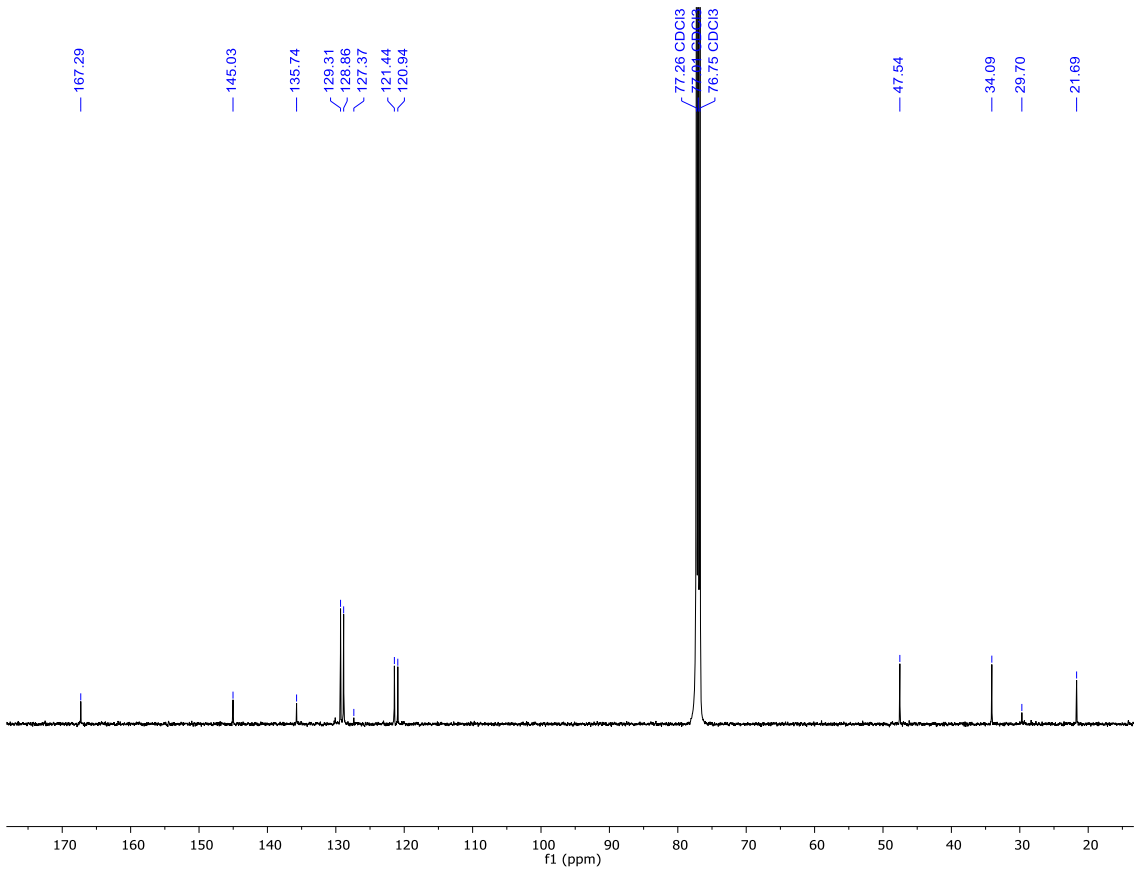

Figure 1.37. ^{13}C {^{1}H} NMR for isolated 1-tosyl-3,6-dihydropyridin-2(1H)-one (**23**). ($CDCl_3$)

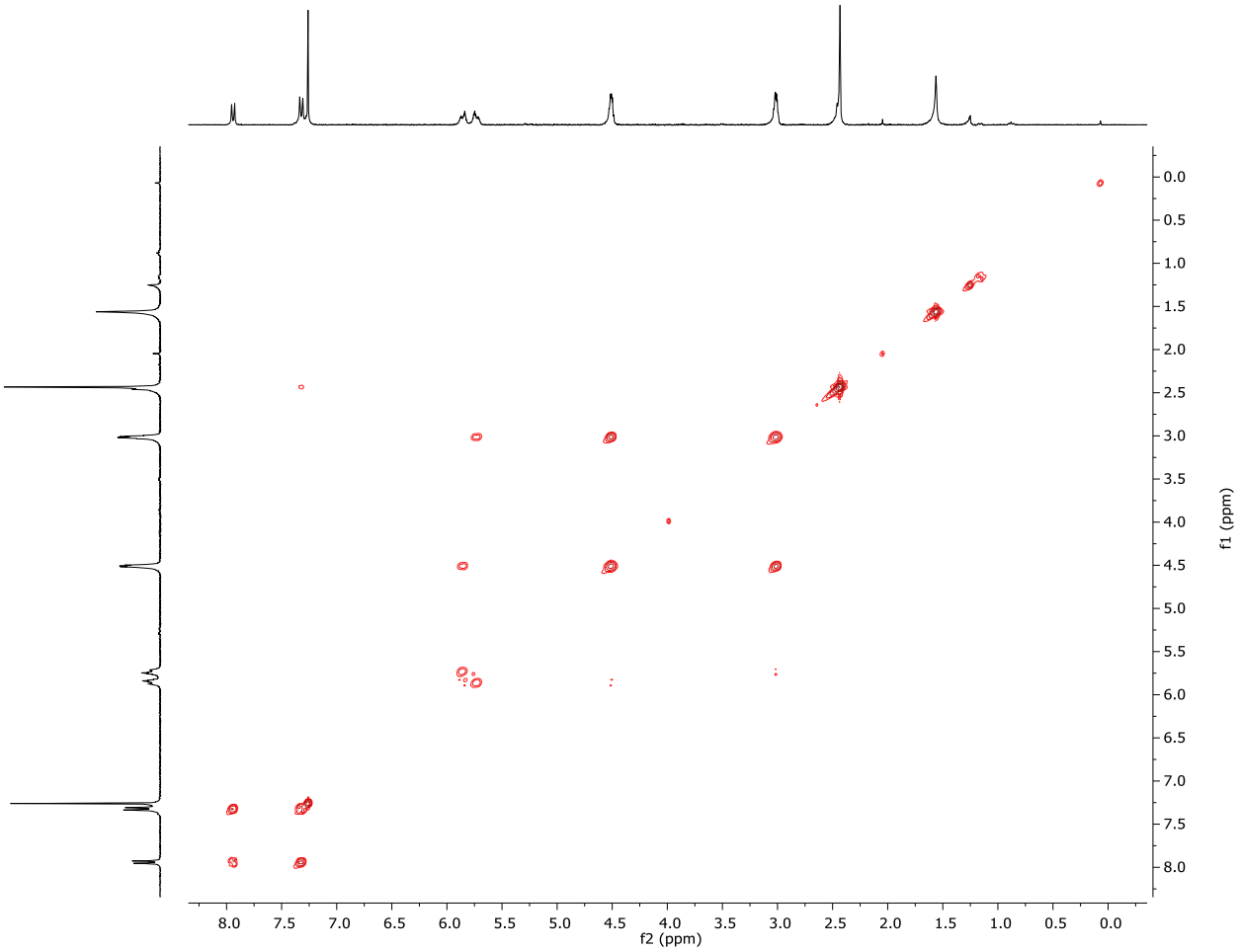

Figure 1.38. COSY for isolated 1-tosyl-3,6-dihydropyridin-2(1H)-one (**23**). ($CDCl_3$)

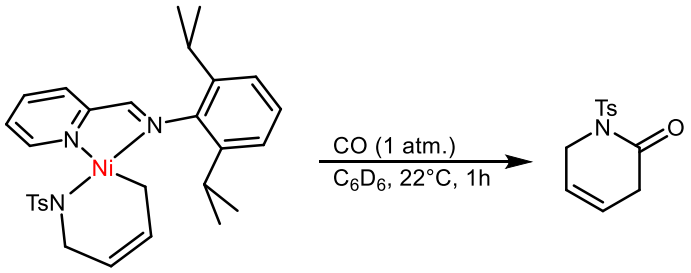

4 23

Stoichiometric generation of 1-tosyl-3,6-dihydropyridin-2(1H)-one (**23**) by [$^{i\text{-}Pr}$IP]Ni(COD). In an N_2-filled glove-box, 1-tosyl-2-vinylaziridine (3 mg, 0.014 mmol, 1 equiv.) and [$^{i\text{-}Pr}$IP]Ni(COD) (6 mg, 0.014 mmol, 1 equiv.) were dissolved in C_6D_6 (0.5 mL), and the

solution was loaded into an NMR tube equipped with a J. Young valve. The reaction mixture was allowed to react at 22 °C for 1 h and allowed to react for 2 hours. At this time, the tube was placed under an atmosphere of CO (1 atm.) and allowed to react for 1 hour. The yield of **23** was determined by ^{1}HNMR integration against the mesitylene standard (92% yield). ^{1}H NMR (300 MHz, $CDCl_3$) δ 7.94 (d, *J* = 8.3 Hz, 1H), 7.32 (d, *J* = 8.1 Hz, 2H), 5.94 – 5.80 (m, 1H), 5.80 – 5.67 (m, 1H), 4.62 – 4.45 (m, 2H), 3.01 (tq, *J* = 3.8, 1.7 Hz, 2H), 2.44 (d, *J* = 7.1 Hz, 4H). ^{13}C NMR (126 MHz, $CDCl_3$) δ 167.29, 145.03, 135.74, 129.31, 128.86, 127.37, 121.44, 120.94, 77.26, 77.01, 76.75, 47.54, 34.09, 29.70, 21.69.

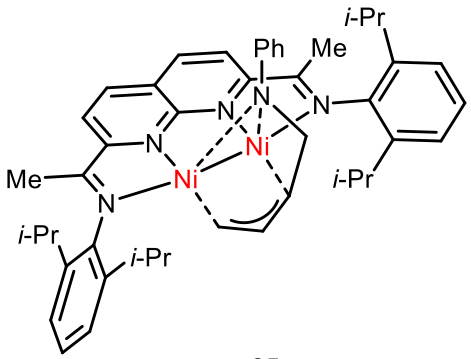

25

In a 20-mL vial, [$^{i\text{-}Pr}$NDI]$Ni_2(C_6H_6)$[42] (20 mg, 0.027 mmol, 1.0 equiv) and 1-phenyl-2-vinylaziridine (**24**) [65] (4 mg, 0.027 mmol, 1.0 equiv) were dissolved in C_6H_6 (5 mL). The solution was observed to undergo an immediate color change from red-brown to green. After stirring at ambient temperature for 30 min, the reaction mixture was filtered through a glass fiber pad, and the filtrate was concentrated to dryness under reduced pressure. Single crystals suitable for XRD were obtained by cooling saturated solutions of **25** in Et_2O to –30 °C in a glovebox freezer. ^{1}H NMR (300 MHz, C_6D_6) δ 8.24 (s, 1H), 7.47 – 7.35 (m, 4H), 7.31 – 7.21 (m, 10H), 7.02 – 6.83 (m, 6H), 6.64 (d, *J* = 8.3 Hz, 1H), 6.11 – 5.83 (m, 5H), 4.19 (d, *J* = 8.0 Hz, 1H), 3.96 – 3.72 (m, 2H), 3.03 – 2.83 (m, 1H), 2.83 – 2.63 (m, 1H), 1.81 (s, 4H), 1.56 – 1.12 (m, 23H), 1.09 – 0.60 (m, 25H), 0.31 (s, 1H).

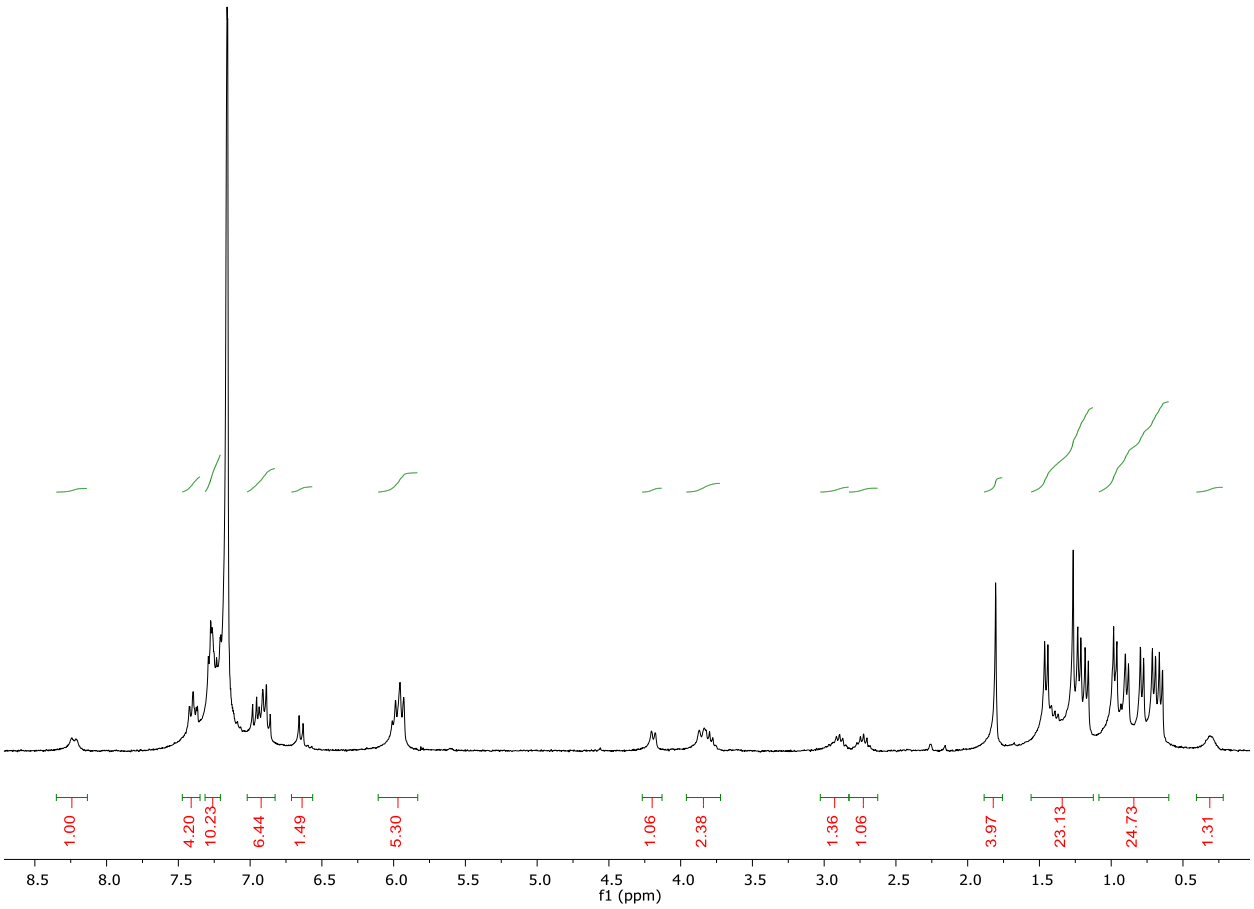

Figure 1.39. ^{1}HNMR for complex **25**. (C_6D_6)

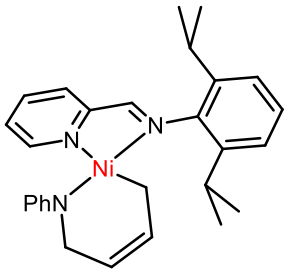

26

In a 20-mL vial, [$^{i\text{-}Pr}$IP]Ni(COD) (**3**)[44] (6 mg, 0.014 mmol, 1.0 equiv) and 1-phenyl-2-vinylaziridine (**24**) (2 mg, 0.014 mmol, 1.0 equiv) were dissolved in THF (5 mL). The solution was observed to undergo a gradual color change from purple to blue. After 2 h, the reaction

mixture was filtered through a glass fiber pad, and the filtrate was concentrated to dryness under reduced pressure. Single crystals suitable for XRD were obtained by cooling saturated solutions of **26** in Et_2O to –30 °C in a glovebox freezer. ^{1}H NMR (300 MHz, $CDCl_3$) δ 9.04 – 8.93 (m, 1H), 7.84 (s, 1H), 7.65 (s, 2H), 7.47 – 7.31 (m, 3H), 7.20 – 7.10 (m, 4H), 6.78 – 6.65 (m, 2H), 6.46 (dq, *J* = 7.5, 4.1 Hz, 3H), 5.76 – 5.55 (m, 5H), 2.37 – 2.17 (m, 10H), 1.38 (dd, *J* = 6.9, 4.5 Hz, 10H), 1.01 (d, *J* = 5.3 Hz, 9H).

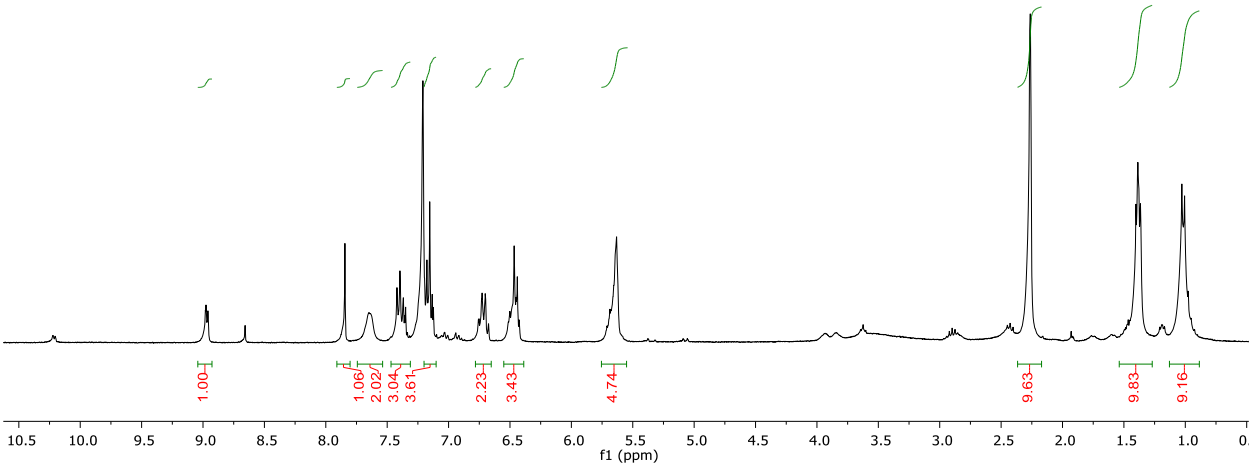

Figure 1.40 ^{1}HNMR for isolated complex **26**. ($CDCl_3$)

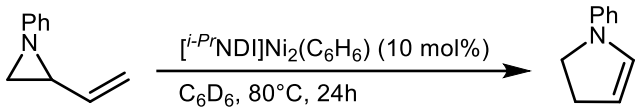

24 27

Catalytic Rearrangement of 1-phenyl-2-vinylaziridine (**24**). In an N_2-filled glove-box, 1-phenyl-2-vinylaziridine (**24**) (3.9 mg, 0.027 mmol) and [$^{i\text{-}Pr}$NDI]$Ni_2(C_6H_6)$ (**1**) (3.3 mg, 0.027 mmol, 10 mol%) were dissolved in C_6D_6 (0.5 mL), and the solution was loaded into an NMR tube equipped with a J. Young valve. The reaction mixture was allowed to react at 80 °C for 24 h. The crude mixture was directly loaded on to a SiO_2 column for purification (mobile phase: 20% EtOAc/Hexanes). 1-phenyl-2,3-dihydro-1H-pyrrole (**27**) was isolated in 96% yield (6.5 mg) as a white solid. ^{1}H NMR (300 MHz, $CDCl_3$) δ 7.21 – 7.12 (m, 1H), 7.12 – 7.04 (m, 2H), 6.90 (td, *J* = 7.4, 1.3 Hz, 1H), 6.82 (dd, *J* = 7.8, 1.3 Hz, 1H), 6.79 – 6.55 (m, 1H), 5.90 – 5.79 (m, 1H), 5.60 – 5.49 (m, 1H), 3.78 (dq, *J* = 4.3, 2.1 Hz, 2H), 3.49 (dd, *J* = 5.5, 2.1 Hz, 2H).

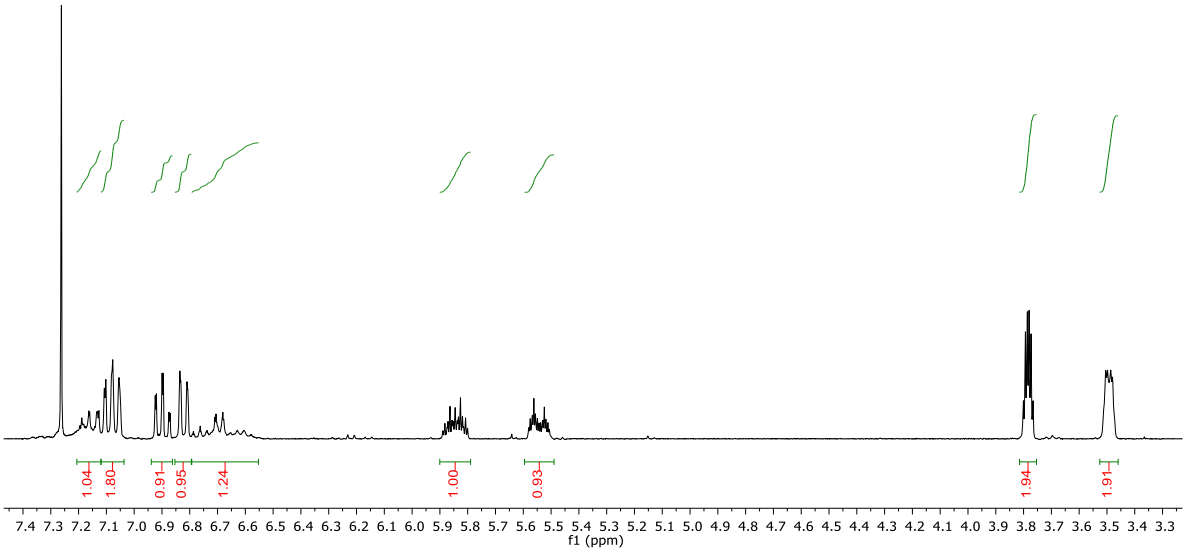

Figure 1.41. ^{1}HNMR for isolated 1-phenyl-2,3-dihydro-1H-pyrrole (**27**). ($CDCl_3$)

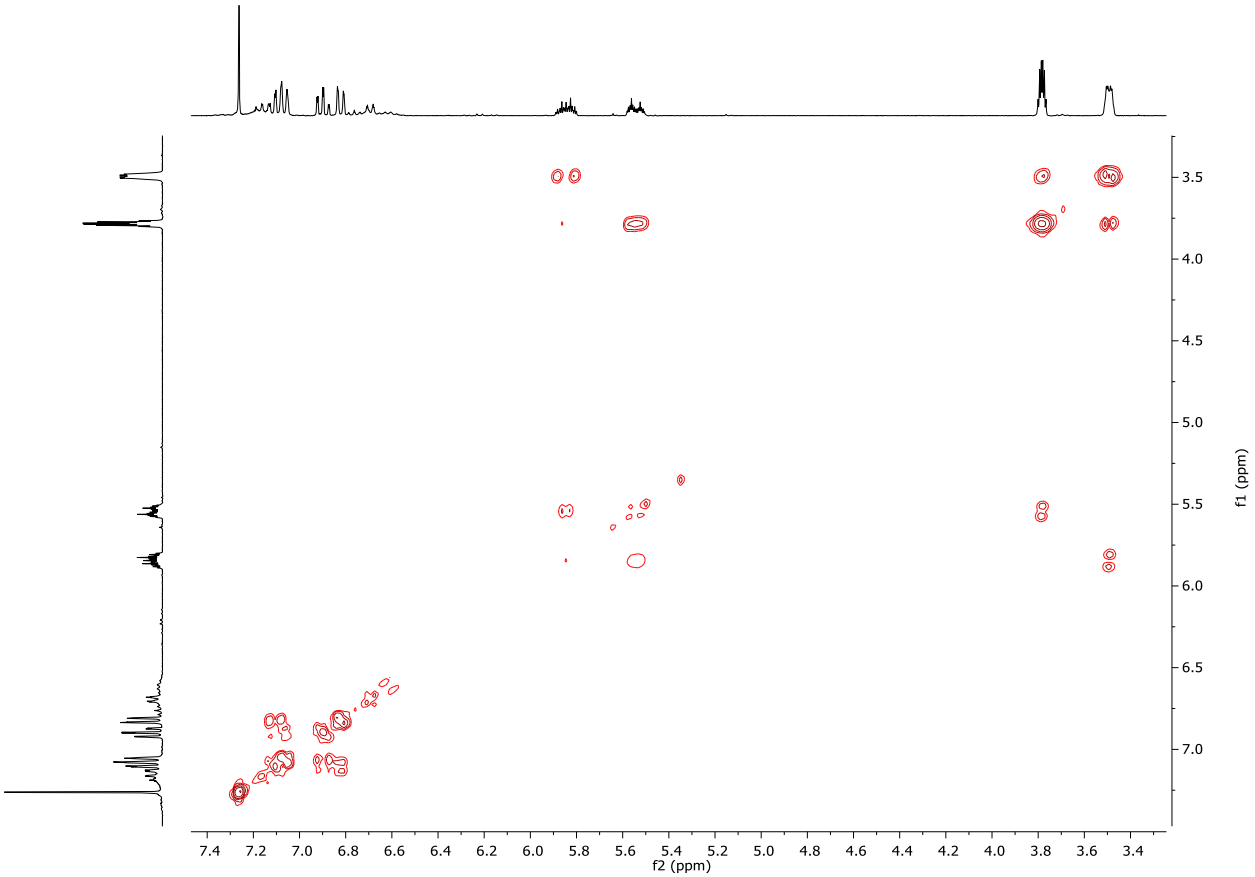

Figure 1.42. COSY for isolated 1-phenyl-2,3-dihydro-1H-pyrrole (**27**). ($CDCl_3$)

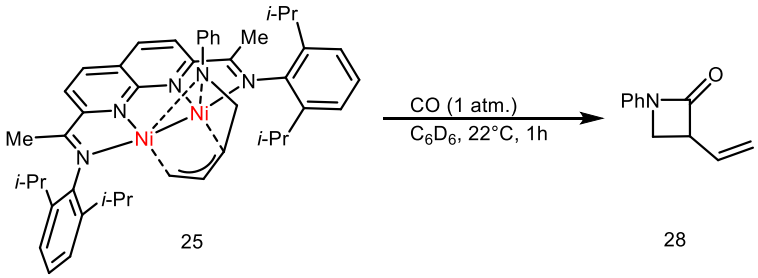

Stoichiometric generation of 1-phenyl-4-vinylazetidin-2-one (**28**). In an N_2-filled glove-box, [$^{i\text{-}Pr}$NDI]$Ni_2(C_6H_6)$ (**1**) (10 mg, 0.014 mmol, 1 equiv.), 1-phenyl-2-vinylaziridine (**24**) (2 mg, 0.014 mmol, 1 equiv.) were dissolved in C_6D_6 (0.5 mL), and the solution was loaded into an NMR tube equipped with a J. Young valve. The reaction mixture was allowed to react at 22 °C for 30 min. At this time, the green mixture was put under CO (1 atm) and allowed to react at

22°C for 1h. The crude mixture was directly loaded on to a SiO_2 column for purification (mobile phase: 25% EtOAc/Hexanes). 1-phenyl-3-vinylazetidin-2-one (**28**) was isolated in 80% yield (1.9 mg) as a white solid. ^{1}H NMR (500 MHz, $CDCl_3$) δ 7.41 – 7.31 (m, 4H), 7.14 – 7.07 (m, 1H), 6.03 – 5.92 (m, 1H), 5.39 (dt, *J* = 17.1, 1.3 Hz, 1H), 5.30 (dt, *J* = 10.3, 1.2 Hz, 1H), 3.99 (dddd, *J* = 7.3, 5.7, 2.7, 1.3 Hz, 1H), 3.86 (td, *J* = 5.8, 1.3 Hz, 1H), 3.51 (ddd, *J* = 5.8, 2.8, 1.3 Hz, 1H). ^{13}C NMR (126 MHz, $CDCl_3$) δ 131.50, 129.18, 124.01, 119.26, 116.35, 77.27, 77.02, 76.76, 52.52, 44.57.

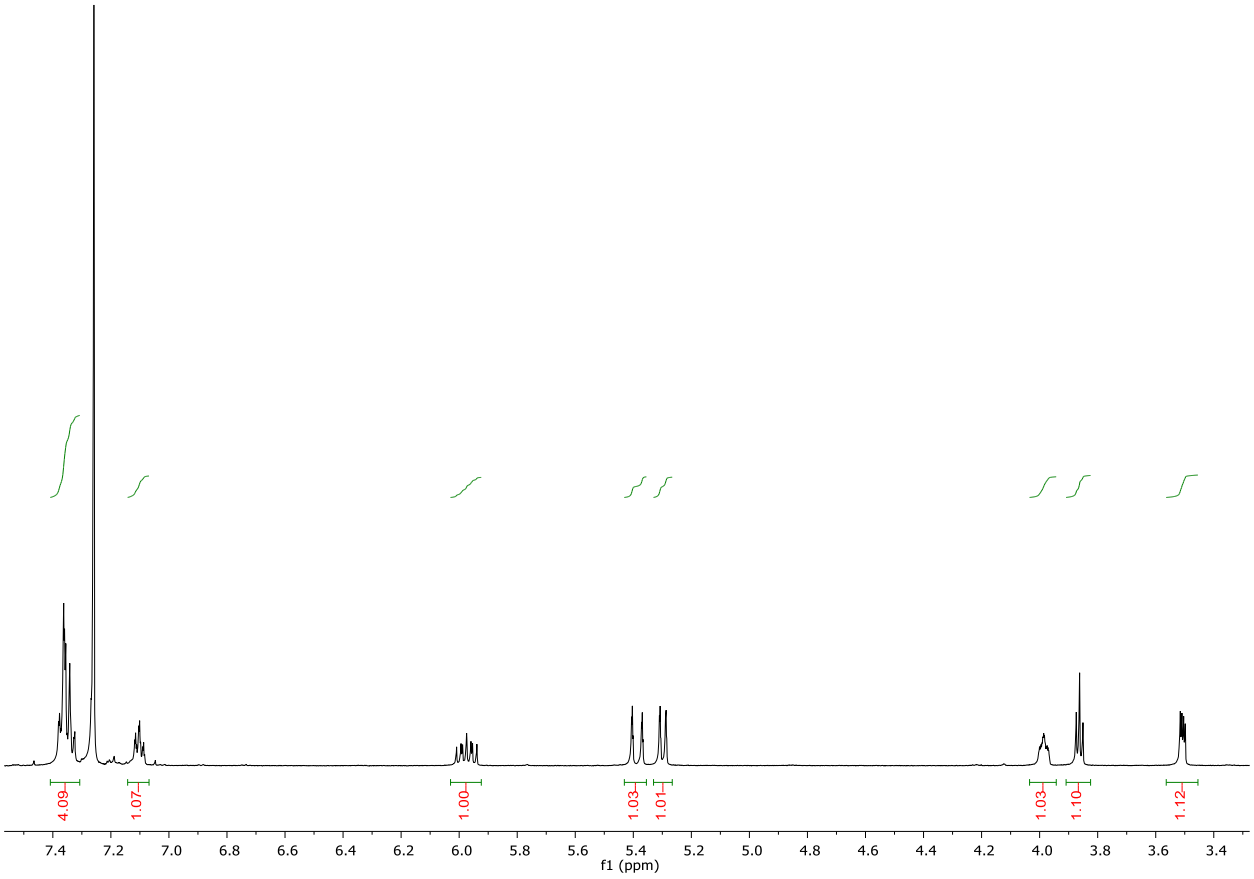

Figure 1.43. ^{1}HNMR for isolated 1-phenyl-4-vinylazetidin-2-one (**28**). ($CDCl_3$)

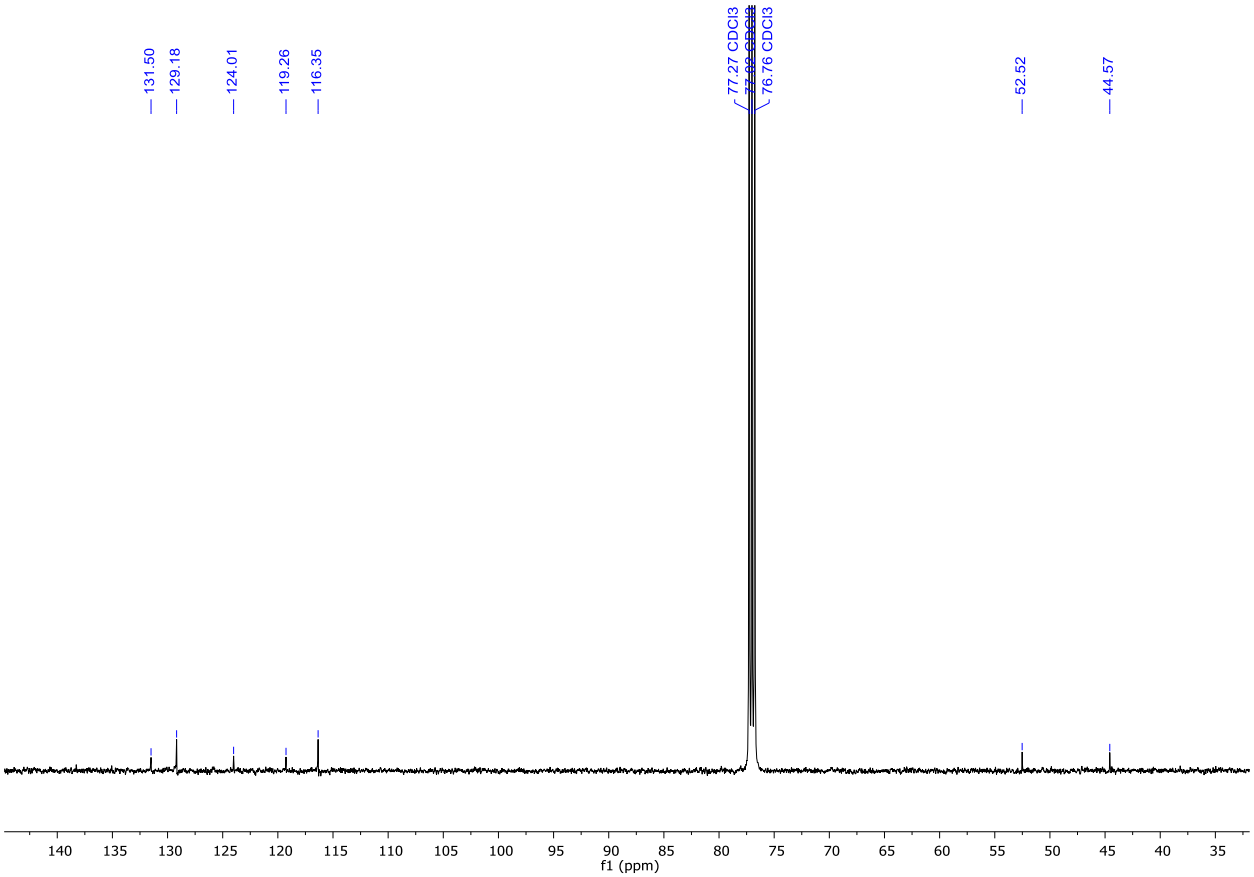

Figure 1.44. ^{13}C {^{1}H} NMR for isolated 1-phenyl-4-vinylazetidin-2-one (**28**). ($CDCl_3$)

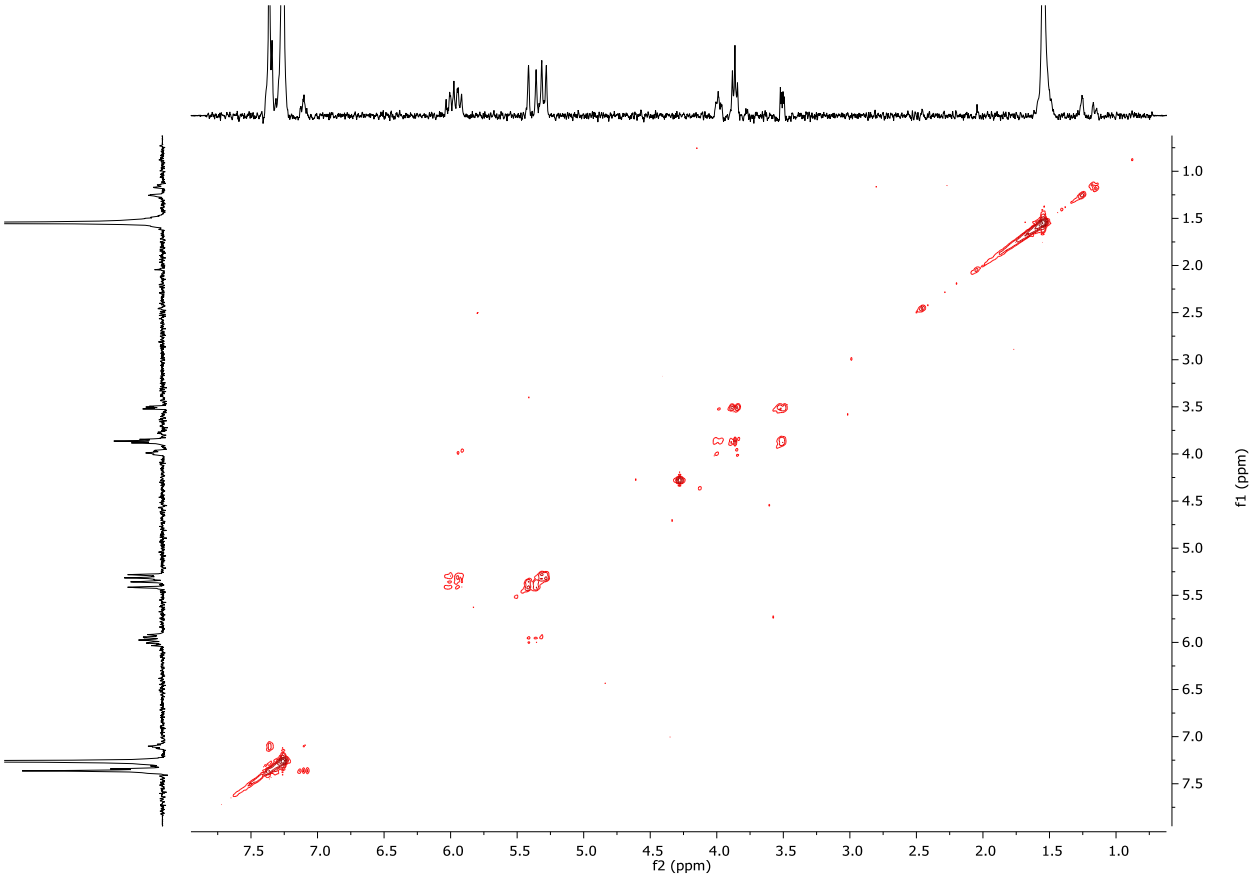

Figure 1.45. COSY for isolated 1-phenyl-4-vinylazetidin-2-one (**28**). ($CDCl_3$)

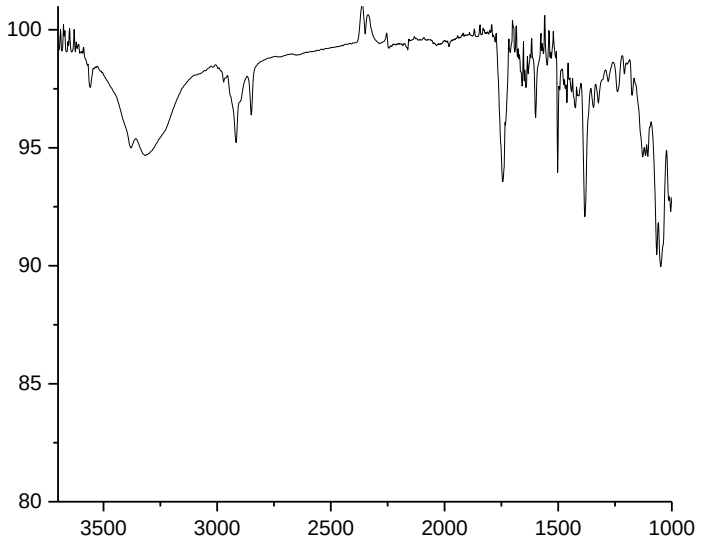

Figure 1.46. IR spectrum for isolated 1-phenyl-4-vinylazetidin-2-one (**28**). (THF)

CHAPTER 2. DINUCLEAR FACILITATED OXIDATIVE TRANSFER REACTIONS

2.1 Heteroatom-Abstraction of Three-Membered Rings

2.1.1 Introduction

The activation of strained, three-membered rings have demonstrated three common reaction pathways. They can undergo 1,3-sigmatropic rearrangement, oxidative addition to a metal to form a new metallacycle, or oxidative transfer of the hetero-atom to a metal. Oxidative transfer reactions can be exhibited by epoxides, aziridines, and thiiranes. When thinking about the reactivity benefits of oxidative transfer two general examples may come to mind. Strained rings containing hetero-atoms such as epoxides could be used as transient protecting groups for alkenes (Figure 2.1a). Another that has been exhibited in the literature is reductive ring contraction in which the hetero-atom, such as sulfur, is removed (Figure 2.1b).

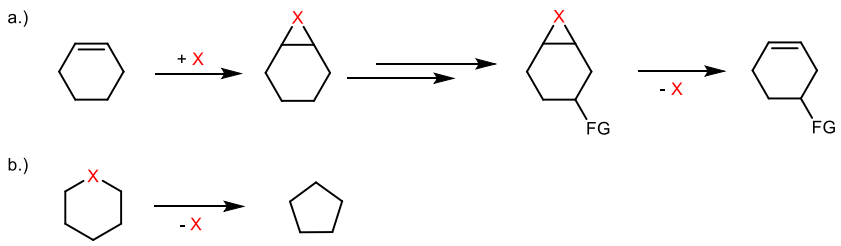

Figure 2.1. Oxidative transfer of hetero-atom containing substrates a.) used as transient protecting groups and b.) ring contraction.

Deoxygenation of epoxides can be thought of as the reverse reaction of the epoxidation of alkenes.[66] Most commonly, deoxygenation of epoxides occurs in the presence of transition metal carbonyl complexes but more recent advances have been demonstrated. A nice example of the synthetic utility of using epoxides as temporary protecting groups came out of a synthesis of triazole bisphosphonates[67] (Figure 2.2). Starting with an allylic alcohol and carrying the synthesis forward without the installation of the epoxide resulted in an allylic azide

rearrangement which gives an undesired product. To prevent this isomerization, an epoxide was installed in which the installation of the azide then subsequent removal of the epoxide afforded the desired isomer.

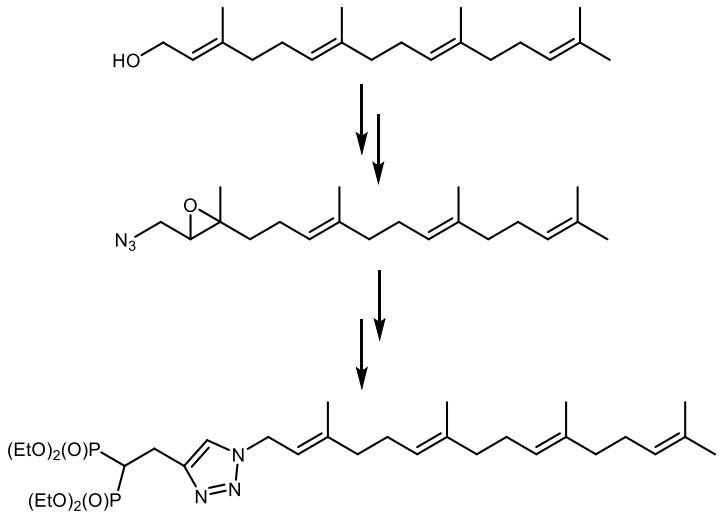

Figure 2.2. Installing an epoxide prevented the unwanted isomerization of the alkene.

Another very interesting and rare example came out of the Luh group. Synthesis and treatment of a thiopyran with a nickel (II) catalyst and excess Grignard reagent resulted in a rather surprising product (Figure 2.3).[68] A C-S bond activation in which the nickel inserts itself into the ring and then and interaction with the alkene fragment guides the reaction to form a nickel allyl complex. It is postulated another C-S bond activation takes place and the sulfur is quenched with an equivalent of Mg to form MgS and the ring closes to form a vinylcyclopropane.

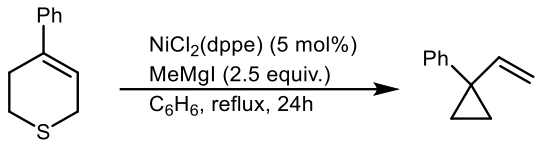

Figure 2.3. Ring contraction instead of the cross-coupling reaction occurred with unsaturated thiopyrans.

2.1.2 Results and Discussion

Strained, three-membered ring heterocycles are sometimes prone to oxidative transfer reactions instead of 1,3-sigmatropic rearrangements or other ring-opening reactions. Discussed in the previous chapter, we wanted to explore reactivity of complex **2**. We first set out by heating the complex **2** at 40°C for 24 hours during which time the solution changed color from dark green to deep purple and observed the formation of butadiene in the ^{1}HNMR (Figure 2.1a). Due to the formation of butadiene, we assume the -NTs fragment has remained bound to the complex as the proposed imido complex. Previously, we have characterized a different imido complex in which an oxygen of the tosyl group is bonded to one of the nickel centers (Figure 2.4b). This complex was synthesized by reacting TsN_3 with [$^{i\text{-}Pr}$NDI]$Ni_2(C_6H_6)$. The imido complex formed is thought to decompose into the amido. To confirm the structure of the amido, it was prepared via salt metathesis with [$^{i\text{-}Pr}$NDI]Ni_2Br. The g-value of the known amido complex was compared with the g-value of the proposed amido complex and was determined the identities were the same. With a similar g-value (2.05 for known amide and 2.07 for unknown), we propose the previously characterized structure and the new complex formed in Figure 2.4a may have the same identity. Other characterization data will need to be obtained to confidently assign the complex as the amido we have previously characterized.

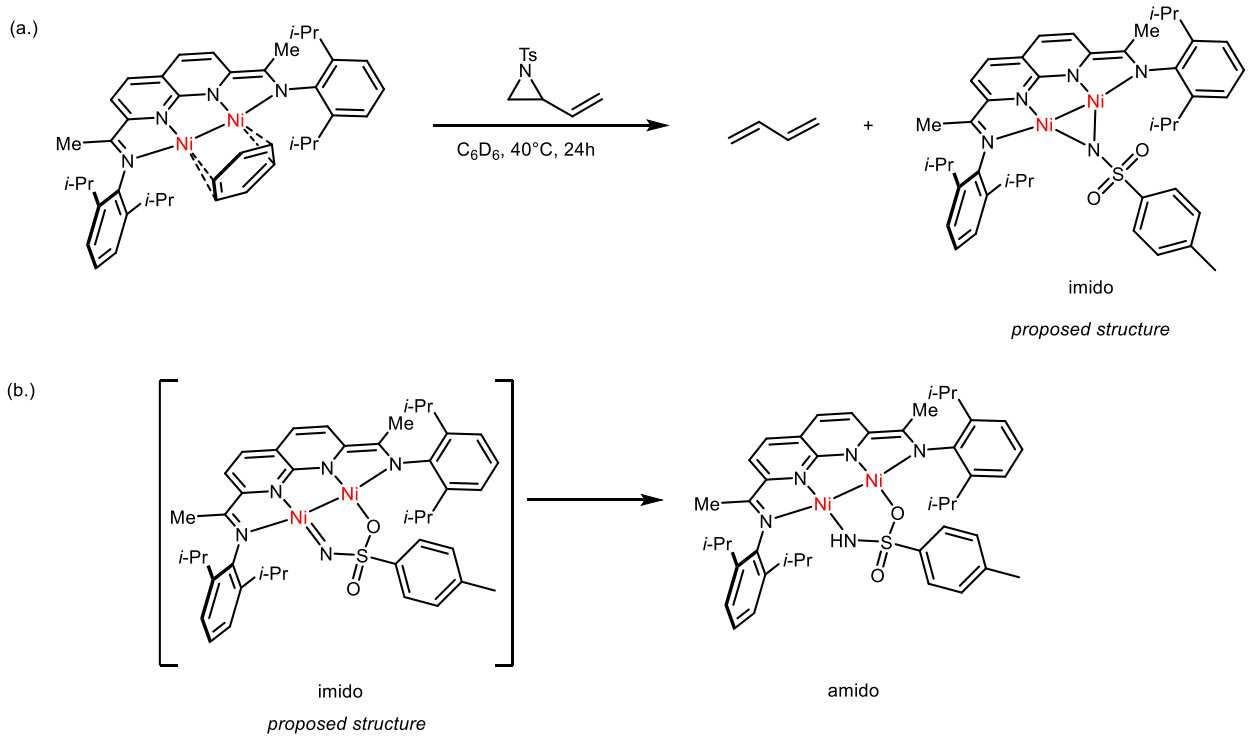

Figure 2.4. Hetero-atom abstraction takes place when heating 1-tosyl-2-vinylaziridine.

This method was extended to other aziridines to include 1-tosylaziridine and 1-tosyl-2-phenylaziridine (Figure 2.5). In the case of these aziridines the red-brown solution turns to deep purple which indicates the formation of the amido complex. By ^{1}HNMR, it was confirmed the organic fragments forming were ethylene and styrene.

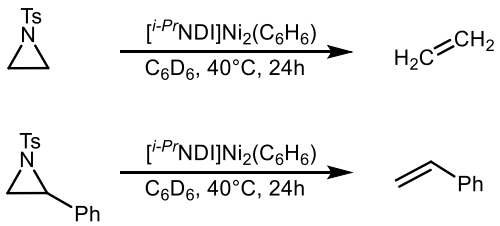

Figure 2.5. Heating 1-tosylaziridine, 1-tosyl-2-phenylaziridine, and styrene oxide results in hetero-atom abstracted products.

Styrene epoxide theoretically forms a similar complex in which the oxygen is bound to the nickel complex (Figure 2.6). Relating the proposed nickel complex from the aziridine ring opening in which may result in the formation of an amido complex, we can postulate the abstraction of oxygen could result in a similar complex but unlikely (Figure 2.4a). From previous studies, we have found the complexation of more than one [$^{i\text{-}Pr}$NDI]Ni_2 complex is common and has been exhibited with hetero-atom abstractions with thiiranes which will be discussed in the next section of this chapter. From these experiments, we can confidently assume the likely complexes formed are clusters with either one or two oxygens present in the binding pocket (Figure 2.6b,c). Other reactivity studies such as XRD will have to be performed to confidently assign the correct complex.

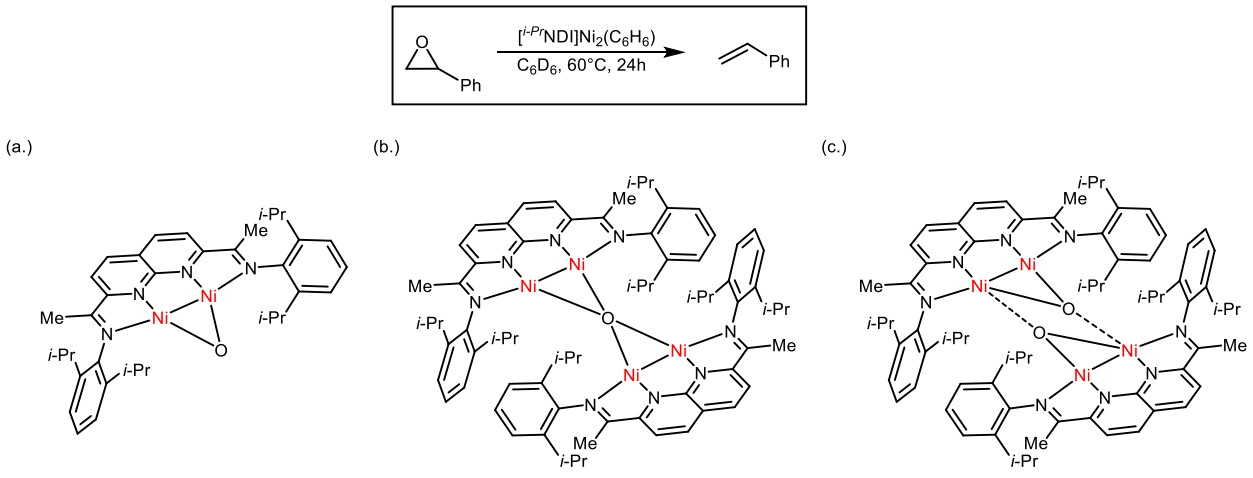

Figure 2.6. Hetero-atom abstraction from an epoxide yields styrene and three theoretical complexes.

We have discovered a few substrates that readily perform hetero-atom abstraction reactions in which the identities of the organic products released were characterized. This substrate scope could be expanded to include other aziridines and epoxides. The vision for continuing this project would be finding more complex substrates where an epoxide or aziridine could be used as a transient protecting group.

2.1.3 Experimental

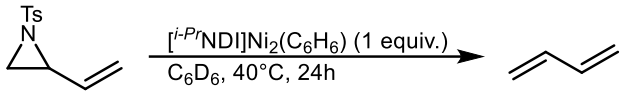

Stoichiometric generation of 1,3-butadiene by [$^{i\text{-}Pr}$NDI]$Ni_2(C_6H_6)$. In an N_2-filled glove-box, 1-tosyl-2-vinylaziridine (3.1 mg, 0.014 mmol, 1 equiv.) and [$^{i\text{-}Pr}$NDI]$Ni_2(C_6H_6)$ (**1**) (10 mg, 0.0014 mmol, 1 equiv.) were dissolved in C_6D_6 (0.5 mL), and the solution was loaded into an NMR tube equipped with a J. Young valve. After reacting at 22 °C for 1 hour, the dark green solution was heated at 40°C for 24 hours. Over the course of the 24 hours, the solution changed from dark green to deep purple. The appearance of ^{1}HNMR peaks corresponding to 1,3-butadiene (**29**) grow in while complex **2** peaks disappeared. Comparison to an authentic sample of 1,3-butadiene confirmed the identity of the product. The crude ^{1}HNMR spectra also shows some polymerized product in the aliphatic region.

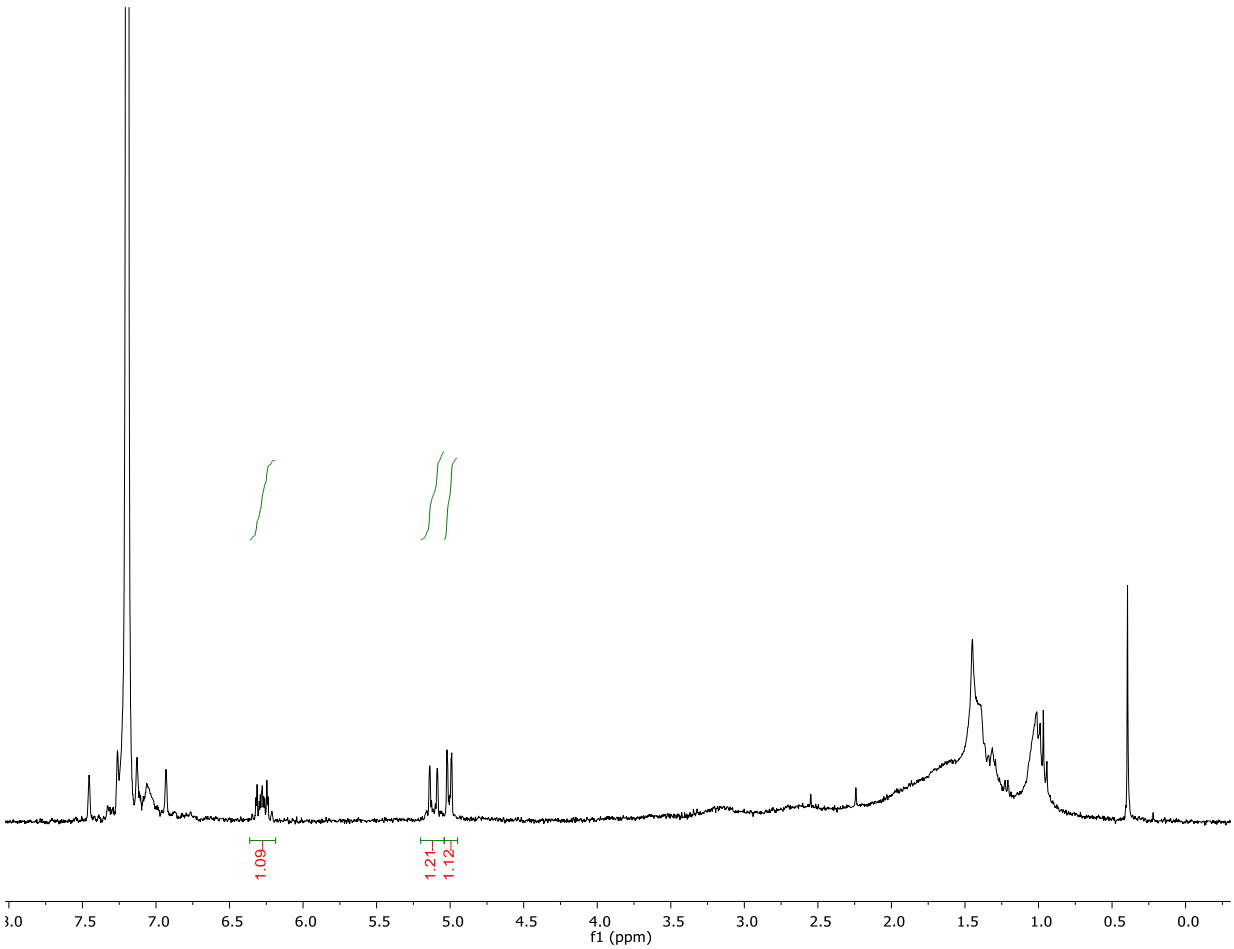

Figure 2.7. ^{1}HNMR spectrum of 1,3-butadiene obtained from heating complex **2**. (C_6D_6)

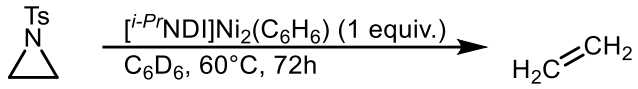

30

Stoichiometric generation of ethylene by [$^{i\text{-}Pr}$NDI]$Ni_2(C_6H_6)$. In an N_2-filled glove-box, 1-tosylaziridine (2.78 mg, 0.014 mmol, 1 equiv.) and [$^{i\text{-}Pr}$NDI]$Ni_2(C_6H_6)$ (**1**) (10 mg, 0.0014 mmol, 1 equiv.) were dissolved in C_6D_6 (0.5 mL), and the solution was loaded into an NMR tube equipped with a J. Young valve. The reaction mixture was heated at 60°C for 72 hours. Comparison to an authentic sample of ethylene (**30**) confirmed the identity of the product. The

crude ^{1}HNMR spectra also shows unreacted 1-tosylaziridine and [$^{i\text{-}Pr}$NDI]Ni$_2$(C$_6$H$_6$).^{1}HNMR (300 MHz, C$_6$D$_6$) δ 5.30 (s, 4H).

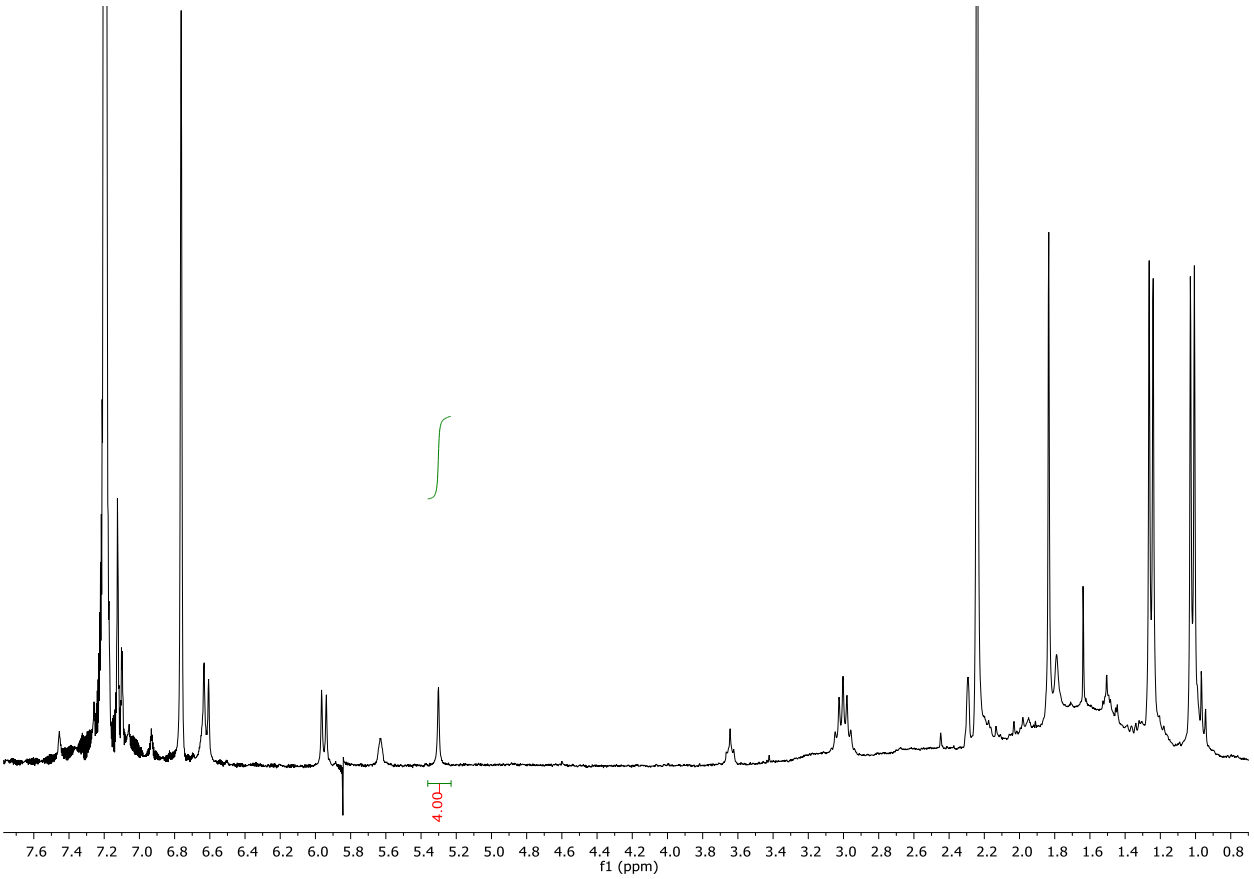

Figure 2.8. ^{1}HNMR spectrum of the generation of ethylene (**30**) from 1-tosylaziridine. (C$_6$D$_6$)

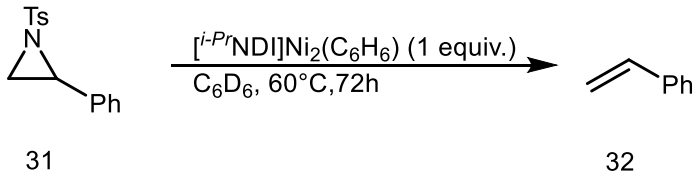

Stoichiometric generation of styrene by [$^{i\text{-}Pr}$NDI]Ni$_2$(C$_6$H$_6$). In an N$_2$-filled glove-box, 1-tosyl-2-phenylaziridine[69] (3.83 mg, 0.014 mmol, 1 equiv.) and [$^{i\text{-}Pr}$NDI]Ni$_2$(C$_6$H$_6$) (**1**) (10 mg, 0.0014 mmol, 1 equiv.) were dissolved in C$_6$D$_6$ (0.5 mL), and the solution was loaded into an

NMR tube equipped with a J. Young valve. The reaction mixture was heated at 60°C for 72 hours. Comparison to an authentic sample of styrene (**32**) confirmed the identity of the product. The crude ^{1}HNMR spectra also shows unreacted 1-tosyl-2-phenylaziridine, [$^{i\text{-}Pr}$NDI]$Ni_2(C_6H_6)$, and mesitylene as an internal standard. Note: the peaks corresponding to styrene at 6.62 ppm are hidden under aromatic peaks from the nickel complex. ^{1}H NMR (300 MHz, $CDCl_3$) δ 6.62 (m, 2H), 5.65 (d, J = 17.2 Hz, 2H), 5.12 (d, J = 10.6 Hz, 1H).

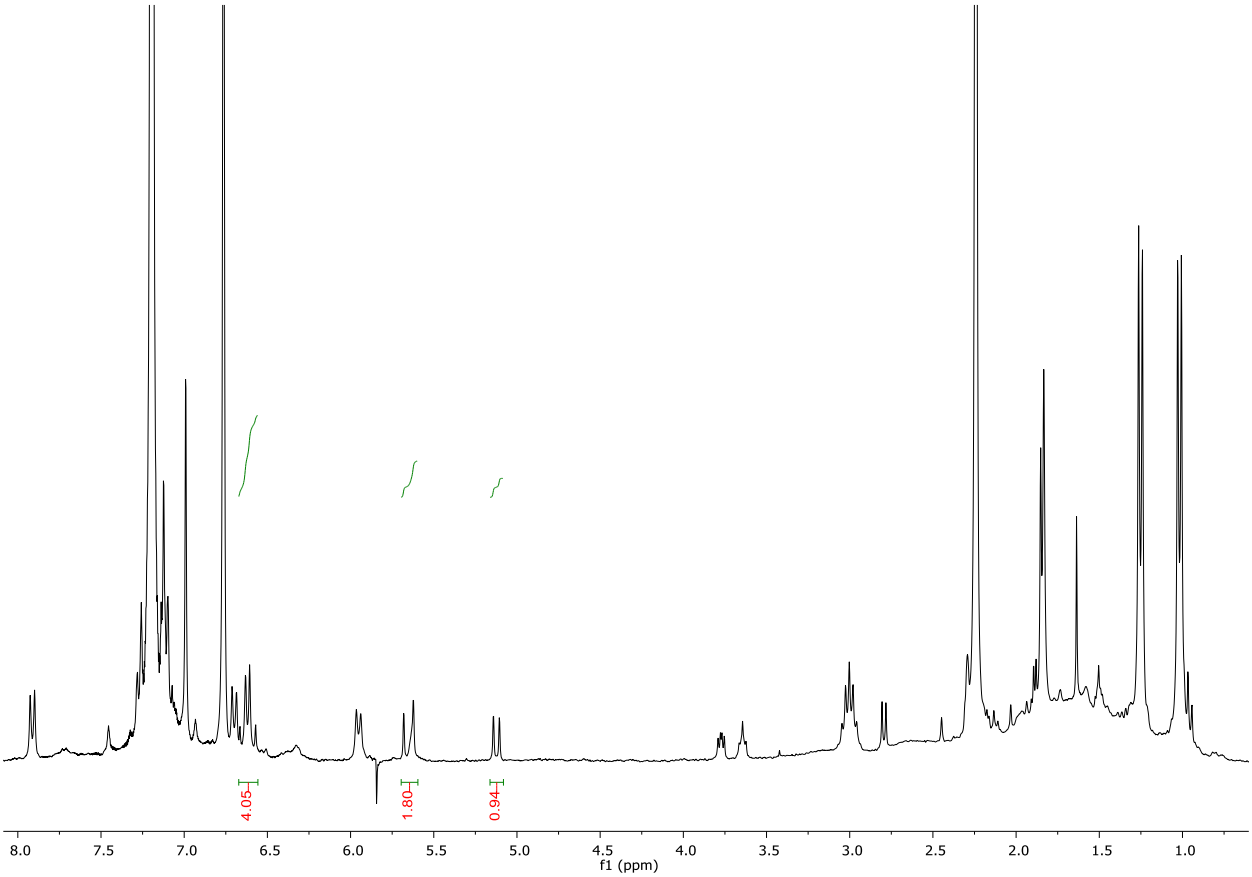

Figure 2.9. ^{1}HNMR spectrum of the generation of styrene (**32**) from 1-tosyl-2-phenylaziridine. (C_6D_6)

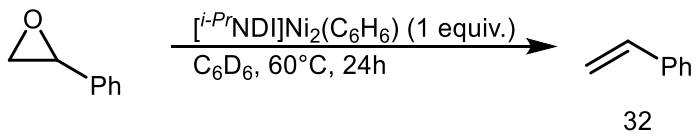

Stoichiometric generation of styrene by [$^{i\text{-}Pr}$NDI]$Ni_2(C_6H_6)$. In an N_2-filled glove-box, styrene oxide (1.68 mg, 0.014 mmol, 1 equiv.) and [$^{i\text{-}Pr}$NDI]$Ni_2(C_6H_6)$ (10 mg, 0.0014 mmol, 1 equiv.) were dissolved in C_6D_6 (0.5 mL), and the solution was loaded into an NMR tube equipped with a J. Young valve. The reaction mixture was heated at 60°C for 24 hours. Comparison to an authentic sample of styrene confirmed the identity of the product. The crude ^{1}HNMR spectra also shows unreacted styrene oxide and mesitylene as an internal standard. ^{1}H NMR (300 MHz, $CDCl_3$) δ 6.63 (dd, J = 17.6, 10.9 Hz, 2H), 5.65 (dd, J = 17.6, 1.1 Hz, 2H), 5.12 (dd, J = 10.9, 1.0 Hz, 1H).

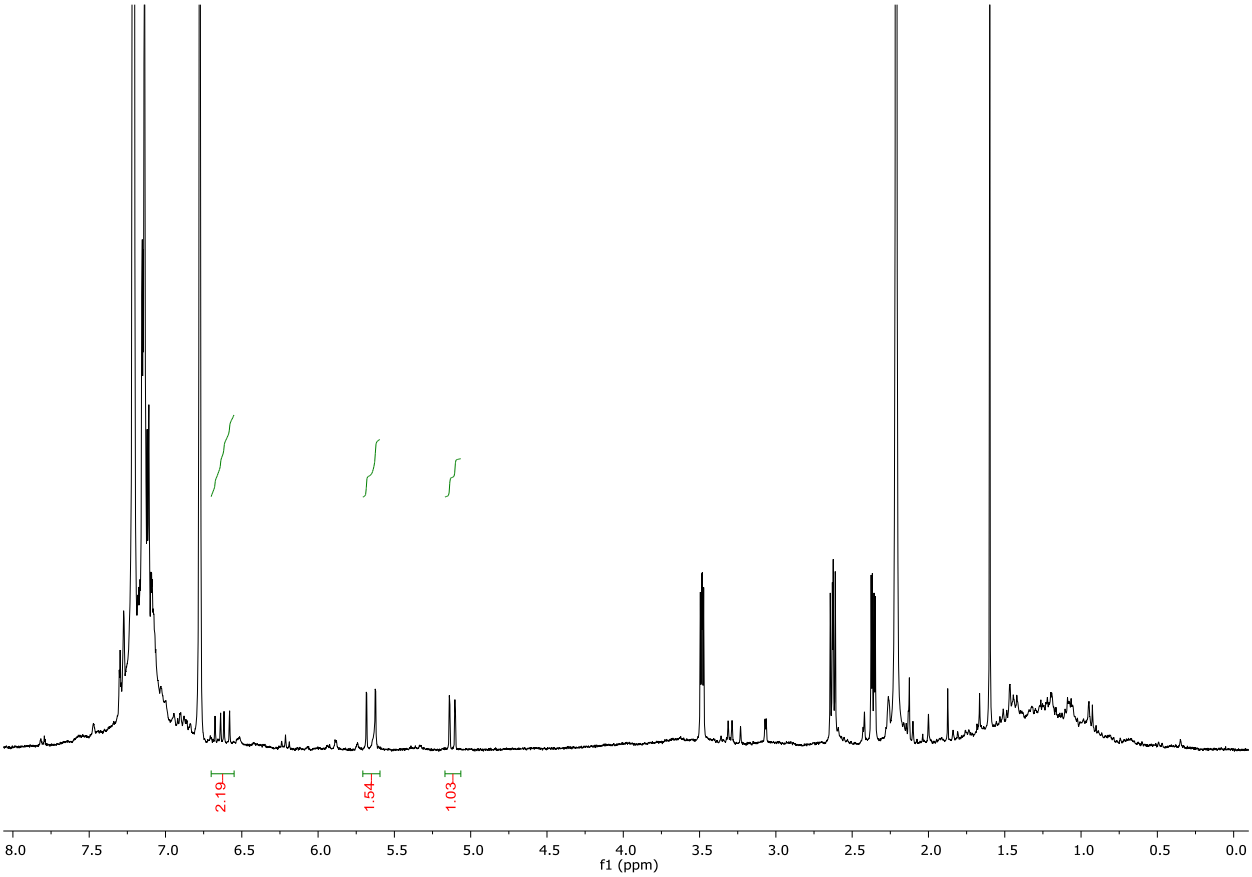

Figure 2.10. ^{1}HNMR spectrum of the generation of styrene (**32**) from styrene oxide. (C_6D_6)

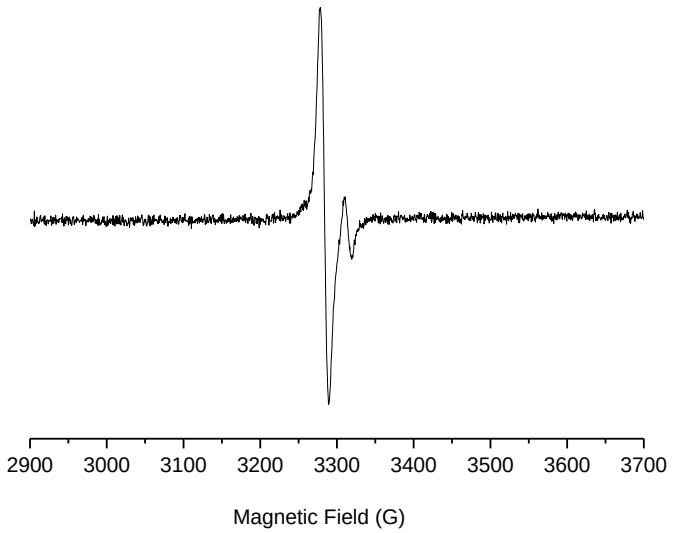

Figure 2.11. EPR spectrum of complex generated from styrene oxide. (298K, THF)

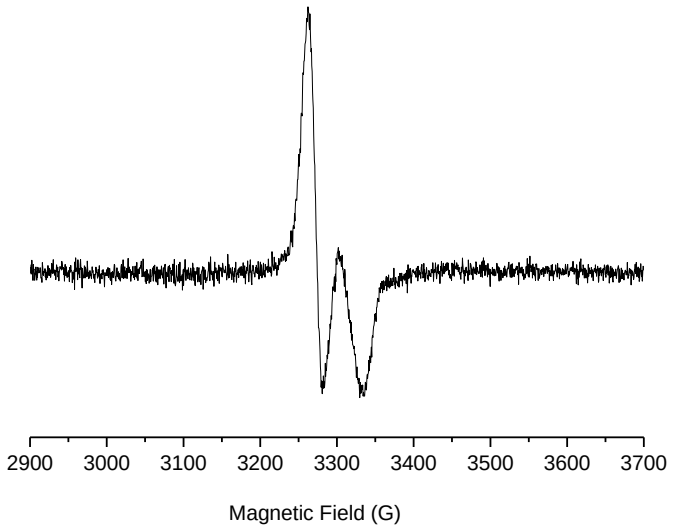

Figure 2.12. EPR spectrum of complex generated from styrene oxide. (125K, THF)

2.2 Catalytic Desulfurization

2.2.1 Introduction

Desulfurization of sulfur-containing substrates is not an unknown reaction. The propensity of sulfur to undergo a C-S bond activation in the presence of transition metals usually results in the oxidative transfer of sulfur to the metal and poisoning of the catalyst.[70] Several strategies have been demonstrated to remove sulfur from the metal and prevent the doom of the reaction. A very well-known reaction that has pioneered this field is the Liebenskiend-Srogl cross-coupling reaction in which copper (I) thiocarboxylate is used as a stoichiometric sulfur scavenger (Figure 2.13). While this reaction works very well and has shifted the way we think about these types of reactions, the use of stoichiometric amounts of a sulfur scavenger is not ideal.

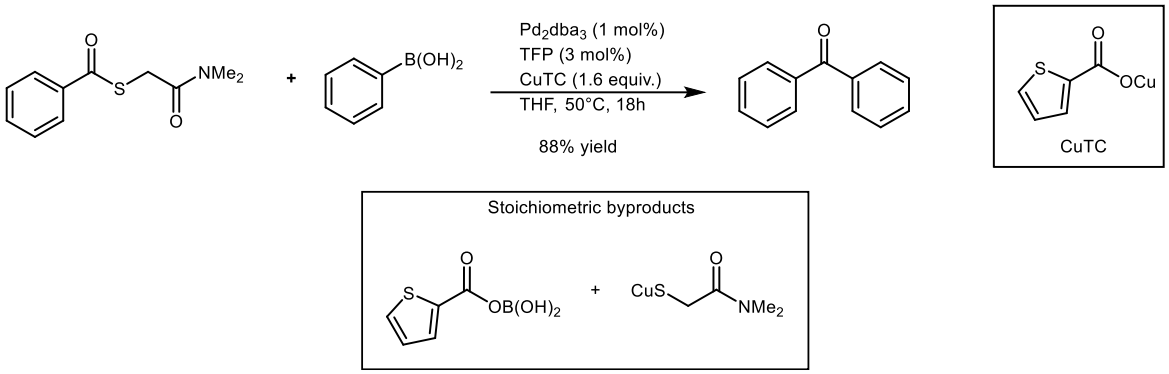

Figure 2.13. The Liebenskiend-Srogl cross coupling reaction uses stoichiometric amounts of a copper containing sulfur scavenger.

This strategy has been applied to transition metal catalyzed desulfurization of thiiranes to prevent catalyst poisoning. Jacob and coworkers applied this strategy to a stereospecific reaction in which various thiiranes were desulfurized using $MeReO_3$ and stoichiometric amounts of triphenylphosphine.[71] Given the gap in the literature we wanted to address catalytic desulfurization of thiiranes and other sulfur-containing substrates by using a reductant for catalytic turnover.

2.2.2 Results and Discussion

In our initial studies, we examined stoichiometric oxidative transfer reactions with aziridines and epoxides. Next, we turned our attention to thiiranes and discovered a desulfurization readily occurs. Subjecting complex **1** to a stoichiometric amount of methyl thiirane results in an oxidative transfer at room temperature in which the sulfur atom is abstracted to form complex **33** and propene (Figure 2.14). To probe the identity of the complex formed from this reaction, we turned to XRD. Concentrating the reaction mixture, dissolving in Et_2O, and subsequent slow evaporation at -30°C yielded dark crystals. Interestingly, the oxidative transfer occurs between two equivalents of [$^{i\text{-}Pr}$NDI]Ni_2 and methyl thiirane to form a tetranickel-disulfide complex. The Ni1-Ni3 bond distance is very elongated at 2.821(1) Å which could mean there is weak to no bonding between them. In contrast, the Ni2-Ni4 bond distance is only slightly elongated at 2.501(1) Å in comparison to complex **1** (2.496(1) Å). The Ni – S bond distances all have similar bond lengths of 2.1 to 2.2 Å.

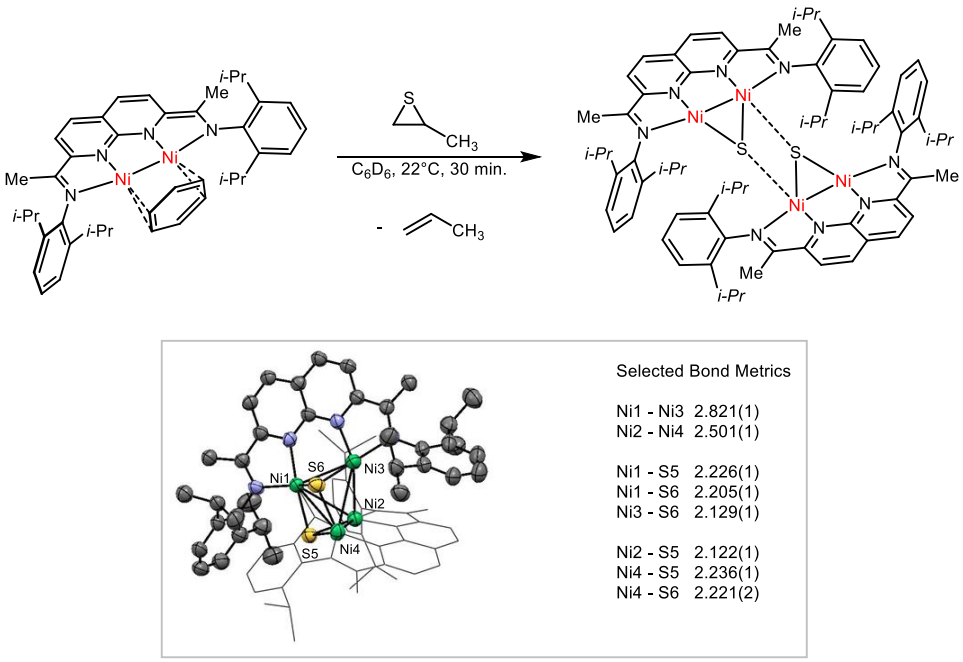

Figure 2.14. Oxidative transfer of the sulfur atom in methyl thiirane transpires to form **33**.

Demonstrating [$^{i\text{-}Pr}$NDI]$Ni_2(C_6H_6)$ is capable of performing an oxidative transfer reaction with methyl thiirane, we sought to expand the substrate scope (Table 2.1). No discrimination was seen between using alkyl substrates (Table 2.1, entries 1 and 4) and aromatic or vinyl substrates (Table 2.1, entries 2,3 and 5). Problems arise with getting accurate yields and isolating the products due to the volatility and polymerization of the reductively eliminated products. We also set out to probe catalytic activity by using 5-10 mol% loading of [$^{i\text{-}Pr}$NDI]$Ni_2(C_6H_6)$, however, once the catalyst was consumed there was no turnover detected.

Table 2.1. Substrate scope for the desulfurization of thiiranes.

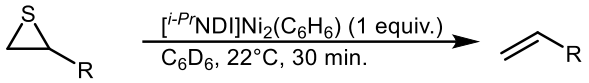

entry	substrate	product	% yield
1	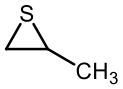	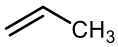	80
2	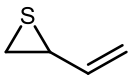	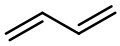	99
3	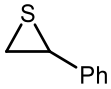	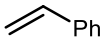	90
4	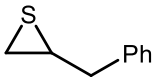	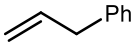	80
5	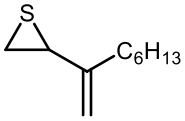	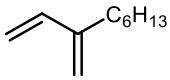	74

Oxidative transfer reactions with thiiranes readily occur at room temperature due to the energy favorability to release ring strain. Seeking out structures that exhibit a higher difficulty in activating the C-S bond we turned our attention to thioureas. Parent thiourea reacts with [$^{i\text{-}Pr}$NDI]$Ni_2(C_6H_6)$ at room temperature to yield a deep purple powder solution that was ^{1}HNMR silent. Crystallizing from benzene revealed the thiourea binds side-on to yields complex **35** (Figure 2.15). The C-S bond distance of thiourea is 1.738 Å which is slightly longer than a C-S double bond but slightly shorter than a C-S single bond. We can conclude the delocalization of

the π-electrons are forming an μ-allyl-type complex. We see similar reactivity for the secondary thiourea in that a purple solution forms and the ^{1}HNMR is silent. Crystals were unable to be obtained but the proposed structure is similar to that of complex **35** (Figure 2.15, bottom).

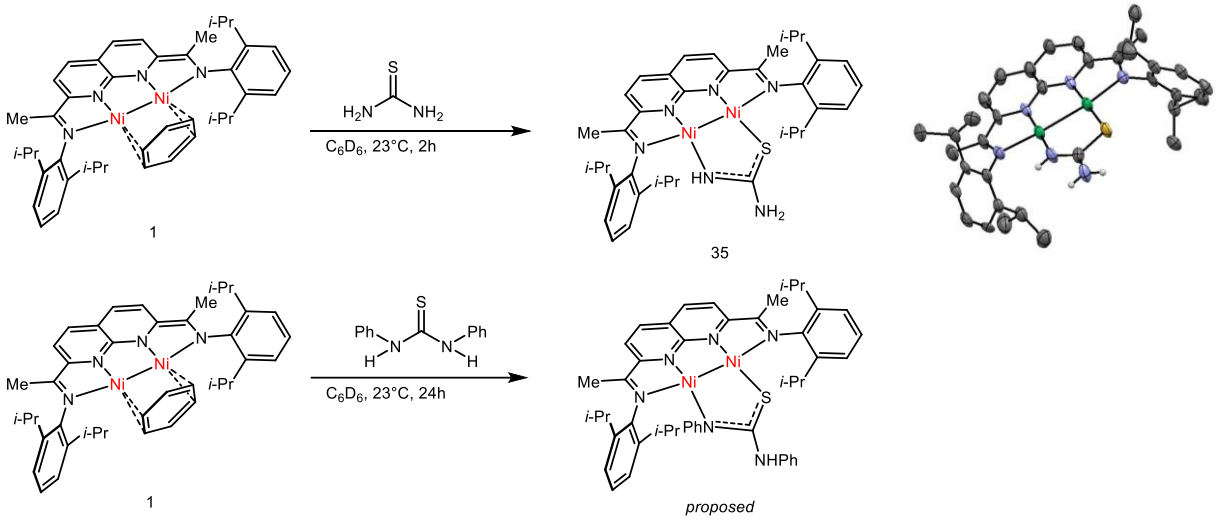

Figure 2.15. Desulfurization attempts with thioureas.

Next, we turned our attention to a tertiary thiourea, tetramethylthiourea, to determine the ability to activate complex substrates. Unlike primary and secondary thioureas which readily exchange with benzene at room temperature, there was no reaction with tetramethylthiourea until heating (Figure 2.16). Unlike thiiranes, which preferentially form $[(^{i\text{-}Pr}\text{NDI})\text{Ni}_2]\text{S}_2$, the reaction with the tetramethylthiourea formed $[(^{i\text{-}Pr}\text{NDI})\text{Ni}_2]_2\text{S}$ (**34**). The Ni-Ni bond length of one fragment, 2.416(1) Å, is slightly longer than the other (2.364(1) Å). An intriguing characteristic of **34** is the napthyridine-diimine backbone of one fragment seems to be π – π stacking with the dipp group of the other fragment.

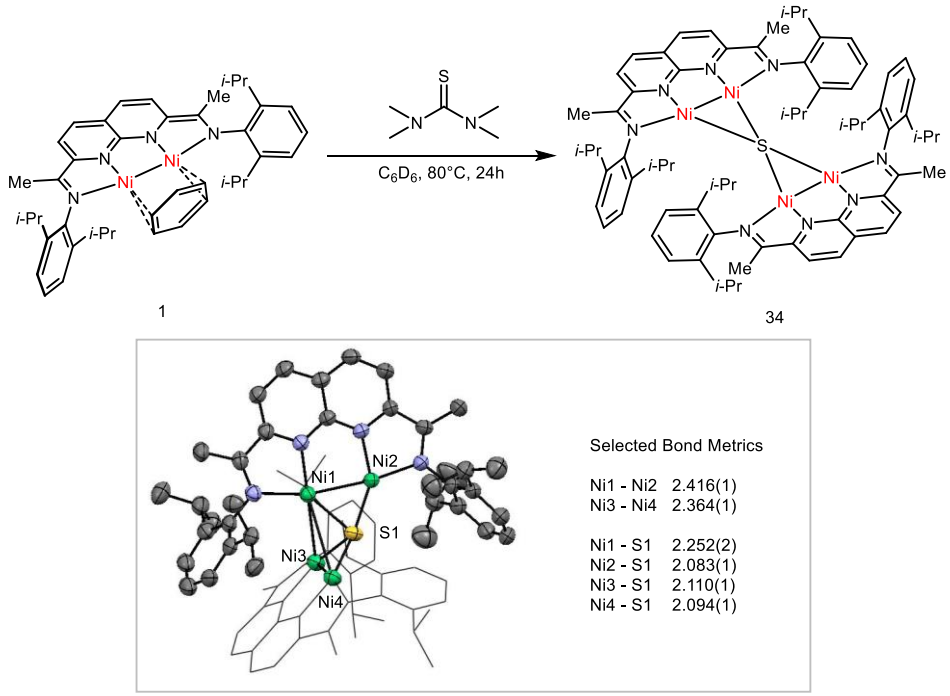

Figure 2.16. Heating complex **1** with tetramethylthiourea yields a tetranickel monosulfide complex.

With the ability to activate strained ring systems in hand, we turned our attention to the activation of sulfur heterocycles larger than thiiranes. We began by looking at the activation of thiophenes. Reaction with parent thiophene is very slow in that after heating for 1 week at 80°C there was still starting material left. Owing this result to the less than favorable act of breaking aromaticity, we decided to try to activate tetrahydrothiophenes.

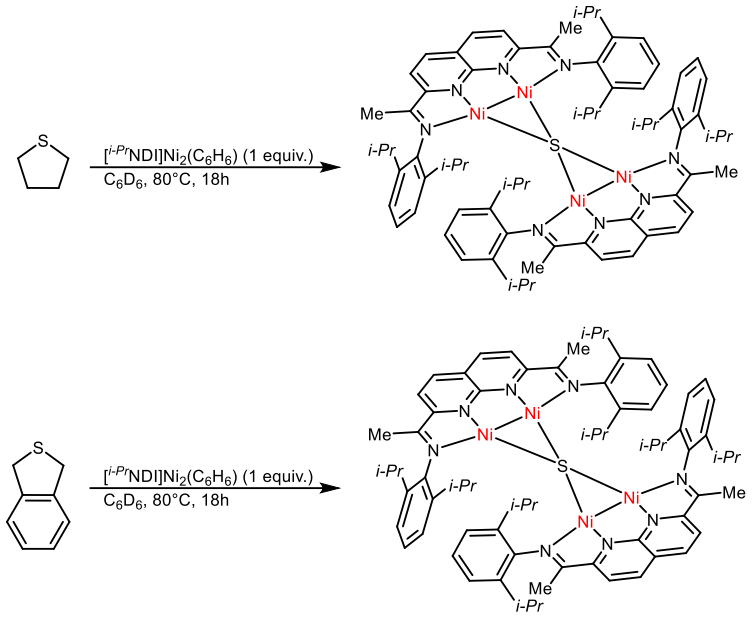

Figure 2.17. Activation of tetrahydrothiophenes led to the formation of $[(^{i\text{-}Pr}NDI)Ni_2]_2S$ (**34**).

First, we decided to activate tetrahydrothiophene due to its commercial availability. Heating tetrahydrothiophene at 80°C for 18 hours yielded complex **34** (Figure 2.17). Likewise, the bicyclic tetrahydrothiophene reacted in the same manner to give the same complex, however, the conversion after 18 hours was a lot lower. In the HNMR spectrum, we could see the presence of unreacted $[^{i\text{-}Pr}NDI]Ni_2(C_6H_6)$ and starting material. The reactivity of this substrate may be lower due to the presence of saturation within the sulfur heterocycle. Another possibility could result from one C-S bond activation exhibiting a lower energy than breaking the second C-S bond within the substrate.

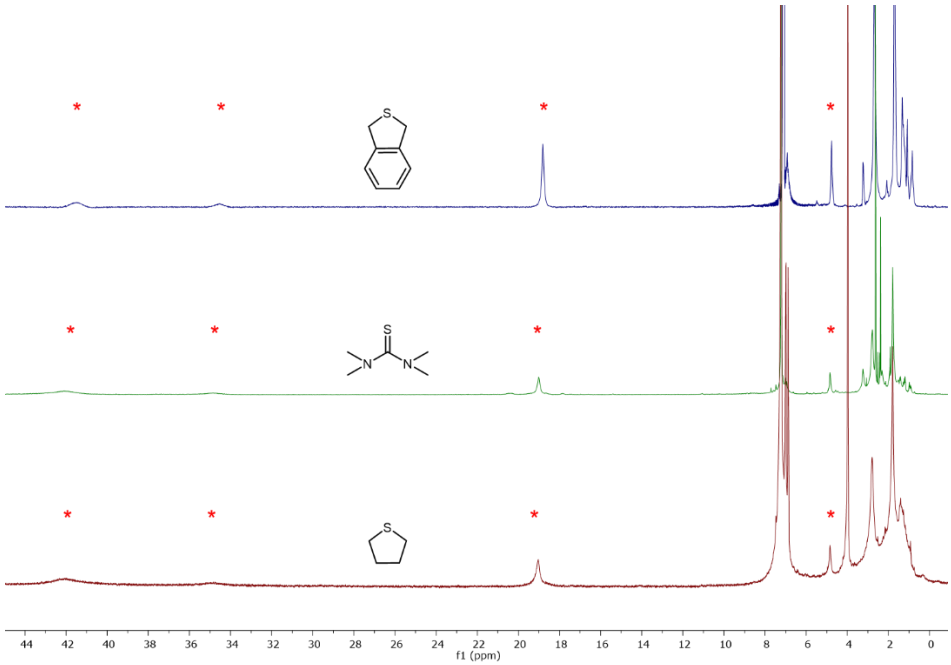

Figure 2.18. Paramagnetic peaks belonging to **34** can be seen in the ^{1}HNMR (red asterisks).

With the formation of **34** we can see broad peaks in the ^{1}HNMR (Figure 2.18). These spectra also show some very broad signals in the aliphatic region which have also been assigned to the complex. If the spectra for the monosulfide complex is compared with the disulfide the same broad peaks are exhibited albeit the signals are not shifted as far downfield.

So far, all the oxidative transfer reactions with sulfur heterocycles are stoichiometric. Turning to further characterizing both the disulfide and monosulfide complexes, we decided to study their redox potentials by cyclic voltammetry (CV). A CV of $[(^{i\text{-}Pr}\text{NDI})\text{Ni}_2]_2\text{S}_2$ exhibited one reversible reduction wave at -2.23 V and a reversible oxidation wave at -1.44 V (Figure 2.19a). Not surprisingly, $[(^{i\text{-}Pr}\text{NDI})\text{Ni}_2]_2\text{S}$ is easier to reduce and exhibits two reversible reduction waves at -1.91 V and -2.37 V and two oxidation waves at -0.845 V and -1.14 V (Figure 2.19b). With this information in hand, we can now choose a proper reductant to reduce the sulfide complexes back to $[^{i\text{-}Pr}\text{NDI}]\text{Ni}_2(\text{C}_6\text{H}_6)$. Further studies are ongoing to address the possibility for catalytic turnover.

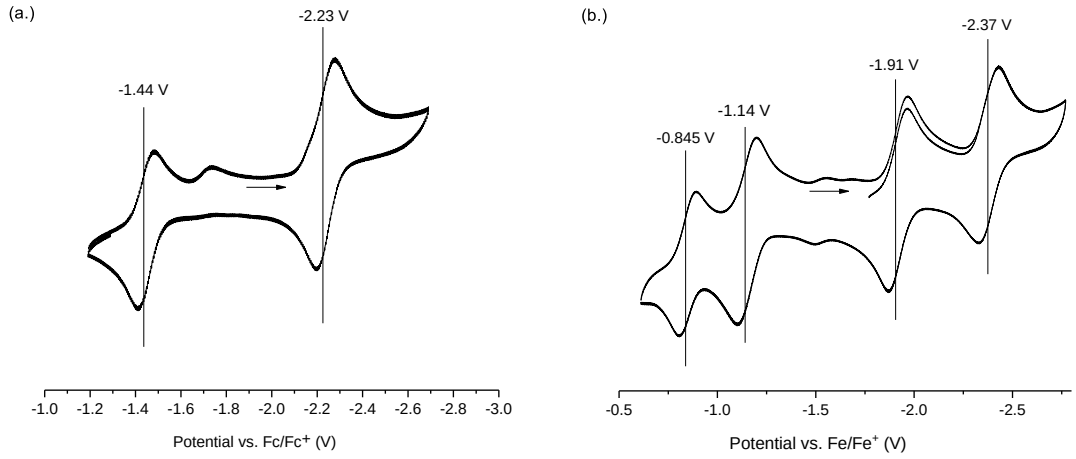

Figure 2.19. Cyclic voltammetry diagrams of a.) $[(^{i\text{-}Pr}NDI)Ni_2]_2S_2$ and b.) $[(^{i\text{-}Pr}NDI)Ni_2]_2S$.

The possible mechanism for the desulfurization of sulfur-containing heterocycles and other substrates is thought-provoking. We can first imagine an oxidative addition in which a C-S bond activation occurs to form a metallacyclic intermediate (Figure 2.20). Next, another equivalent of $[^{i\text{-}Pr}NDI]Ni_2(C_6H_6)$ may come in and activate the other C-S bond and concurrently release of the organic fragment and benzene occurs to form a sulfide complex. The dotted arrow signifies the reductive elimination of sulfur to reform $[^{i\text{-}Pr}NDI]Ni_2(C_6H_6)$ and the next cycle can begin. We are currently working on the reductive elimination part of the mechanism and we are excited to tackle this problem.

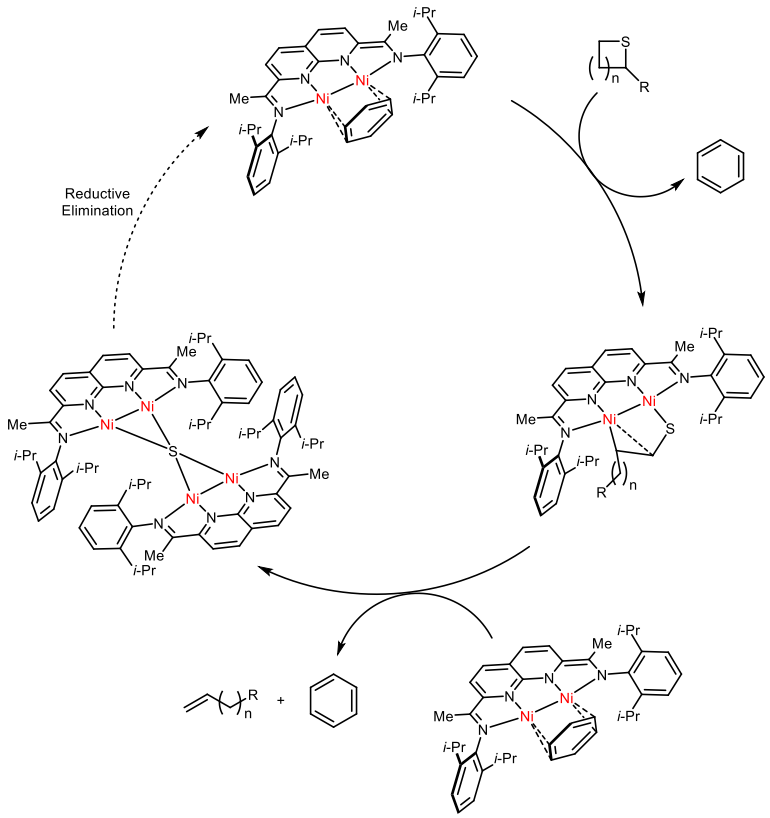

Figure 2.20. Proposed mechanism for C-S bond activation of sulfur containing substrates.

2.2.3 Experimental

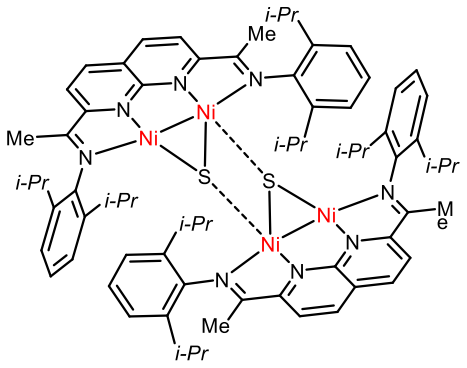

33

In a 20 mL vial, [$^{i\text{-}Pr}$NDI]$Ni_2(C_6H_6)$ (**1**) (20 mg, 0.027 mmol, 1.0 equiv) and methyl thiirane (2.6 mg, 0.036 mmol, 1.0 equiv) were dissolved in C_6H_6 (5 mL). The solution was observed to undergo an immediate color change from red-brown to blackish-green. After stirring at ambient temperature for 30 min, the reaction mixture was concentrated. Single crystals suitable for XRD were obtained by cooling saturated solutions of **33** in Et_2O to −30°C in a glovebox freezer. ^{1}H NMR (300 MHz, C_6D_6) δ 9.72 (s, 1H), 5.06 (s, 2H), 1.96 (d, J = 96.2 Hz, 215H), 1.42 (s, 58H), 0.94 (s, 13H).

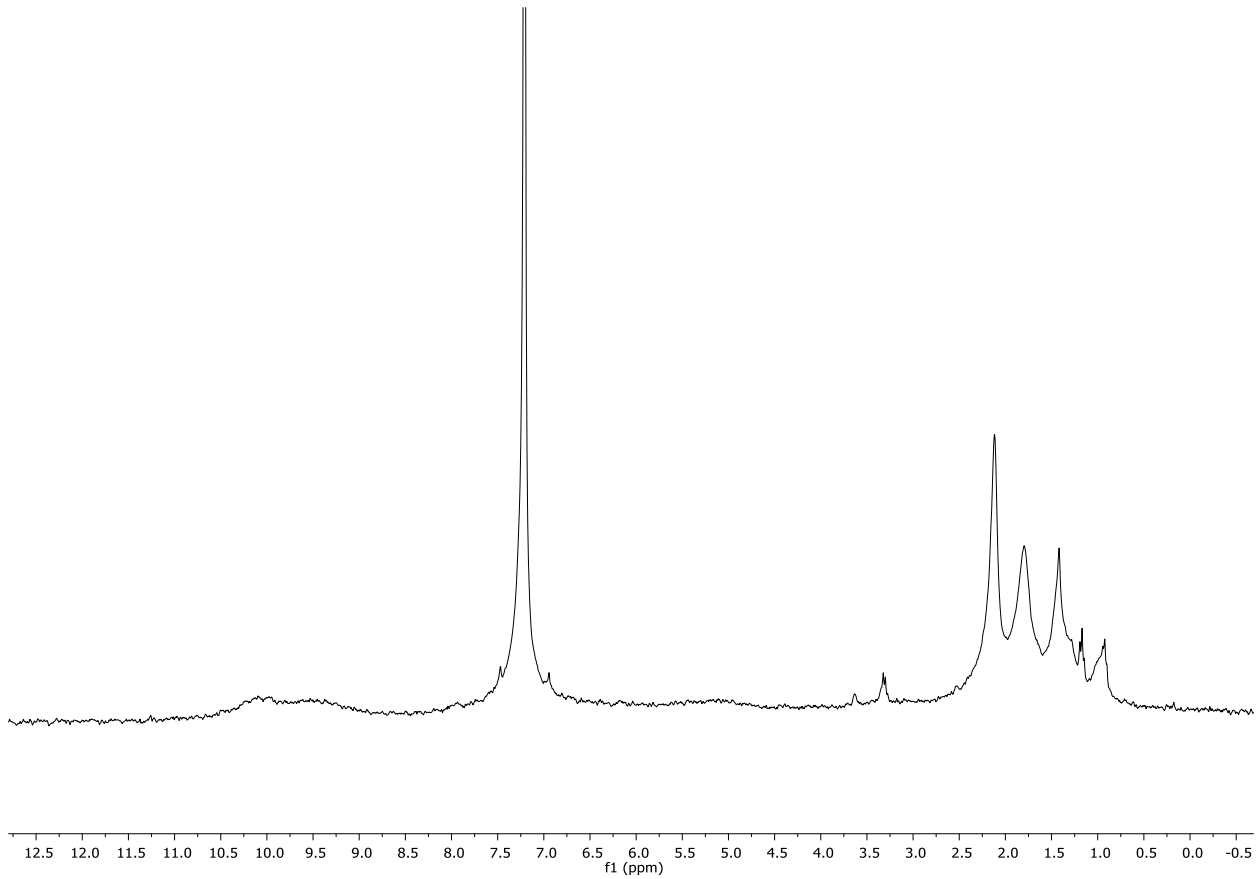

Figure 2.21. ^{1}HNMR for isolated Complex **33**. (C_6D_6)

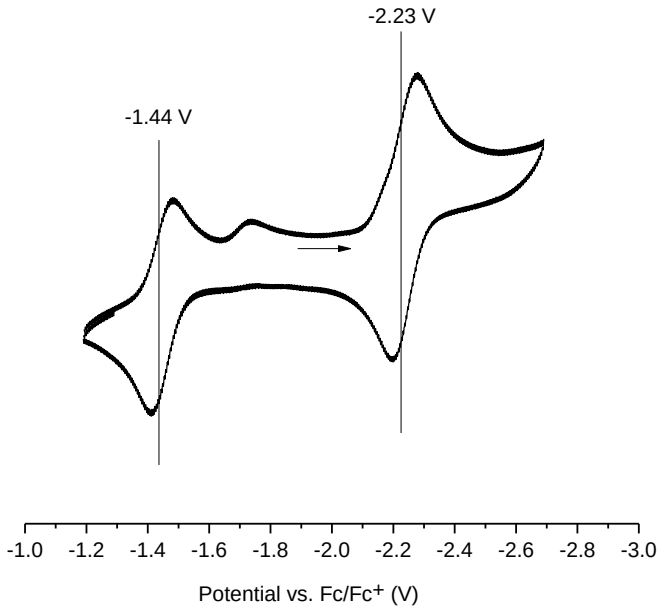

Figure 2.22. EPR spectrum for isolated Complex **33**.

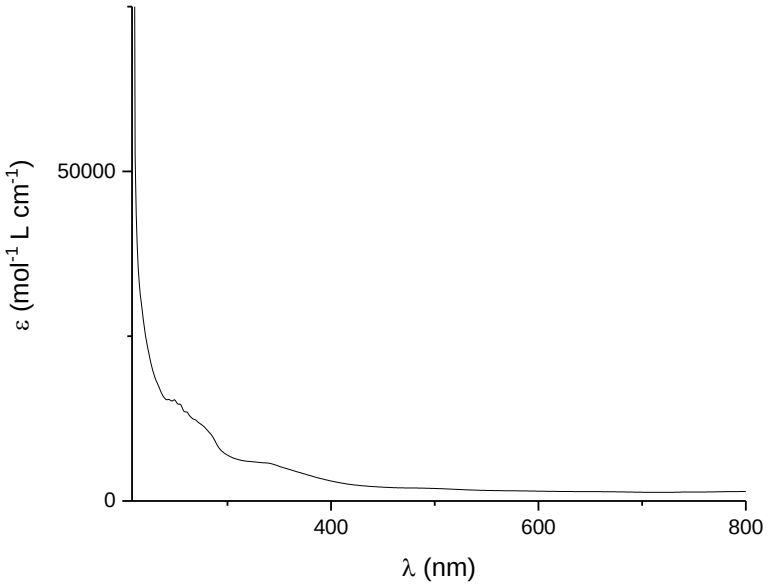

Figure 2.23. UV-Vis spectrum for Complex **33**.

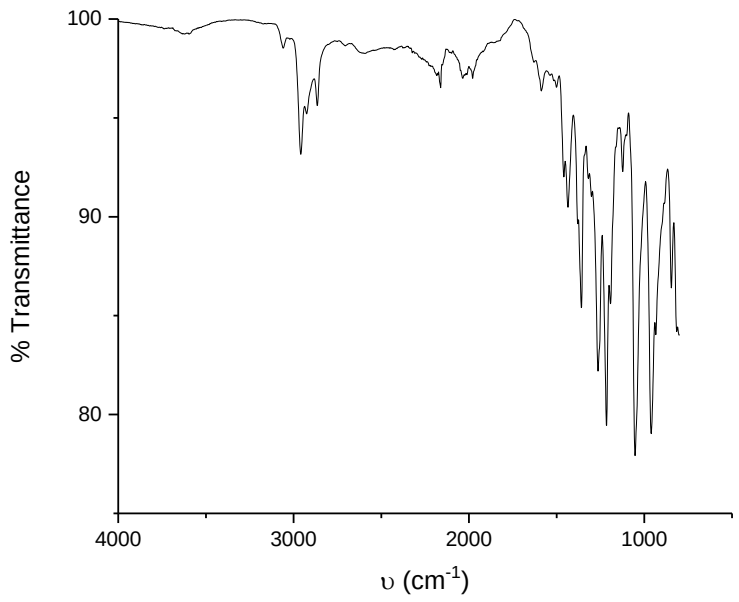

Figure 2.24. FT-IR spectrum of Complex **33**.

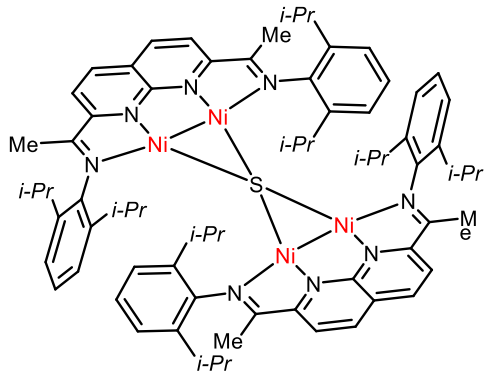

34

In a 10-mL Schlenk round bottom flask, [$^{i\text{-}Pr}$NDI]$Ni_2(C_6H_6)$ (**1**) (20 mg, 0.027 mmol, 1.0 equiv) and tetrahydrothiophene (9.5 mg, 0.11 mmol, 1.0 equiv) were dissolved in C_6H_6 (5 mL). After stirring at 80°C for 18h, the reaction mixture was filtered through a glass fiber pad and concentrated. Single crystals suitable for XRD were obtained by cooling saturated solutions of **34** in C_6H_6 to −30°C in a glovebox freezer.

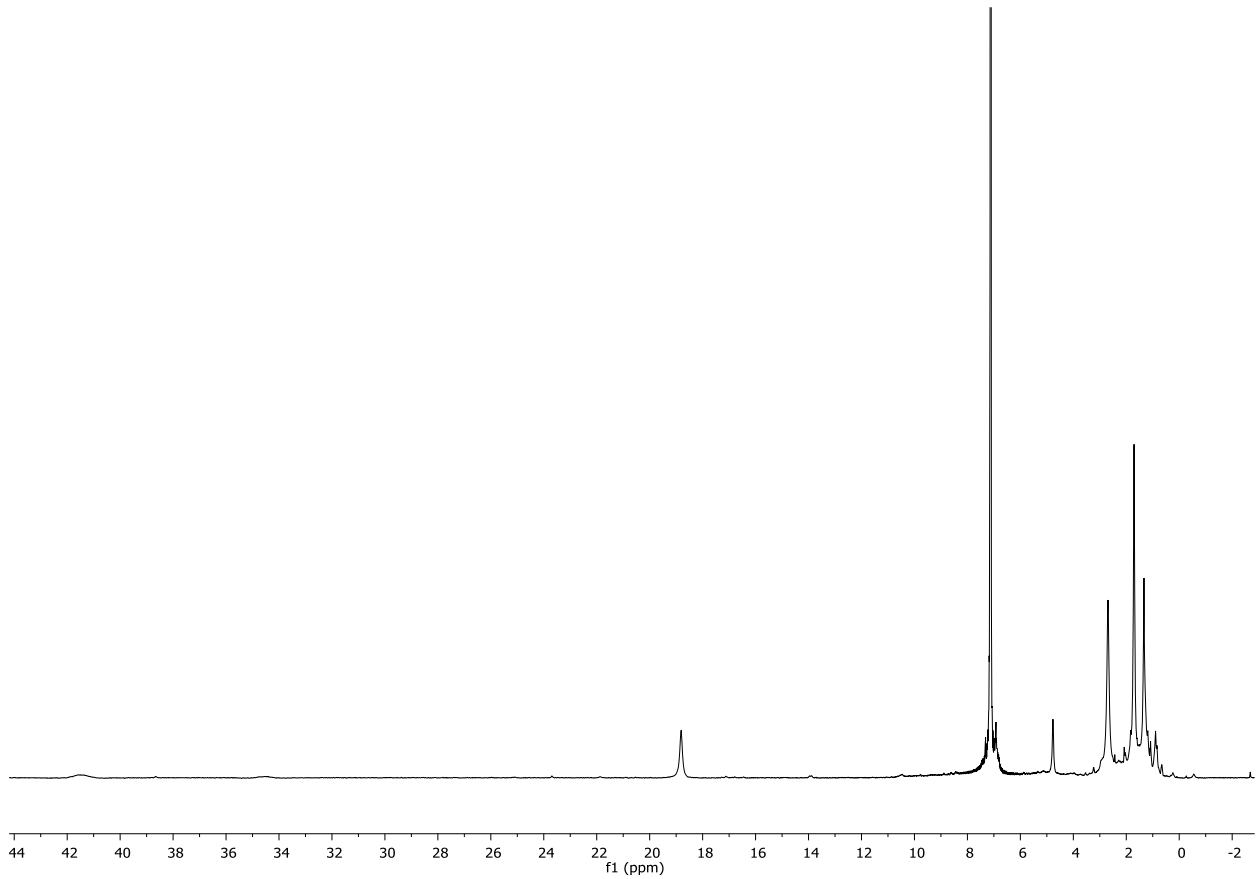

Figure 2.25. ^{1}HNMR for isolated Complex **34**. (C_6D_6)

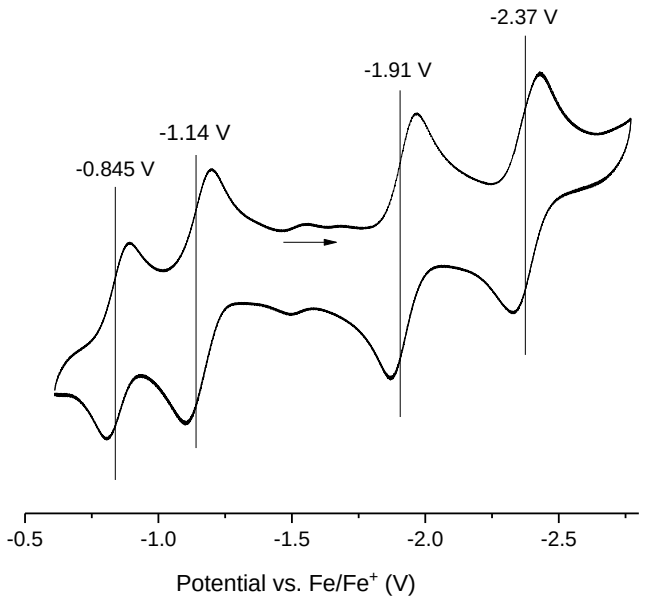

Figure 2.26. EPR spectrum for Complex **34**.

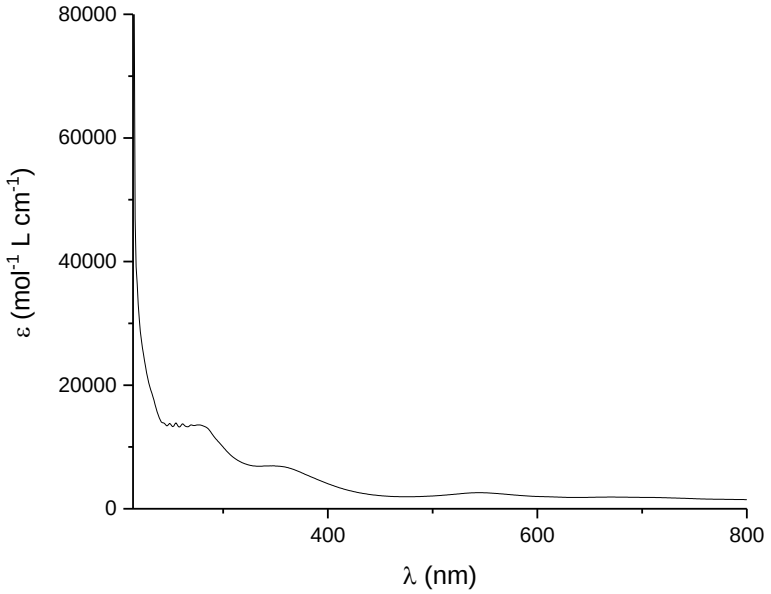

Figure 2.27. UV-Vis spectrum of Complex **34**.

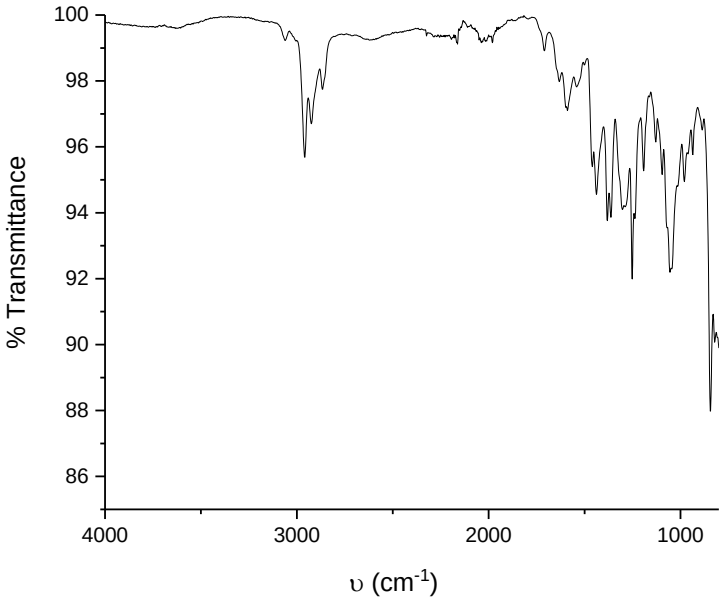

Figure 2.28. FT-IR spectrum of Complex **34**.

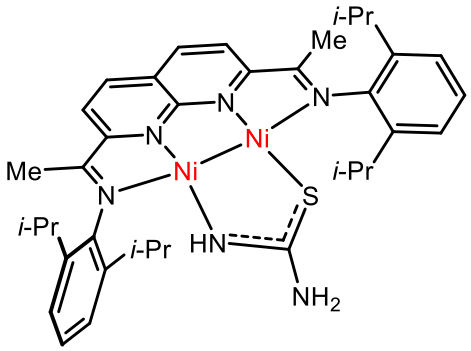

35

In an NMR tube equipped with a J-Young valve, [$^{i\text{-}Pr}$NDI]$Ni_2(C_6H_6)$ (**1**) (5 mg, 0.007 mmol, 1.0 equiv) and thiourea (0.5 mg, 0.007 mmol, 1.0 equiv) were dissolved in C_6H_6 (5 mL). After stirring at ambient temperature for 24 hours, the reaction mixture was filtered through a glass fiber pad and concentrated. Single crystals suitable for XRD were obtained by cooling saturated solutions of **35** in C_6H_6 to −30°C in a glovebox freezer.

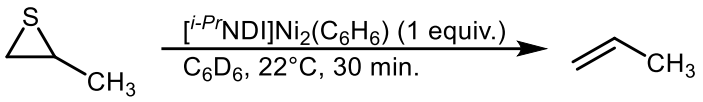

36

In an NMR tube equipped with a J-Young valve, [$^{i\text{-}Pr}$NDI]$Ni_2(C_6H_6)$ (**1**) (5 mg, 0.007 mmol, 1.0 equiv) and methyl thiirane (0.5 mg, 0.007 mmol, 1.0 equiv) were dissolved in C_6D_6 (0.5 mL). The solution was observed to undergo an immediate color change from red-brown to blackish-green. The reaction was monitored by ^{1}HNMR which revealed the presence of propene (**36**) (80% yield) and mesitylene as internal standard. ^{1}H NMR (300 MHz, C_6D_6) δ 5.77 (ddd, J = 16.8, 10.4, 6.7 Hz, 1H), 5.21 – 4.94 (m, 2H), 1.59 (dp, J = 6.6, 1.7 Hz, 4H).

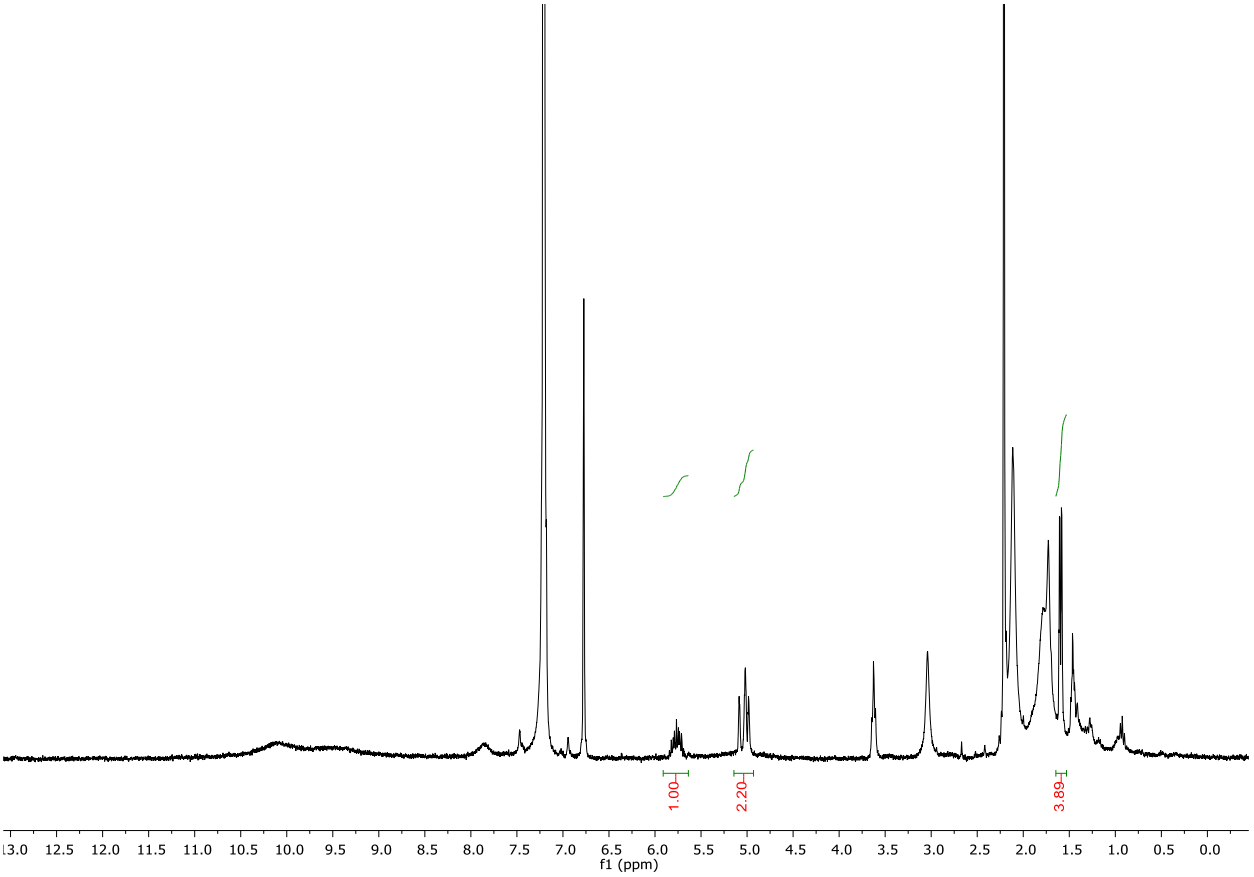

Figure 2.29. Crude ^{1}HNMR for reaction with methyl thiirane to form propene (**36**). (C_6D_6)

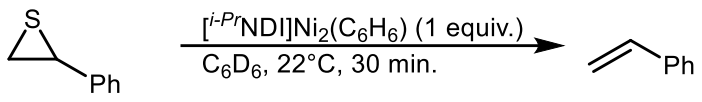

37 32

In an NMR tube equipped with a J-Young valve, [$^{i\text{-}Pr}$NDI]$Ni_2(C_6H_6)$ (**1**) (5 mg, 0.007 mmol, 1.0 equiv) and phenyl thiirane[72] (9.4 mg, 0.007 mmol, 1.0 equiv) were dissolved in C_6D_6 (0.5 mL). The solution was observed to undergo an immediate color change from red-brown to blackish-green. The reaction was monitored by ^{1}HNMR which revealed the presence of styrene (**32**) (90% yield), mesitylene as internal standard, and unreacted starting material. ^{1}HNMR (300 MHz, C_6D_6) δ 7.20 – 7.00 (m, 5H), 6.58 (dd, *J* = 17.6, 10.9 Hz, 1H), 5.61 (d, *J* = 17.7 Hz, 1H), 5.07 (d, *J* = 10.8 Hz, 1H).

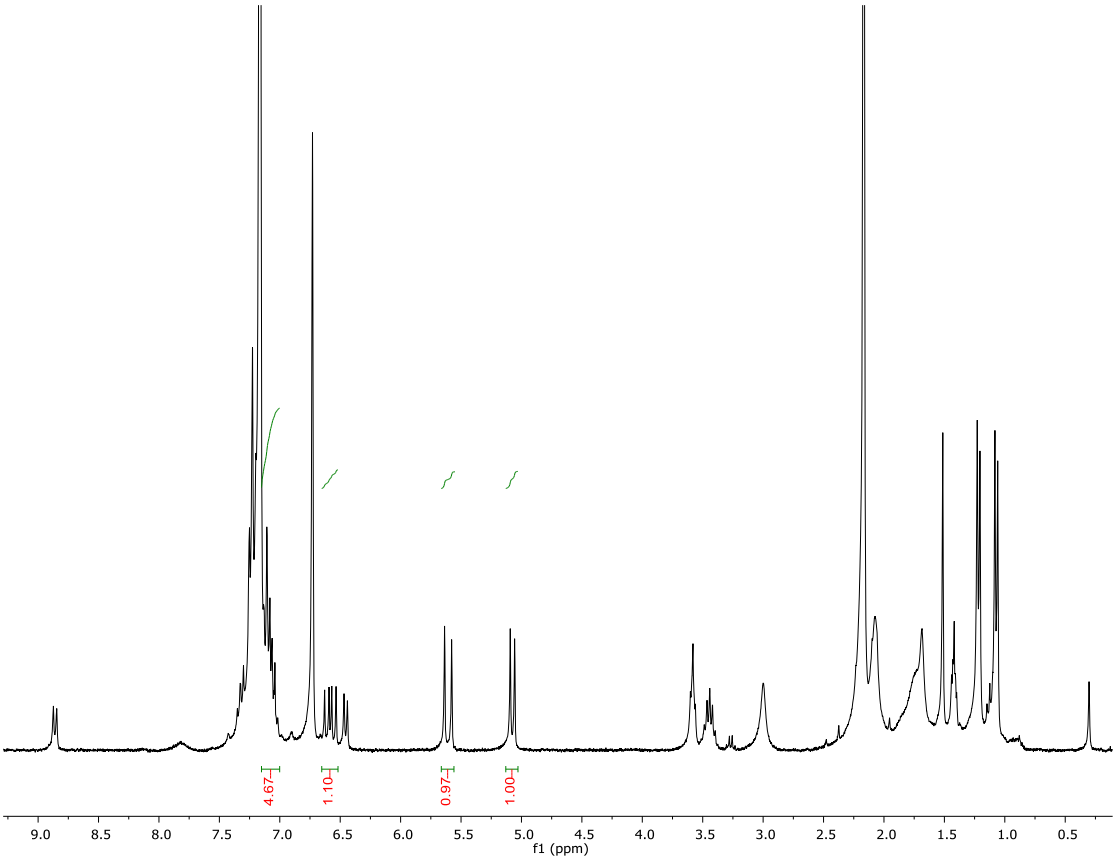

Figure 2.30. Crude ^{1}HNMR for reaction with phenylthiirane to form styrene (**32**). (C_6D_6)

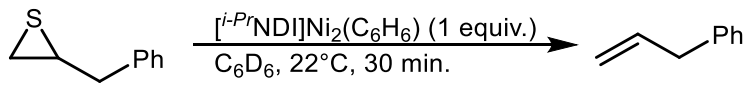

38 39

In an NMR tube equipped with a J-Young valve, [$^{i\text{-}Pr}$NDI]$Ni_2(C_6H_6)$ (**1**) (2 mg, 0.0027 mmol, 1.0 equiv) and 2-benzylthiirane[73] (**38**) (0.41 mg, 0.0027 mmol, 1.0 equiv) were dissolved in C_6D_6 (0.5 mL). The solution was observed to undergo an immediate color change from red-brown to blackish-green. The reaction was monitored by ^{1}HNMR which revealed the presence of allylbenzene (**39**) (80% yield) and unreacted starting material. ^{1}HNMR (300 MHz, C_6D_6) δ 7.10 – 7.04 (m, 5H), 6.00 – 5.81 (m, 1H), 5.11 – 4.96 (m, 2H), 3.23 (d, J = 6.8 Hz, 2H).

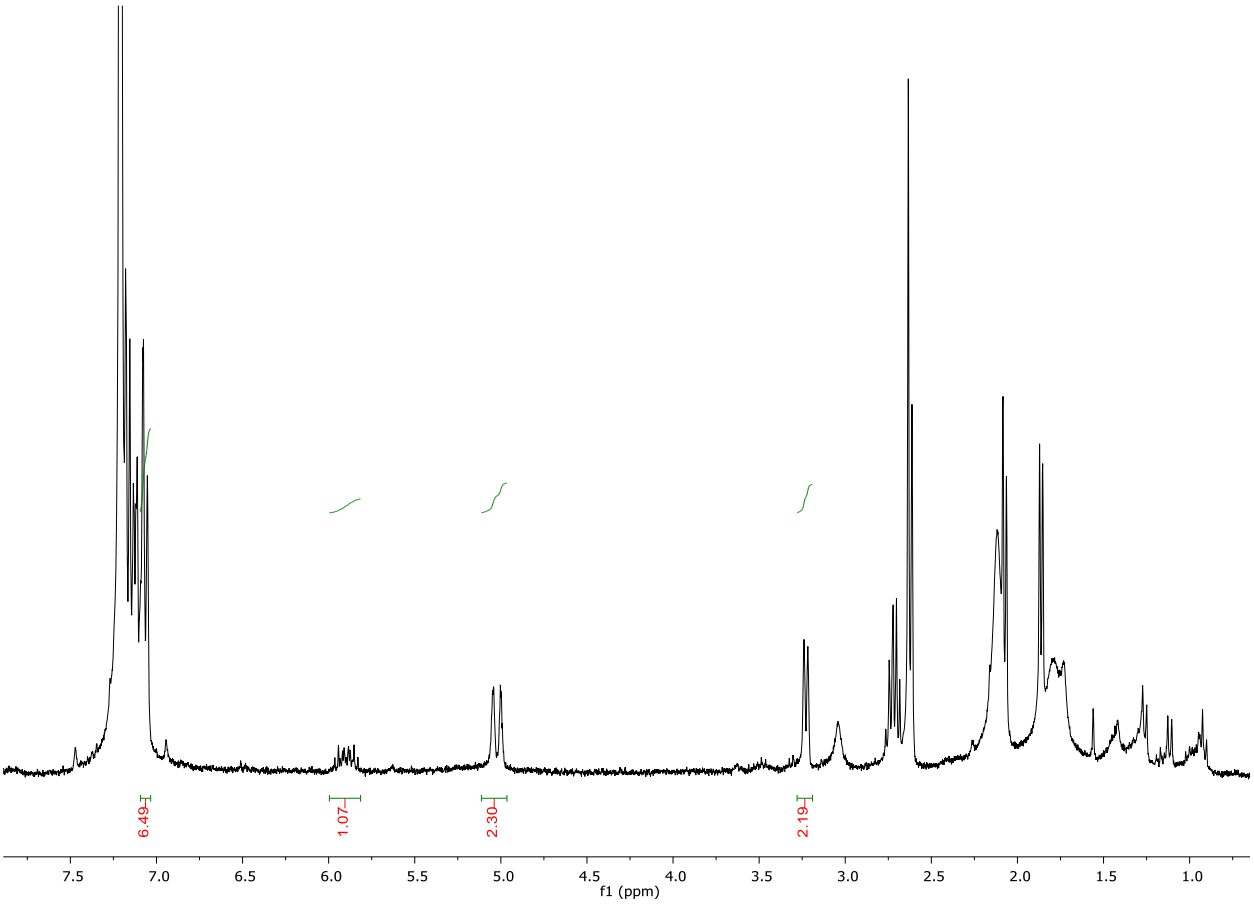

Figure 2.31. Crude ^{1}HNMR for reaction with 2-benzylthiirane to form allylbenzene (**39**). (C_6D_6)

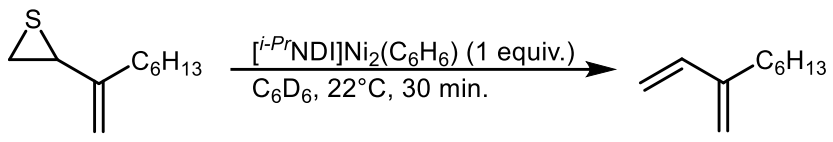

40 41

In an NMR tube equipped with a J-Young valve, [$^{i\text{-}Pr}$NDI]$Ni_2(C_6H_6)$ (**1**) (2 mg, 0.0027 mmol, 1.0 equiv) and 2-(oct-1-en-2-yl)thiirane[70] (**40**) (0.46 mg, 0.0027 mmol, 1.0 equiv) were dissolved in C_6D_6 (0.5 mL). The solution was observed to undergo an immediate color change from red-brown to blackish-green. The reaction was monitored by ^{1}HNMR which revealed the presence of 3-methylenenon-1-ene (**41**) (74% yield), unreacted starting material, and mesitylene as an internal standard. ^{1}HNMR (300 MHz, C_6D_6) δ 6.43 (dd, *J* = 17.3, 10.9 Hz, 1H), 5.26 (d, *J* = 17.6 Hz, 2H), 5.03 (d, *J* = 6.7 Hz, 5H), 1.27 (s, 14H). GC/MS: m/z = 138.34 g/mol

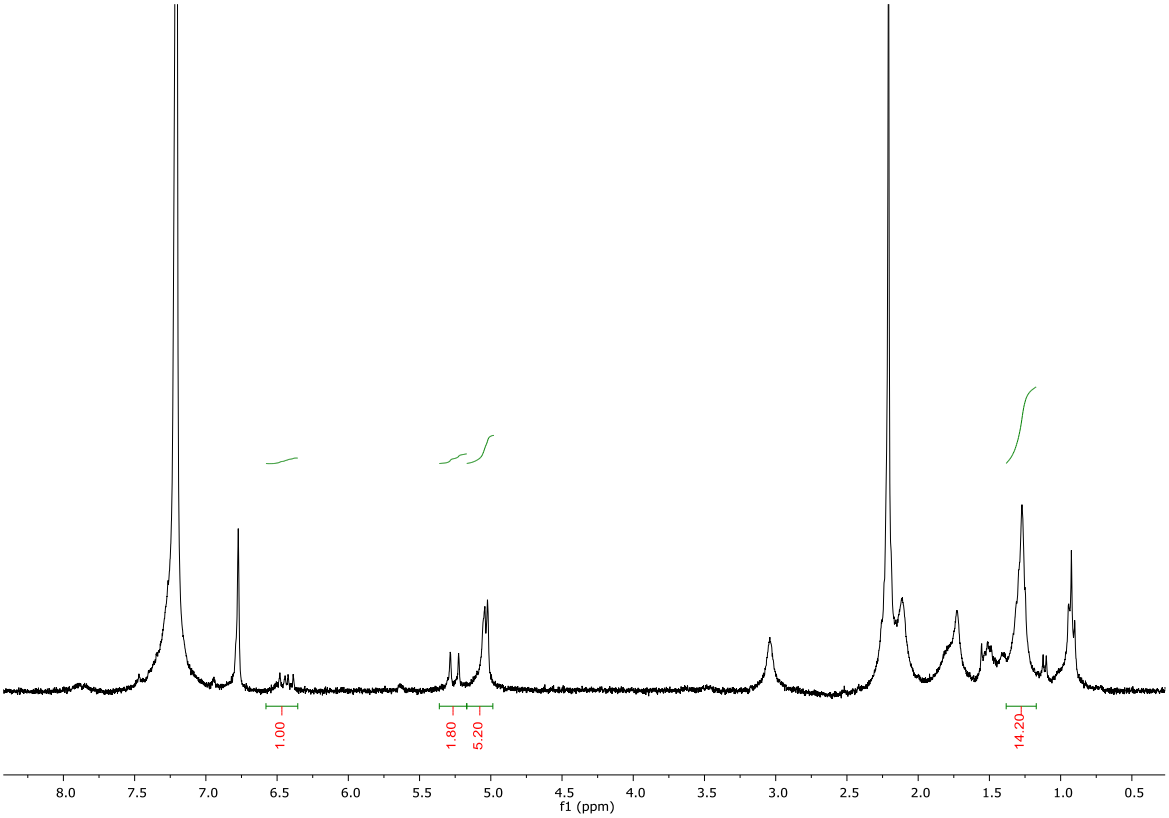

Figure 2.32. Crude ^{1}HNMR of 3-methylenenon-1-ene (**41**). (C_6D_6)

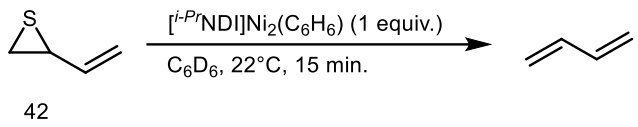

In an NMR tube equipped with a J-Young valve, [$^{i\text{-}Pr}$NDI]$Ni_2(C_6H_6)$ (**1**) (2 mg, 0.0027 mmol, 1.0 equiv) and vinylthiirane[74] (**38**) (0.24 mg, 0.0027 mmol, 1.0 equiv), and mesitylene (0.33 mg, 0.0027 mmol, 1.0 equiv.) were dissolved in C_6D_6 (0.5 mL). The solution was observed to undergo an immediate color change from red-brown to blackish-green. The reaction was monitored by ^{1}HNMR which revealed the presence of 1,3-butadiene (**42**) (99% yield) and mesitylene as an internal standard. ^{1}HNMR (400 MHz, C_6D_6) δ 6.28 – 6.12 (m, 1H), 5.08 – 4.96 (m, 1H), 4.95 – 4.88 (m, 1H).

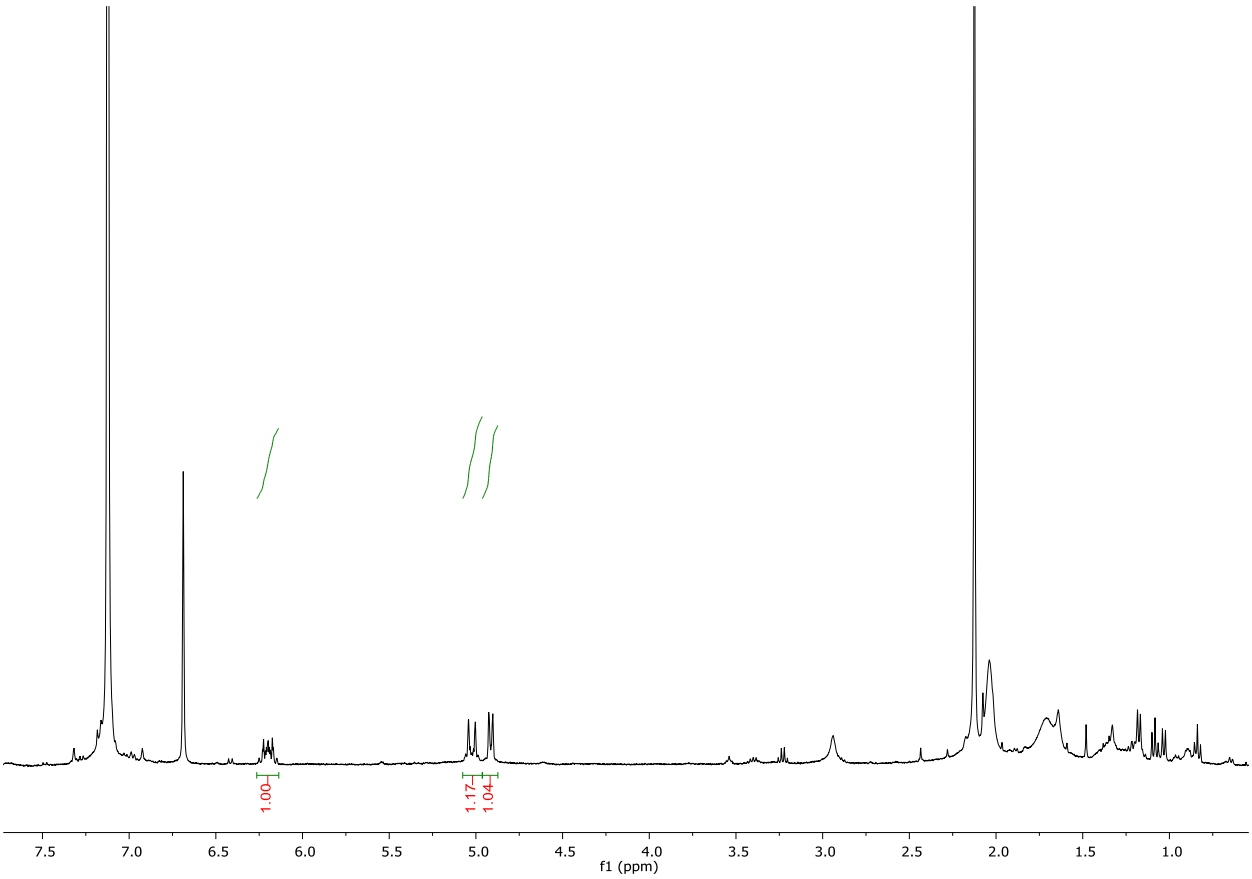

Figure 2.33. Crude ^{1}HNMR of 1,3-butadiene. (C_6D_6)

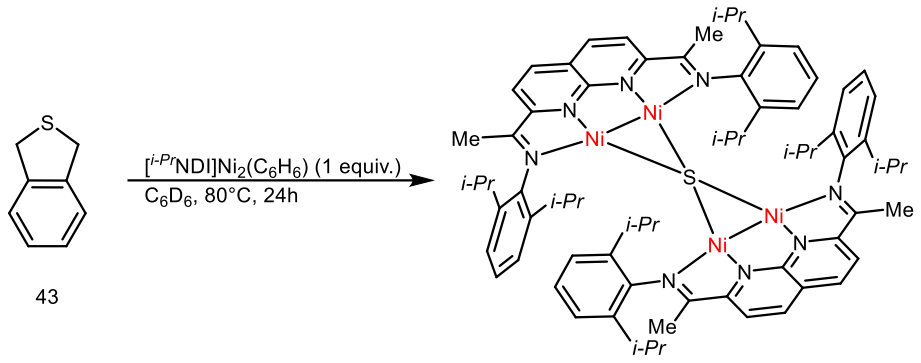

In an NMR tube equipped with a J-Young valve, [$^{i\text{-}Pr}$NDI]$Ni_2(C_6H_6)$ (**1**) (2 mg, 0.0027 mmol, 1.0 equiv) and 1,3-dihydrobenzo[c]thiophene (**43**)[75] (0.37 mg, 0.0027 mmol, 1.0 equiv) were dissolved in C_6H_6 (5 mL). After stirring at 80°C for 24 hours, the reaction mixture was filtered through a glass fiber pad and concentrated. Single crystals suitable for XRD were obtained by cooling saturated solutions of **34** in C_6H_6 to −30°C in a glovebox freezer.

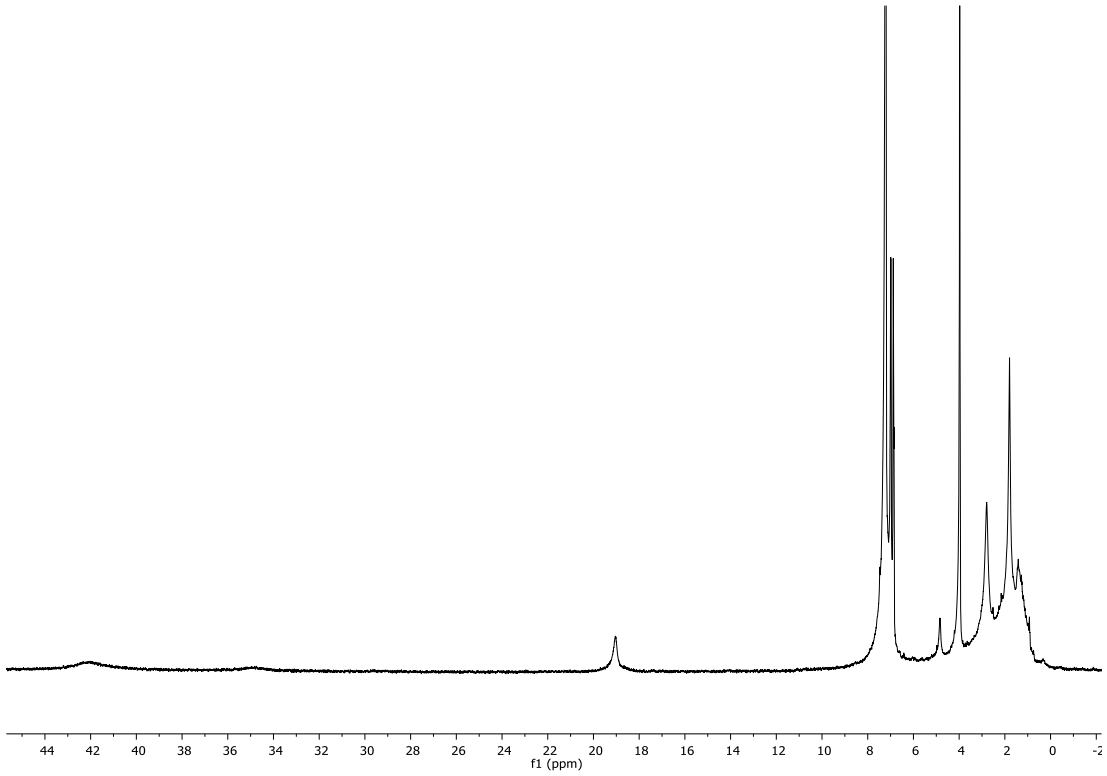

Figure 2.34. ^{1}HNMR of isolated Complex (**43**). (C_6D_6)

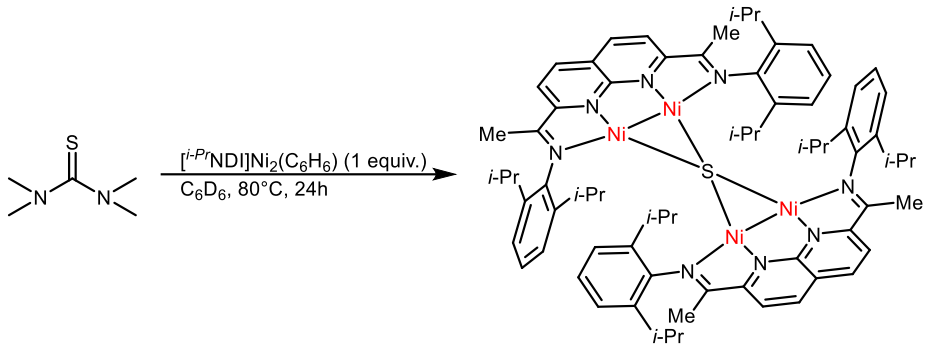

In an NMR tube equipped with a J-Young valve, [$^{i\text{-}Pr}$NDI]$Ni_2(C_6H_6)$ (**1**) (11 mg, 0.015 mmol, 2.0 equiv) and tetramethylthiourea (1 mg, 0.008 mmol, 1.0 equiv) were dissolved in C_6H_6 (5 mL). After stirring at 80°C for 24 hours, the reaction mixture was filtered through a glass fiber pad and concentrated. Single crystals suitable for XRD were obtained by cooling saturated solutions of **34** in C_6H_6 to −30°C in a glovebox freezer.

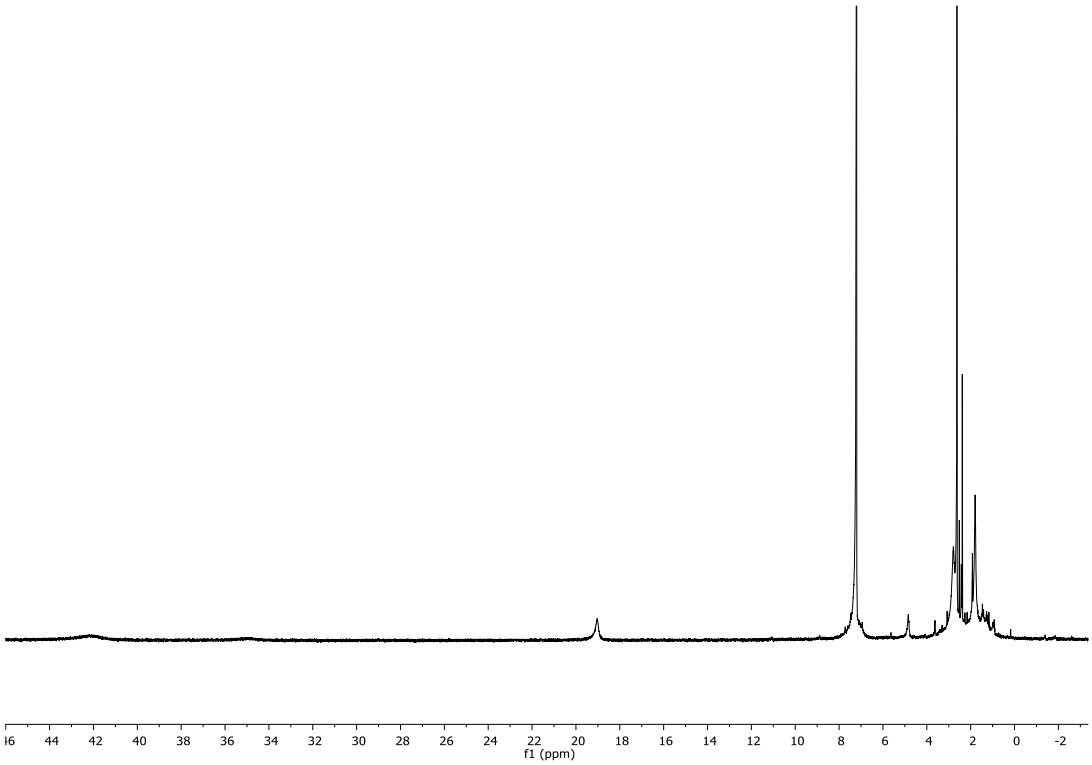

Figure 2.35. ^{1}HNMR of isolated Complex (**34**). (C_6D_6)

APPENDIX A. CRYSTAL STRUCTURE DATA

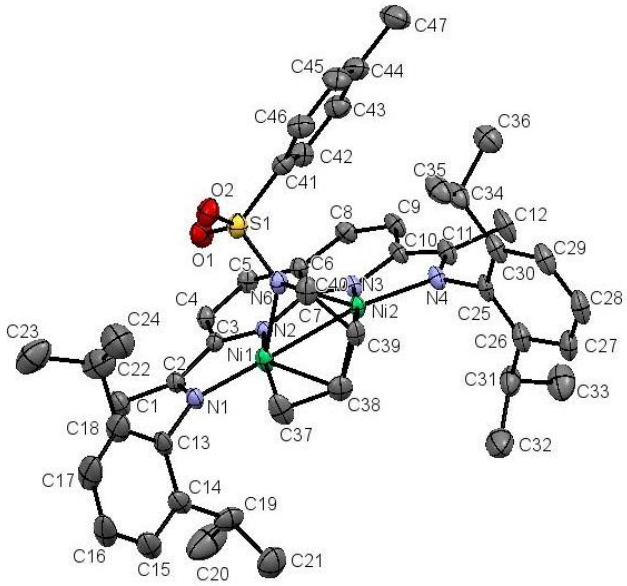

Figure A1. Crystal structure ORTEP diagram of complex **2.** Ellipsoids are shown at 50% probability level.

Table A1. Crystal, Data Collection and Refinement Parameters.

Complex 2	
Crystal data	
Chemical formula	$C_{47}H_{57}N_5Ni_2O_2S\cdot1.427(C_4H_{10}O)$
Temperature (K)	100
M_r	979.19
Crystal System	monoclinic
Space group	$P2_1/n$
a, b, c (Å)	16.3857 (6), 17.7788 (6), 18.3150 (6)
β (°)	108.6811 (11)
V (Å^3)	5054.4 (3)
Z	4
F(000)	2087.7
D_x (Mg m^{-3})	1.287

Radiation type	Mo $K\alpha$
No. of reflections for cell measurement	9826
θ range (°) for cell measurement	2.3–30.5
μ (mm^{-1})	0.83
Crystal shape	Block
Colour	Black
Crystal size (mm)	0.35 × 0.26 × 0.18
Data collection	
Diffractometer	Bruker AXS D8 Quest CMOS diffractometer
Radiation source	I-mu-S microsource X-ray tube
Monochromator	Laterally graded multilayer (Goebel) mirror
Scan method	ω and phi scans
Absorption correction	Multi-scan Apex2 v2014.1-1 (Bruker, 2014)
T_{min}, T_{max}	0.594, 0.746
No. of measured, independent and observed [$I > 2\square(I)$] reflections	42234, 12459, 9102
R_{int}	0.048
θ values (°)	θ_{max} = 28.3, θ_{min} = 2.3
$(\sin \theta/\lambda)_{max}$ ($Å^{-1}$)	0.667
Range of h, k, l	h = -21→21, k = -23→23, l = -24→23
Refinement	
Refinement on	F^2
$R[F^2 > 2\sigma(F^2)]$, $wR(F^2)$, S	0.072, 0.165, 1.10
H-atom parameters	constrained
No. of reflections	12459

No. of parameters	722
No. of restraints	306
	$w = 1/[\sigma^2(F_o^2) + (0.0139P)^2 + 24.8175P]$ where $P = (F_o^2 + 2F_c^2)/3$
$(\Delta/\sigma)_{max}$	< 0.001
$\Delta\rho_{max}$, $\Delta\rho_{min}$ (e Å^{-3})	1.33, -1.07
Extinction method	*SHELXL2014*/7 (Sheldrick 2014, $Fc^*=kFc[1+0.001xFc^2\lambda^3/\sin(2\theta)]^{-1/4}$
Extinction coefficient	0.0012 (2)

Complex 2:

Areas within the structure are filled with disordered solvate molecules. The roughly rectangular area was modeled as being occupied by four partially occupied ether molecules arranged around an inversion center. The four molecules were refined as having similar geometries, and U_{ij} components of ADPs were restrained as being similar if closer than 1.7 Å. Occupancies refined to 0.423(7), 0.442(8), 0.131(7) and 0.431(8).

Ni atom Ni2 was refined as disordered over two positions. The two atoms were constrained to have identical ADPs. The occupancy ratio refined to 0.918(5) to 0.082(5).

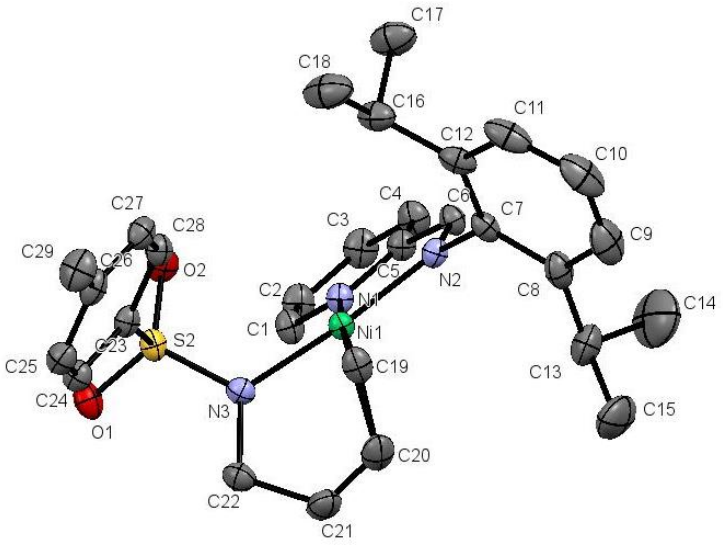

Figure A2. Crystal structure ORTEP diagram of complex 4. Ellipsoids are shown at 50% probability level.

Table A2. Crystal, Data Collection and Refinement Parameters.

	Complex 4
Crystal data	
Chemical formula	$C_{29}H_{35}N_3NiO_2S\cdot1.285(C_4H_{10}O)$
Temperature (K)	100
M_r	643.59
Crystal System	monoclinic
Space group	$P2_1/n$
a, b, c (Å)	15.2562 (2), 10.9383 (2), 21.2687 (4)
β (°)	108.5589 (6)
V (Å^3)	3364.68 (10)
Z	4
F(000)	1375.9
D_x (Mg m^{-3})	1.270
Radiation type	Mo $K\alpha$
No. of reflections for cell measurement	37511

θ range (°) for cell measurement	2.0–27.9
μ (mm^{-1})	0.68
Crystal shape	Block
Colour	Blue
Crystal size (mm)	0.41 × 0.37 × 0.29
Data collection	
Diffractometer	Nonius Kappa CCD diffractometer
Radiation source	fine focus X-ray tube
Monochromator	Graphite
Scan method	ω and ϕ scans
Absorption correction	Multi-scan *SCALEPACK* (Otwinowski & Minor, 1997)
T_{min}, T_{max}	0.591, 0.828
No. of measured, independent and observed [$I > 2\sigma(I)$] reflections	37511, 7829, 6670
R_{int}	0.122
□ values (°)	θ_{max} = 27.9, θ_{min} = 2.0
$(\sin \theta/\lambda)_{max}$ ($Å^{-1}$)	0.659
Range of *h*, *k*, *l*	h = -20→20, k = -13→13, l = -28→28
Refinement	
Refinement on	F^2
$R[F^2 > 2\sigma(F^2)]$, $wR(F^2)$, S	0.057, 0.154, 1.07
H-atom parameters	constrained
No. of reflections	7829
No. of parameters	522
No. of restraints	531

	$w = 1/[\sigma^2(F_o^2) + (0.0748P)^2 + 3.9318P]$ where $P = (F_o^2 + 2F_c^2)/3$
$(\Delta/\sigma)_{max}$	0.002
$\Delta\rho_{max}$, $\Delta\rho_{min}$ (e Å^{-3})	0.84, -0.62
Extinction method	*SHELXL2014*/7 (Sheldrick 2014, $Fc^{*}=kFc[1+0.001xFc^2\lambda^3/\sin(2\theta)]^{-1/4}$
Extinction coefficient	0.0087 (10)

Complex 4:

Channels between molecules is occupied by disordered solvate molecules. The solvate was tentatively refined as diethyl ether, and four different consecutively overlapping moieties were refined. All four moieties were restrained to have similar geometries, and U_{ij} components of ADPs of all partially occupied atoms were restrained to be similar if closer than 1.7 Å. Ether O-C bonds were restrained to 1.40(2) Å, ether C-C bonds to 1.45(2) Å. A weak anti-bumping restraint was applied to keep low occupancy methyl ether groups from approaching the main molecule too closely. Subject to these conditions the occupancy rates for the ether molecules refined to 0.540(6), 0.223(6), 0.308(6) and 0.214(5).

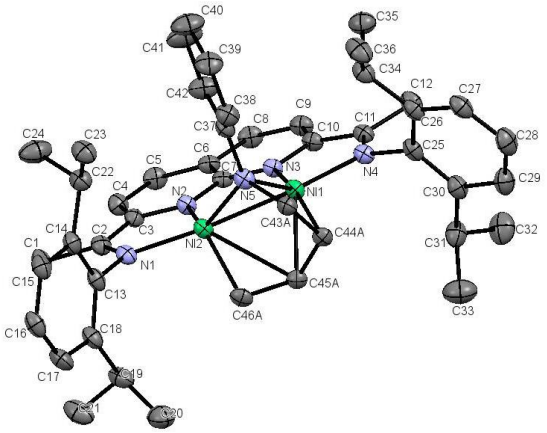

Figure A3. Crystal structure ORTEP diagram of complex **25** showing the atom-labelling scheme. Displacement ellipsoids are drawn at the 50% probability level. H atoms and minor moieties are omitted for clarity.

Table A3. Experimental details for complex **25**.

Crystal data	
Chemical formula	$2(C_{46}H_{55}N_5Ni_2)\cdot C_5H_{12}$
M_r	1662.88
Crystal system, space group	Triclinic, *P*1
Temperature (K)	100
a, *b*, *c* (Å)	10.7300 (5), 14.4010 (7), 15.2250 (13)
α, β, γ (°)	75.227 (3), 80.308 (3), 70.869 (2)
V (Å^3)	2139.9 (2)
Z	1
Radiation type	Cu *K*α
μ (mm^{-1})	1.38
Crystal size (mm)	0.12 × 0.09 × 0.09
Data collection	
Diffractometer	Bruker AXS D8 Quest CMOS diffractometer
Absorption correction	Multi-scan *SADABS* 2016/2: Krause, L., Herbst-Irmer, R., Sheldrick G.M. & Stalke D., J. Appl. Cryst. 48 (2015) 3-10
T_{min}, T_{max}	0.563, 0.754
No. of measured, independent and observed [$I > 2\sigma(I)$] reflections	26774, 8450, 7186

R_{int}	0.056
$(\sin \theta/\lambda)_{max}$ ($Å^{-1}$)	0.625
Refinement	
$R[F^2 > 2\sigma(F^2)]$, $wR(F^2)$, S	0.052, 0.146, 1.03
No. of reflections	8450
No. of parameters	596
No. of restraints	124
H-atom treatment	H atoms treated by a mixture of independent and constrained refinement
$\Delta\rho_{max}$, $\Delta\rho_{min}$ (e $Å^{-3}$)	0.70, −0.46

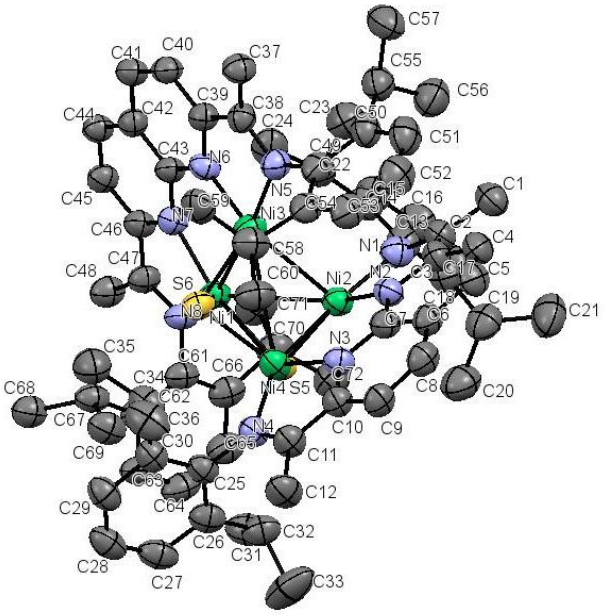

A4. Crystal structure ORTEP diagram of complex **33**. Ellipsoids are shown at 50% probability level.

Table A4. Experimental details of complex **33**.

Crystal data	
Chemical formula	$C_{72}H_{88}N_8Ni_4S_2 \cdot 0.654(C_6H_{16}OSi_2) \cdot 1.692(C_6H_6)$
M_r	1601.43
Crystal system, space group	Monoclinic, $P2_1/n$
Temperature (K)	100
a, b, c (Å)	14.8576 (4), 24.4483 (7), 23.1164 (6)
β (°)	107.126 (2)
V (Å^3)	8024.6 (4)
Z	4
Radiation type	Cu $K\alpha$
μ (mm^{-1})	2.11
Crystal size (mm)	0.25 × 0.08 × 0.02
Data collection	
Diffractometer	Rigaku Rapid II curved image plate diffractometer
Absorption correction	Multi-scan *SCALEPACK* (Otwinowski & Minor, 1997)
T_{min}, T_{max}	0.643, 0.959
No. of measured, independent and observed [$I > 2\sigma(I)$] reflections	160488, 15044, 9724
R_{int}	0.115
$(\sin \theta/\lambda)_{max}$ (Å^{-1})	0.619
Refinement	
$R[F^2 > 2\sigma(F^2)]$, $wR(F^2)$, S	0.069, 0.198, 1.07
No. of reflections	15044
No. of parameters	1073
No. of restraints	504
H-atom treatment	H-atom parameters constrained $w = 1/[\sigma^2(F_o^2) + (0.0703P)^2 + 16.7547P]$ where $P = (F_o^2 + 2F_c^2)/3$
$\Delta\rho_{max}$, $\Delta\rho_{min}$ (e Å^{-3})	0.86, −0.70

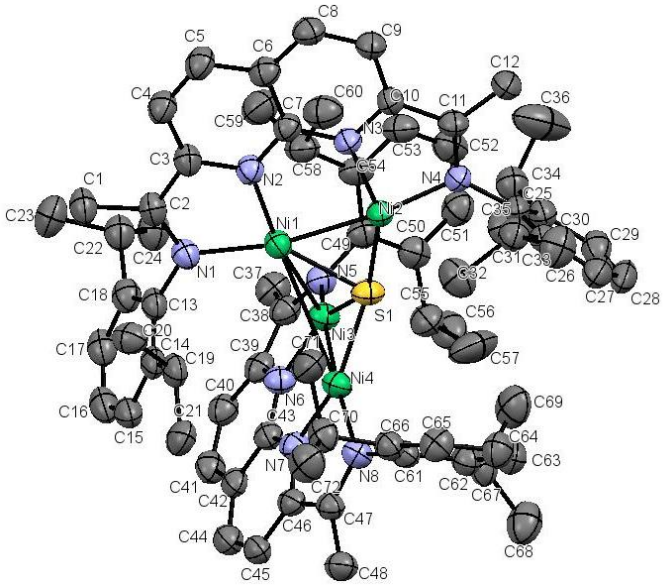

A5. Crystal structure ORTEP diagram of complex **34**. Ellipsoids are shown at 50% probability level.

Table A5. Experimental details of complex **34**.

Crystal data	
Chemical formula	$C_{72}H_{88}N_8Ni_4S$
M_r	1332.40
Crystal system, space group	Orthorhombic, $Pna2_1$
Temperature (K)	150
a, b, c (Å)	23.2910 (14), 16.1954 (10), 17.7232 (12)
V (Å^3)	6685.3 (7)
Z	4
Radiation type	Cu $K\alpha$
μ (mm^{-1})	1.91
Crystal size (mm)	0.40 × 0.34 × 0.03
Data collection	
Diffractometer	Bruker AXS D8 Quest CMOS diffractometer
Absorption correction	Multi-scan *SADABS* 2016/2: Krause, L., Herbst-Irmer, R., Sheldrick G.M. & Stalke D., J. Appl. Cryst. 48 (2015) 3-10

T_{min}, T_{max}	0.439, 0.754
No. of measured, independent and observed [$I > 2\sigma(I)$] reflections	20726, 10838, 9659
R_{int}	0.046
$(\sin \theta/\lambda)_{max}$ (Å^{-1})	0.626
Refinement	
$R[F^2 > 2\sigma(F^2)]$, $wR(F^2)$, S	0.050, 0.136, 1.04
No. of reflections	10838
No. of parameters	786
No. of restraints	1
H-atom treatment	H-atom parameters constrained
$\Delta\rho_{max}$, $\Delta\rho_{min}$ (e Å^{-3})	0.85, −0.72
Absolute structure	Flack x determined using 3251 quotients [(I+)-(I-)]/[(I+)+(I-)] (Parsons, Flack and Wagner, Acta Cryst. B69 (2013) 249-259).
Absolute structure parameter	0.001 (16)

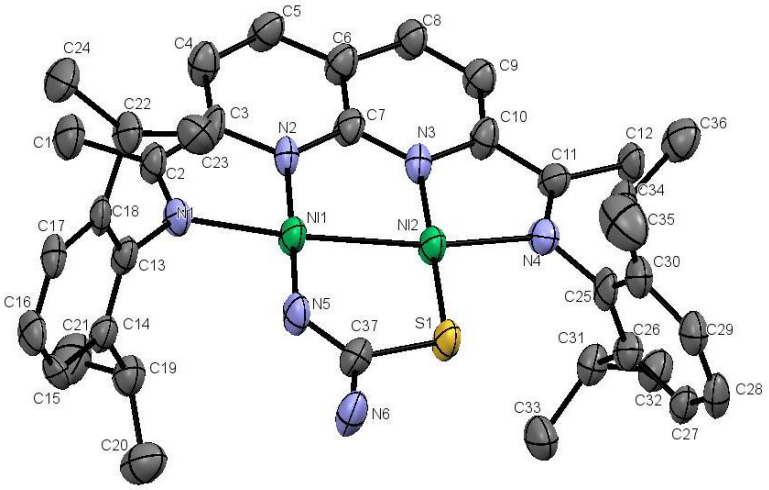

A6. Crystal structure ORTEP diagram of complex **35**. Ellipsoids are shown at 50% probability level.

Table A6. Experimental details of complex **35**.

Crystal data	
Chemical formula	$C_{37}H_{47}N_6Ni_2S$
M_r	677.91
Crystal system, space group	Triclinic, *P*1
Temperature (K)	293
a, *b*, *c* (Å)	8.4489 (17), 12.940 (3), 16.202 (3)
α, β, γ (°)	84.81 (3), 85.53 (3), 81.67 (3)
V (Å^3)	1741.7 (6)
Z	2
Radiation type	Cu *K*α
μ (mm^{-1})	2.17
Crystal size (mm)	× ×
Data collection	
Diffractometer	?
Absorption correction	–
No. of measured, independent and observed [$I > 2\sigma(I)$] reflections	13487, 4566, 2752
R_{int}	0.086
$(\sin \theta/\lambda)_{max}$ (Å^{-1})	0.618
Refinement	

$R[F^2 > 2\sigma(F^2)]$, $wR(F^2)$, S	0.084, 0.260, 1.09
No. of reflections	4566
No. of parameters	425
H-atom treatment	H-atom parameters constrained
$\Delta\rho_{max}$, $\Delta\rho_{min}$ (e Å^{-3})	1.34, −0.77

APPENDIX B. DFT CALCULATIONS

Computational Methods. Geometry optimizations were performed using the Gaussian09 software package.[i] All geometries were fully optimized at the BP86/6-311G(d,p) level of DFT. Stationary points were verified by frequency analysis.

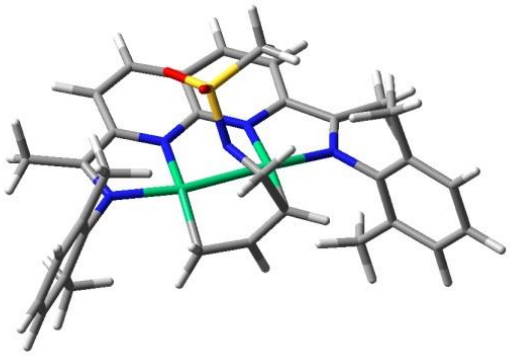

Structure 01

Charge: 0

Multiplicity: 1

Imaginary Frequencies: 0

Energy: –5118.31624927

Free Energy (298 K): –5117.743882

C	-4.81423500	1.81310700	-0.43711400
Ni	-1.17536700	-0.25991800	-0.34530900
C	-3.39919200	1.34839100	-0.49370300
Ni	1.22076100	-0.20826800	-0.10481400
C	-2.30400500	2.27363200	-0.51654700
C	-2.39457700	3.67976600	-0.49701900
C	-1.24440800	4.43937500	-0.51100800
C	0.01918800	3.80411500	-0.51847800
C	0.02651600	2.38783500	-0.50442000
C	1.28512700	4.44926400	-0.55894600

C	2.43916100	3.70463200	-0.56605700
C	2.37612400	2.29008000	-0.52138400
C	3.45925200	1.36643300	-0.51278600
C	4.88682000	1.75177700	-0.70170600
C	-4.00120500	-0.95873500	-0.51049000
C	-4.58388900	-1.31956100	-1.73717700
C	-5.50260300	-2.37017900	-1.74888400
C	-5.82842000	-3.04740100	-0.57926000
C	-5.22617600	-2.68457200	0.62036000
C	-4.29892100	-1.64286500	0.67941600
C	4.04868400	-0.93032400	-0.49062800
C	4.33430200	-1.41240900	-1.78019300
C	5.25512000	-2.45347900	-1.90819800
C	5.87164300	-3.00830000	-0.79181300
C	5.56309200	-2.53030800	0.47700500
C	4.64745900	-1.49125200	0.64815600
C	-1.19583800	-2.12026800	-0.78663200
C	0.22758600	-2.01050400	-0.91949500
C	1.12536200	-2.10469400	0.19527400
C	0.48290100	-1.93578900	1.54846900
N	-3.02346100	0.07399400	-0.49426200
N	-1.09877200	1.64725100	-0.54137700
N	1.16257000	1.65859400	-0.48683100
N	3.07289700	0.09125100	-0.34310000
C	-3.60702400	-1.28266500	1.95378300
H	-4.00833400	-1.84082500	2.80238900
H	-2.53347400	-1.49967700	1.89200900
H	-3.66976200	-0.21374300	2.18571000
C	-4.20911500	-0.59393300	-2.99186700
C	3.64176200	-0.82826400	-2.97209300
H	2.55480000	-0.80576900	-2.82534500

H	3.93595900	0.21253300	-3.15525300
H	3.86042500	-1.39877000	-3.87760400
C	4.27162600	-0.98642200	2.00369700
H	4.49808300	0.07946600	2.12938500
H	3.18814800	-1.07826700	2.15398100
H	4.78004300	-1.53902800	2.79703100
H	-5.46938700	-3.21765900	1.53698600
H	-6.54506000	-3.86351400	-0.60422000
H	-5.95928900	-2.65666500	-2.69403900
H	-4.64197000	-1.07628800	-3.87149700
H	-3.12034300	-0.55439400	-3.11776900
H	-4.55043800	0.44867700	-2.98556200
H	-5.03973500	2.24892000	0.54384400
H	-5.00822700	2.59092400	-1.18335500
H	-5.51427500	0.99295000	-0.60359300
H	-3.37057800	4.15327800	-0.45325800
H	-1.29637000	5.52486800	-0.51024100
H	1.32808700	5.53460600	-0.59363900
H	3.40599100	4.19776300	-0.59138200
H	5.52374300	1.33440900	0.08615800
H	5.28652000	1.36823000	-1.64876400
H	5.01763600	2.83513000	-0.70563100
H	6.03098200	-2.96838700	1.35613800
H	6.58465800	-3.81904200	-0.91024700
H	5.48072800	-2.83422600	-2.90218100
H	0.66064100	-2.10072200	-1.91554700
H	2.07721000	-2.62527100	0.09739400
H	-0.29865500	-2.66846100	1.81415200
H	1.22874700	-1.96366800	2.35473900
H	-1.57478500	-2.69822000	0.06364800
H	-1.75383500	-2.31502100	-1.70337100

N	-0.07602400	-0.56947600	1.36720000
S	-0.38797200	0.28120200	2.76364200
O	-0.86046700	-0.63453700	3.80592600
O	-1.18754000	1.44886600	2.39137700
C	1.21494200	0.89499100	3.28678700
H	1.86899500	0.05112200	3.51423600
H	1.64169000	1.50945700	2.49044100
H	1.05915500	1.49047200	4.18731000

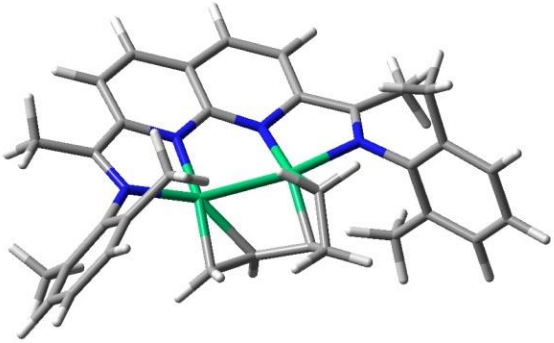

Structure 02

Charge: 0

Multiplicity: 1

Imaginary Frequencies: 0

Energy: –4514.34236588

Free Energy (298 K): –4513.793433

C	-4.88091400	1.85807900	0.61354700
Ni	-1.27213300	-0.11537100	-0.31631200
C	-3.48516700	1.41428100	0.32013200
Ni	1.12115600	-0.08594100	-0.08881700
C	-2.41236400	2.34726000	0.23964000
C	-2.49924400	3.72796300	0.39264600

C	-1.35096500	4.50986000	0.33153300
C	-0.09328800	3.90776700	0.13762300
C	-0.07434100	2.48221200	-0.02711600
C	1.15594900	4.57063600	0.13123300
C	2.32624400	3.83580600	0.05177400
C	2.29032900	2.44454200	-0.07263500
C	3.37228100	1.55325400	0.04264000
C	4.80354300	1.96842500	0.00491100
C	-4.05333300	-0.91752100	0.19664200
C	-4.99522500	-1.07967800	-0.83694900
C	-5.84539700	-2.18857600	-0.79655800
C	-5.76547000	-3.12180000	0.22944400
C	-4.80750100	-2.96650400	1.22647600
C	-3.93877400	-1.87781400	1.22126300
C	3.99716200	-0.74656700	0.10363800
C	4.39226700	-1.19471900	-1.17533600
C	5.26376400	-2.28139700	-1.26676600
C	5.74729600	-2.90934800	-0.12421000
C	5.37277700	-2.44319000	1.13091500
C	4.50280000	-1.35946000	1.26705400
C	-1.46609600	-1.76706600	-1.18629800
C	-0.13335500	-1.28910100	-1.43738800
C	1.05121500	-1.93935700	-0.82442200
C	0.91143000	-3.08501500	0.11382900
N	-3.11488600	0.13997800	0.18683200
N	-1.19147900	1.74738300	-0.01634700
N	1.06555700	1.79149100	-0.23007900
N	3.01575300	0.26614500	0.21433500
C	-2.86961400	-1.73074300	2.25358000
H	-2.85811700	-2.57481600	2.94765600
H	-1.88969200	-1.66004400	1.75918500

H	-2.97279900	-0.80553900	2.83089200
C	-5.05695200	-0.11506300	-1.98124400
C	3.89318100	-0.50401300	-2.40949900
H	2.84880400	-0.18558600	-2.30266300
H	4.46180200	0.41038900	-2.62160800
H	3.97856200	-1.14736200	-3.28913400
C	4.15100300	-0.82215200	2.62162500
H	4.33259600	-1.56293200	3.40469400
H	4.75241500	0.06197100	2.86624800
H	3.10830700	-0.49529300	2.67780800
H	-4.72164400	-3.70321800	2.02259300
H	-6.43445000	-3.97759800	0.24201100
H	-6.57088000	-2.31953900	-1.59711100
H	-5.52476400	-0.57550200	-2.85526500
H	-4.05697600	0.23092300	-2.26598900
H	-5.64111300	0.78166800	-1.74148600
H	-4.90215200	2.50242300	1.49809500
H	-5.30325300	2.44367000	-0.21126600
H	-5.54037500	1.00772900	0.79634600
H	-3.46834400	4.19014400	0.55935800
H	-1.40881300	5.58683100	0.46276800
H	1.18697000	5.64932700	0.25541700
H	3.28610100	4.33755100	0.13562600
H	4.91207100	3.05191600	-0.05893300
H	5.34427200	1.62051800	0.89251100
H	5.32458900	1.53225000	-0.85593000
H	5.76052600	-2.92163400	2.02823900
H	6.41769400	-3.75971500	-0.21192700
H	5.56187600	-2.63610400	-2.25154000
H	0.07036700	-0.86233900	-2.42116700
H	1.99622900	-1.92422800	-1.36444900

H	-0.05640800	-3.57673600	0.15920700
H	1.75049500	-3.77536600	0.12480800
H	-1.62777200	-2.66216900	-0.58168100
H	-2.19961300	-1.67976900	-1.98977700
C	1.10601000	-1.83460900	0.89932300
H	2.02944400	-1.78306500	1.46686900
H	0.20126800	-1.47536300	1.40374600

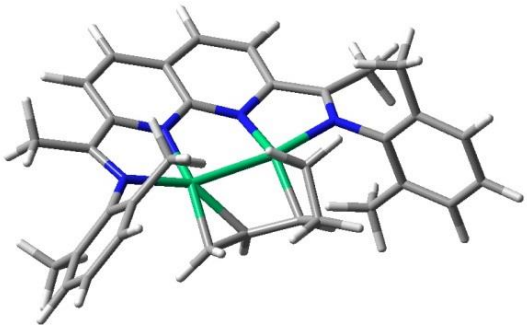

Structure 03

Charge: 0

Multiplicity: 1

Imaginary Frequencies: 1

Energy: –4514.34235178

Free Energy (298 K): –4513.792653

C	-4.88200100	1.85724300	0.60756500
Ni	-1.27179300	-0.11681900	-0.31491600
C	-3.48580900	1.41319200	0.31661800
Ni	1.12169500	-0.08820500	-0.08528100
C	-2.41299800	2.34627200	0.23657000

C	-2.50072200	3.72703500	0.38821200
C	-1.35251900	4.50923900	0.32899900
C	-0.09434400	3.90729600	0.13866300
C	-0.07449600	2.48164600	-0.02579900
C	1.15485800	4.57042700	0.13526100
C	2.32557600	3.83597700	0.05901600
C	2.29049900	2.44465600	-0.06564400
C	3.37253900	1.55385400	0.05122900
C	4.80365100	1.97057000	0.02397800
C	-4.05431800	-0.91851900	0.19493200
C	-4.99360300	-1.08211800	-0.84081700
C	-5.84409600	-2.19076900	-0.80076000
C	-5.76689300	-3.12234200	0.22697000
C	-4.81157300	-2.96552200	1.22626500
C	-3.94277700	-1.87687100	1.22161200
C	3.99774800	-0.74706600	0.10398000
C	4.39705700	-1.18351500	-1.17832700
C	5.26614100	-2.27099500	-1.27780100
C	5.74332900	-2.91252100	-0.13987600
C	5.36484900	-2.45860300	1.11817100
C	4.49728800	-1.37359300	1.26262100
C	-1.46496900	-1.77056300	-1.18263200
C	-0.13598100	-1.28764700	-1.44246300
C	1.05489900	-1.92679600	-0.83556000
C	0.92845300	-3.06739700	0.11051700
N	-3.11552000	0.13876600	0.18544300
N	-1.19148700	1.74641700	-0.01647200
N	1.06610300	1.79131000	-0.22554600
N	3.01693100	0.26581200	0.21849200
C	1.10141400	-1.82095400	0.90887800
H	0.18744700	-1.48131400	1.41042300

H	2.01706100	-1.76590800	1.48934000
C	-2.87683000	-1.72760400	2.25687000
H	-2.86593500	-2.57122800	2.95147600
H	-1.89572300	-1.65568000	1.76516100
H	-2.98312500	-0.80224700	2.83339400
C	-5.05196900	-0.11926500	-1.98677000
C	3.90418200	-0.48002400	-2.40779900
H	2.85944300	-0.16220200	-2.30341500
H	4.47426700	0.43613100	-2.60818600
H	3.99368000	-1.11478600	-3.29323600
C	4.14520900	-0.85153300	2.62332500
H	4.23435300	-1.62999800	3.38587400
H	4.81563600	-0.03511800	2.91981300
H	3.13340600	-0.43681100	2.65509300
H	-4.72794500	-3.70089400	2.02386000
H	-6.43597200	-3.97806700	0.23916300
H	-6.56759700	-2.32290200	-1.60291500
H	-5.52021600	-0.57993800	-2.86042500
H	-4.05083800	0.22368400	-2.27123600
H	-5.63393800	0.77941600	-1.74897900
H	-4.90469200	2.50126800	1.49231000
H	-5.30255000	2.44327800	-0.21783000
H	-5.54198700	1.00699800	0.78886700
H	-3.47030800	4.18899300	0.55259500
H	-1.41101100	5.58632400	0.45900000
H	1.18524100	5.64916100	0.25923700
H	3.28499000	4.33815400	0.14539200
H	4.91150800	3.05369800	-0.04669600
H	5.33531600	1.63004700	0.91997000
H	5.33391300	1.52857400	-0.82808500
H	5.74722800	-2.94804200	2.01192100

H	6.41162700	-3.76389200	-0.23387600
H	5.56698700	-2.61622500	-2.26509900
H	0.05960000	-0.85455100	-2.42504400
H	1.99744700	-1.90454700	-1.38014500
H	-0.03153100	-3.57551700	0.15157400
H	1.77631700	-3.74742300	0.12368500
H	-1.61825900	-2.66555600	-0.57558700
H	-2.20404800	-1.68748200	-1.98132800

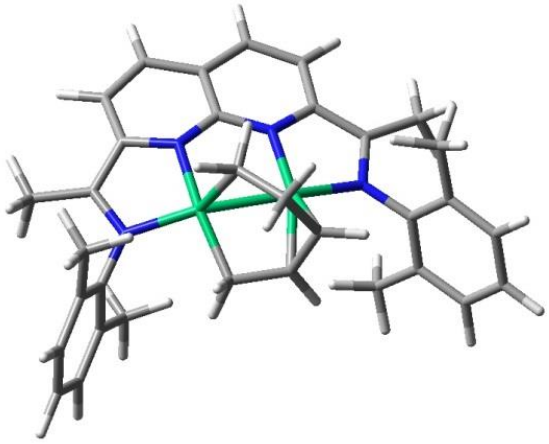

Structure 04

Charge: 0

Multiplicity: 1

Imaginary Frequencies: 0

Energy: –4514.36973831

Free Energy (298 K): –4513.822995

C	4.88676100	1.59532100	0.33467700
Ni	1.16722700	-0.07837500	-0.65032000
C	3.44226900	1.31741600	0.08943700
Ni	-1.11980600	-0.07390600	-0.39993200

C	2.47185200	2.33873600	-0.11793900
C	2.58835800	3.69567600	0.18773400
C	1.44356100	4.47216700	0.31771200
C	0.16603800	3.87656700	0.24007700
C	0.12118700	2.48889600	-0.12640200
C	-1.06505500	4.49548200	0.54667900
C	-2.22811400	3.73994700	0.60276500
C	-2.20714900	2.37605800	0.30771500
C	-3.24392400	1.43066700	0.50070900
C	-4.62829900	1.80017500	0.91424500
C	3.80479700	-1.02364900	0.36166600
C	3.92261800	-1.49026900	1.68188600
C	4.71855400	-2.61117500	1.92348200
C	5.37063000	-3.26265200	0.88201100
C	5.22073600	-2.80454300	-0.42284100
C	4.43445600	-1.68664500	-0.70472400
C	-3.81331000	-0.89520900	0.44021400
C	-3.79238400	-1.72081200	1.57987500
C	-4.67626500	-2.79867800	1.64109800
C	-5.55328300	-3.06424300	0.59482300
C	-5.54731600	-2.25491800	-0.53603300
C	-4.68069000	-1.16494500	-0.63694300
C	0.86110600	-1.94733800	-0.39997000
C	-0.60765700	-2.01845100	-0.36002000
C	-1.37396000	-1.69781800	-1.49027000
C	-0.65020900	-1.24941100	-2.72875900
N	2.94875300	0.07386600	0.10537300
N	1.23372700	1.81581100	-0.44540700
N	-1.03241200	1.78947200	-0.15708700
N	-2.86501900	0.14930500	0.35819800
C	0.23163000	-0.06452400	-2.33901000

H	1.18326500	-0.06684200	-2.90179900
H	-0.25112100	0.89171100	-2.56595500
C	4.21760900	-1.21072300	-2.10683000
H	4.75767700	-1.82757800	-2.82902300
H	3.14965300	-1.23880100	-2.36265400
H	4.53059500	-0.16931000	-2.24925400
C	3.17746100	-0.79965600	2.78120700
C	-2.84094900	-1.42392400	2.69666800
H	-1.81360500	-1.32020000	2.32605500
H	-3.07340200	-0.47124700	3.18671500
H	-2.86251200	-2.20813000	3.45735100
C	-4.63382100	-0.33062000	-1.88073800
H	-5.16573800	0.62252000	-1.77249600
H	-3.60066100	-0.07464900	-2.14532300
H	-5.08892400	-0.85632600	-2.72403800
H	5.71294300	-3.32208000	-1.24362100
H	5.98507900	-4.13501000	1.08585500
H	4.81538600	-2.97767800	2.94347500
H	3.32150900	-1.30445800	3.73962800
H	2.10211000	-0.76552400	2.56439400
H	3.48731700	0.24534700	2.90092700
H	5.51214700	1.08294600	-0.40554800
H	5.11405900	2.66120600	0.28933200
H	5.20398600	1.21297100	1.31166800
H	3.56323900	4.12757100	0.39568900
H	1.52038400	5.52095200	0.59087900
H	-1.08145800	5.55088200	0.80248500
H	-3.15876300	4.20828100	0.91019600
H	-5.36115200	1.59077500	0.12669500
H	-4.94555700	1.21999700	1.78766100
H	-4.70678700	2.85937200	1.16311900

H	-6.21456000	-2.47467500	-1.36715900
H	-6.23112800	-3.91119600	0.65382300
H	-4.66839900	-3.43639000	2.52243600
H	-1.10688800	-2.52536700	0.46903900
H	-2.40332600	-2.04870500	-1.54882700
H	-0.03880800	-2.07334400	-3.13212900
H	-1.36256700	-0.97447600	-3.51612800
H	1.28632600	-2.50137400	-1.25212900
H	1.34311700	-2.28789700	0.52298400

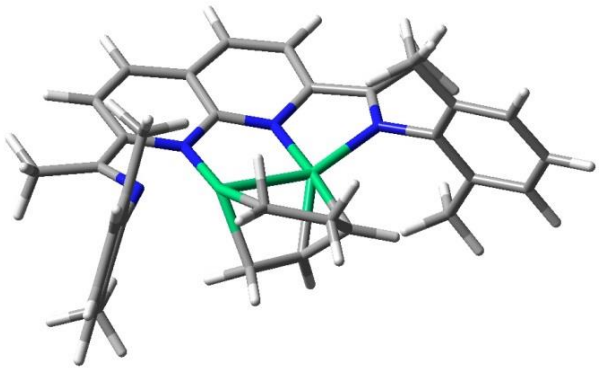

Structure 05

Charge: 0

Multiplicity: 1

Imaginary Frequencies: 1

Energy: –4514.333448387

Free Energy (298 K): –4513.787088

C	-4.84247000	1.87339700	0.21626400
Ni	-1.11159600	-0.08748600	-0.19480100
C	-3.40751400	1.46833000	0.17364700
Ni	1.20344700	-0.07995500	-0.46746600

C	-2.33793600	2.40302500	0.07712800
C	-2.40417800	3.78307200	0.27115800
C	-1.24255600	4.54251500	0.30879400
C	0.01573700	3.92162400	0.17137100
C	0.01788300	2.51043900	-0.08207500
C	1.27678000	4.54479500	0.29858300
C	2.43302800	3.78020700	0.25857100
C	2.36792600	2.40429100	0.02757900
C	3.41496800	1.45852100	0.16537000
C	4.84009300	1.83285200	0.39698800
C	-3.97530100	-0.85276400	0.22257800
C	-4.61840300	-1.25153700	-0.96451800
C	-5.44815300	-2.37718100	-0.92629600
C	-5.65188200	-3.08406600	0.25034200
C	-5.02547200	-2.66800400	1.42189600
C	-4.18256900	-1.55889100	1.42683000
C	3.96326100	-0.86083800	0.22701500
C	4.66842400	-1.26279200	-0.92223500
C	5.55099500	-2.33924700	-0.82274500
C	5.72379700	-3.01276200	0.38198200
C	4.99298700	-2.62589300	1.50082900
C	4.09993700	-1.55517700	1.44124400
C	-1.06234400	-1.51026100	-1.52122600
C	0.37112100	-1.24349100	-1.77012100
C	1.21986800	-1.94363700	-0.84971600
C	0.38633900	-2.75267700	0.11484000
N	-3.02425500	0.19286300	0.23456900
N	-1.11838400	1.79733400	-0.17455000
N	1.14796600	1.81000500	-0.27251600
N	3.01011400	0.17983800	0.13945200
C	-0.87674900	-1.94524800	0.35021000

H	-1.77798800	-2.51036000	0.60102500
H	-0.67633900	-1.19447400	1.17177500
C	-3.51806600	-1.09383400	2.68476900
H	-3.70189000	-1.78581300	3.51027700
H	-2.43565900	-0.98722200	2.55388900
H	-3.87755700	-0.10383500	2.98935900
C	-4.44636000	-0.50535200	-2.25500500
C	4.40722100	-0.57786800	-2.22769800
H	3.32664800	-0.52133700	-2.41916600
H	4.76272200	0.45954200	-2.24174700
H	4.88374200	-1.10363600	-3.05851100
C	3.27549700	-1.15144400	2.62303500
H	3.53986600	-0.15364700	2.99226300
H	2.21337700	-1.09229000	2.35229500
H	3.38994700	-1.85698900	3.44998500
H	-5.18708400	-3.21038000	2.35117700
H	-6.29810300	-3.95710300	0.25697900
H	-5.94065500	-2.69478600	-1.84363600
H	-4.15559400	-1.17868800	-3.06830600
H	-3.69225000	0.28307400	-2.18879900
H	-5.38570700	-0.03230200	-2.56552200
H	-5.41357000	1.23348700	0.89577300
H	-4.96122400	2.91038700	0.53558300
H	-5.31304500	1.78248600	-0.77074400
H	-3.36753100	4.25997700	0.42448200
H	-1.29059100	5.61243000	0.49163200
H	1.32613400	5.61124700	0.49938100
H	3.39541100	4.24892600	0.44329700
H	5.20523800	1.42925600	1.34858300
H	5.49552700	1.41637400	-0.37647200
H	4.98373800	2.91412500	0.40935800

H	5.10642600	-3.16418900	2.43994500
H	6.41284900	-3.85048700	0.44368900
H	6.09675700	-2.65601200	-1.70942100
H	0.69017000	-0.99353700	-2.78322500
H	2.19836700	-2.32799500	-1.13951800
H	0.13295400	-3.73453200	-0.31776200
H	0.91082700	-2.95282600	1.05774700
H	-1.41917100	-2.53579600	-1.67210200
H	-1.77209700	-0.83561500	-2.02509800

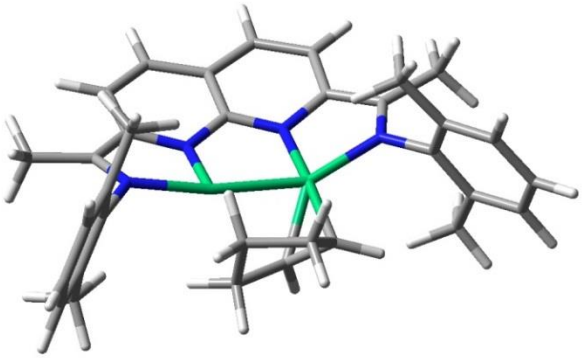

Structure 06

Charge: 0

Multiplicity: 1

Imaginary Frequencies: 0

Energy: –4514.35411850

Free Energy (298 K): –4513.802884

C	-4.82900200	1.88244000	0.31214300
Ni	-1.12194600	-0.00929600	-0.18958700
C	-3.39277900	1.49998700	0.20780300
Ni	1.16861300	-0.04706500	-0.47676700
C	-2.34005800	2.44173100	0.06330200

C	-2.40315000	3.82174700	0.25884200
C	-1.24308800	4.58439100	0.28071600
C	0.01454500	3.96017200	0.14758600
C	0.01662900	2.54983600	-0.10665500
C	1.27836700	4.57304900	0.29497400
C	2.43185900	3.80132900	0.27435300
C	2.36031900	2.42568700	0.04586100
C	3.39500000	1.46534500	0.20360200
C	4.81400600	1.82822900	0.48764000
C	-3.89337900	-0.84671600	0.29396500
C	-4.60822000	-1.22561800	-0.85923200
C	-5.38994900	-2.38371100	-0.80649100
C	-5.47640700	-3.14262700	0.35291800
C	-4.77498700	-2.75072900	1.48997200
C	-3.97544900	-1.60976900	1.47834000
C	3.91415500	-0.85995200	0.25936400
C	4.66284800	-1.24155800	-0.86917800
C	5.52612700	-2.33293800	-0.75992700
C	5.63803700	-3.03987800	0.43251800
C	4.86410000	-2.67235100	1.52887400
C	3.98783000	-1.58887100	1.45887000
C	-1.08983900	-1.76479900	-1.63083700
C	0.27718800	-1.13059700	-1.79677800
C	1.20003600	-1.87493400	-0.96471200
C	0.40922600	-2.86216600	-0.13319700
N	-2.97804800	0.23055700	0.27744200
N	-1.12249900	1.84158800	-0.23072000
N	1.14163000	1.84370700	-0.26996100
N	2.97763700	0.19389000	0.16017000
C	-1.01108100	-2.30378300	-0.19033400
H	-1.81162000	-3.01177500	0.04455000

H	-1.10294700	-1.53676700	0.63633400
C	-3.22276600	-1.17483100	2.69581300
H	-3.29685700	-1.91481600	3.49620900
H	-2.16316900	-0.99876200	2.47386500
H	-3.59911700	-0.21977600	3.08050900
C	-4.55064900	-0.42651900	-2.12730800
C	4.47055800	-0.52266900	-2.16893800
H	3.40318400	-0.46464400	-2.42364100
H	4.82316000	0.51523200	-2.13876200
H	4.99440500	-1.02717900	-2.98436500
C	3.11442300	-1.20567600	2.61178100
H	3.35009200	-0.20655200	2.99613000
H	2.06181700	-1.15959000	2.30239400
H	3.20764200	-1.91599900	3.43734000
H	-4.84160000	-3.33819600	2.40322700
H	-6.08749600	-4.04046700	0.37152400
H	-5.93570900	-2.68786200	-1.69756500
H	-4.48781900	-1.07952800	-3.00299100
H	-3.69937200	0.25975400	-2.15338400
H	-5.45525200	0.18090400	-2.25608800
H	-5.37322700	1.19485700	0.96650900
H	-4.94641000	2.89538800	0.70284500
H	-5.32761300	1.85403400	-0.66497100
H	-3.36638800	4.29466300	0.42589000
H	-1.29093000	5.65442900	0.46195300
H	1.33175000	5.63828600	0.50128600
H	3.39354300	4.26559800	0.47357000
H	5.13360300	1.42961600	1.45767800
H	5.49748700	1.39826700	-0.25270200
H	4.96756100	2.90818300	0.49753700
H	4.92963800	-3.23655600	2.45728400

H	6.31358200	-3.88796600	0.50173400
H	6.10512600	-2.63470500	-1.63050400
H	0.54183600	-0.77804500	-2.79582300
H	2.19172000	-2.17854800	-1.30486800
H	0.41789000	-3.85716300	-0.60613400
H	0.78260800	-2.99213500	0.88937900
H	-1.19136200	-2.63049000	-2.30507300
H	-1.95418100	-1.12127900	-1.85537300

REFERENCES

1. Jun, C. H., Transition metal-catalyzed carbon-carbon bond activation. *Chem. Soc. Rev.,* **2004,** *33* (9), 610-8.
2. Huang, C. Y.; Doyle, A. G., The chemistry of transition metals with three-membered ring heterocycles. *Chem. Rev.,* **2014,** *114* (16), 8153-98.
3. Lu, B. L.; Dai, L.; Shi, M., Strained small rings in gold-catalyzed rapid chemical transformations. *Chem. Soc. Rev.,* **2012,** *41* (8), 3318-39.
4. Tasker, S. Z.; Standley, E. A.; Jamison, T. F., Recent advances in homogeneous nickel catalysis. *Nature,* **2014,** *509* (7500), 299-309.
5. Chen, P. H.; Billett, B. A.; Tsukamoto, T.; Dong, G., "Cut and Sew" Transformations via Transition-Metal-Catalyzed Carbon-Carbon Bond Activation. *ACS Catal.,* **2017,** *7* (2), 1340-1360.
6. Gao, Y.; Fu, X. F.; Yu, Z. X., Transition metal-catalyzed cycloadditions of cyclopropanes for the synthesis of carbocycles: C-C activation in cyclopropanes. *Top. Curr. Chem.,* **2014,** *346*, 195-231.
7. Souillart, L.; Cramer, N., Catalytic C-C Bond Activations via Oxidative Addition to Transition Metals. *Chem Rev* **2015,** *115* (17), 9410-64.
8. Rybtchinski, B.; Milstein, D., Metal Insertion into C−C Bonds in Solution. *Angew. Chemie Int.Ed.,* **1999,** *38* (7), 870-883.
9. Wender, P. A.; Inagaki, F.; Pfaffenbach, M.; Stevens, M. C., Propargyltrimethylsilanes as allene equivalents in transition metal-catalyzed [5 + 2] cycloadditions. *Org. Lett.,* **2014,** *16* (11), 2923-5.
10. Shintani, R.; Nakatsu, H.; Takatsu, K.; Hayashi, T., Rhodium-catalyzed asymmetric [5+2] cycloaddition of alkyne-vinylcyclopropanes. *Chem. Eur. J.,* **2009,** *15* (35), 8692-4.
11. Sebelius, S.; Olsson, V. J.; Szabo, K. J., Palladium pincer complex catalyzed substitution of vinyl cyclopropanes, vinyl aziridines, and allyl acetates with tetrahydroxydiboron. An efficient route to functionalized allylboronic acids and potassium trifluoro(allyl)borates. *J. Am. Chem. Soc.,* **2005,** *127* (30), 10478-9.
12. Li, C. F.; Xiao, W. J.; Alper, H., Palladium-catalyzed ring-opening thiocarbonylation of vinylcyclopropanes with thiols and carbon monoxide. *J. Org. Chem.,* **2009,** *74* (2), 888-90.
13. Moran, J.; Smith, A. G.; Carris, R. M.; Johnson, J. S.; Krische, M. J., Polarity inversion of donor-acceptor cyclopropanes: disubstituted delta-lactones via enantioselective iridium catalysis. *J. Am. Chem. Soc.,* **2011,** *133* (46), 18618-21.
14. Korotvicka, A.; Cisarova, I.; Roithova, J.; Kotora, M., Synthesis of aromatic compounds by catalytic C-C bond activation of biphenylene or angular [3]phenylene. *Chem. Eur. J.,***2012,** *18* (14), 4200-7.

15. Tamaki, T.; Nagata, M.; Ohashi, M.; Ogoshi, S., Synthesis and reactivity of six-membered oxa-nickelacycles: a ring-opening reaction of cyclopropyl ketones. *Chem. Eur. J.,* **2009,** *15* (39), 10083-91.

16. Liu, L.; Montgomery, J., [3+2] cycloaddition reactions of cyclopropyl imines with enones. *Org. Lett.,* **2007,** *9* (20), 3885-7.

17. Sumida, Y.; Yorimitsu, H.; Oshima, K., Nickel-catalyzed arylative ring-opening of 3-methylenecycloalkane-1,1-dicarboxylates. *Org. Lett.,* **2010,** *12* (10), 2254-7.

18. Dieskau, A. P.; Holzwarth, M. S.; Plietker, B., Fe-catalyzed allylic C-C-bond activation: vinylcyclopropanes as versatile a1,a3,d5-synthons in traceless allylic substitutions and [3 + 2]-cycloadditions. *J. Am. Chem. Soc.,* **2012,** *134* (11), 5048-51.

19. Sherry, B. D.; Furstner, A., Iron-catalyzed addition of Grignard reagents to activated vinyl cyclopropanes. *Chem. Commun.,* **2009,** (46), 7116-8.

20. Tipper, C. F. H., Some Reactions Of Cyclopropane, And A Comparison With The Lower Olefins. 2. Some Platinous-Cyclopropane Complexes. *J. Chem. Soc.,* **1955**, 2045-2046.

21. Adams, D. M.; Chatt, J.; Guy, R. G.; Sheppard, N., 149. The structure of "cyclopropane platinous chloride". *J. Chem. Soc. (Res.),* **1961,** (0), 738-742.

22. Schlodder, R.; Ibers, J. A.; Lenarda, M.; Graziani, M., Structure and mechanism of formation of the metallooxacyclobutane complex bis(triphenylarsine)tetracyanooxiraneplatinum, the product of the reaction between tetracyanooxirane and tetrakis(triphenylarsine)platinum. *J. Am. Chem. Soc.,* **1974,** *96* (22), 6893-6900.

23. Lin, B. L.; Clough, C. R.; Hillhouse, G. L., Interactions of Aziridines with Nickel Complexes: Oxidative-Addition and Reductive-Elimination Reactions that Break and Make C−N Bonds. *J. Am. Chem. Soc.,* **2002,** *124* (12), 2890-2891.

24. Ney, J. E.; Wolfe, J. P., Synthesis and Reactivity of Azapalladacyclobutanes. *J. the Am. Chem. Soc.,* **2006,** *128* (48), 15415-15422.

25. Desnoyer, A. N.; Bowes, E. G.; Patrick, B. O.; Love, J. A., Synthesis of 2-Nickela(II)oxetanes from Nickel(0) and Epoxides: Structure, Reactivity, and a New Mechanism of Formation. *J. Am. Chem.Soc.,* **2015,** *137* (40), 12748-12751.

26. Zuo, G.; Louie, J., Highly Active Nickel Catalysts for the Isomerization of Unactivated Vinyl Cyclopropanes to Cyclopentenes. *Angew. Chem., Int. Ed.,* **2004,** *43* (17), 2277-2279.

27. Zuo, G.; Louie, J., Highly Active Nickel Catalysts for the Isomerization of Unactivated Vinyl Cyclopropanes to Cyclopentenes. *Angew. Chemie. Int.Ed.,* **2004,** *43*, 2277-2279.

28. Wang, S. C.; Troast, D. M.; Conda-Sheridan, M.; Zuo, G.; LaGarde, D.; Louie, J.; Tantillo, D. J., Mechanism of the Ni(0)-Catalyzed Vinylcyclopropane−Cyclopentene Rearrangement. *J. Org. Chem.,* **2009,** *74* (20), 7822-7833.

29. Behlen, M. J.; Zhou, Y.-Y.; Steiman, T. J.; Pal, S.; Hartline, D. R.; Zeller, M.; Uyeda, C., Dinuclear oxidative addition reactions using an isostructural series of Ni2, Co2, and Fe2 complexes. *Dalton Trans.,* **2017,** *46* (17), 5493-5497.

30. Hartline, D. R.; Zeller, M.; Uyeda, C., Catalytic Carbonylative Rearrangement of Norbornadiene via Dinuclear Carbon–Carbon Oxidative Addition. *J. Am. Chem. Soc.,* **2017,** *139* (39), 13672-13675.

31. Zhou, Y.-Y.; Hartline, D. R.; Steiman, T. J.; Fanwick, P. E.; Uyeda, C., Dinuclear Nickel Complexes in Five States of Oxidation Using a Redox-Active Ligand. *Inorg. Chem.,* **2014,** *53* (21), 11770-11777.

32. Manuel, T. D.; Rohde, J.-U., Reaction of a Redox-Active Ligand Complex of Nickel with Dioxygen Probes Ligand-Radical Character. *J. Am. Chem. Soc.,* **2009,** *131* (43), 15582-15583.

33. Dong, Q.; Yang, X.-J.; Gong, S.; Luo, Q.; Li, Q.-S.; Su, J.-H.; Zhao, Y.; Wu, B., Distinct Stepwise Reduction of a Nickel□Nickel-Bonded Compound Containing an α-Diimine Ligand: From Perpendicular to Coaxial Structures. *Chem. Eur. J.,* **2013,** *19* (45), 15240-15247.

34. Dible, B. R.; Sigman, M. S.; Arif, A. M., Oxygen-Induced Ligand Dehydrogenation of a Planar Bis-μ-Chloronickel(I) Dimer Featuring an NHC Ligand. *Inorg. Chem.,* **2005,** *44* (11), 3774-3776.

35. Marvell, E. N.; Lin, C., The aromatic Cope rearrangement. Thermal reactions of cis-1-aryl-2-vinylcyclopropanes. *J. Am. Chem. Soc.,* **1978,** *100* (3), 877-883.

36. Baldwin, J. E.; Bonacorsi, S. J., Stereochemistry of the Thermal Isomerizations of trans-1-Ethenyl-2-phenylcyclopropane to 4-Phenylcyclopentene. *J. Am. Chem. Soc.,* **1996,** *118* (35), 8258-8265.

37. Kamitani, A.; Chatani, N.; Morimoto, T.; Murai, S., Carbonylative [5 + 1] Cycloaddition of Cyclopropyl Imines Catalyzed by Ruthenium Carbonyl Complex. *J. Org. Chem.,* **2000,** *65* (26), 9230-9233.

38. Ogoshi, S.; Nagata, M.; Kurosawa, H., Formation of Nickeladihydropyran by Oxidative Addition of Cyclopropyl Ketone. Key Intermediate in Nickel-Catalyzed Cycloaddition. *J. Am. Chem. Soc.,* **2006,** *128* (16), 5350-5351.

39. Tamaki, T.; Nagata, M.; Ohashi, M.; Ogoshi, S., Synthesis and Reactivity of Six-Membered Oxa-Nickelacycles: A Ring-Opening Reaction of Cyclopropyl Ketones. *Chem. Eur. J.,* **2009,** *15* (39), 10083-10091.

40. Ye, R.; Yuan, B.; Zhao, J.; Ralston, W. T.; Wu, C.-Y.; Unel Barin, E.; Toste, F. D.; Somorjai, G. A., Metal Nanoparticles Catalyzed Selective Carbon–Carbon Bond Activation in the Liquid Phase. *J. Am. Chem. Soc.,* **2016,** *138* (27), 8533-8537.

41. Okumoto, H.; Jinnai, T.; Shimizu, H.; Harada, Y.; Mishima, H.; Suzuki, A., Pd-Catalyzed Ring Opening of Cyclopropanols. *Synlett.,* **2000,** *2000* (05), 0629-0630.

42. Zhou, Y.-Y.; Hartline, D. R.; Steiman, T. J.; Fanwick, P. E.; Uyeda, C., Dinuclear Nickel Complexes in Five States of Oxidation Using a Redox-Active Ligand. *Inorg. Chem.,* **2014,** *53*, 11770-11777.

43. Cunha, R. L. O. R.; G.Diego, D.; Simonelli, F.; Comasseto, J. V., Selectivity aspects of the ring opening reaction of 2-alkenyl aziridines by carbon nucleophiles. *Tet. Lett.,* **2005,** *46* (15), 2539.

44. Diercks, R.; Dieck tom, H., Diazadiene als Steuerliganden in der homogenen Katalyse, IX. Katalytische Cyclotetramerisierung von Propiolsäureestern. *Chemische Berichte,* **1985,** *118* (2), 428-435.

45. Fischetti, W.; Heck, R. F., The Mechanism of Reactions of Organopalladium Salts with Vinylcyclopropanes. *J. Organomet. Chem.,* **1985,** *293* (3), 391-405.

46. Itoh, T.; Matsueda, T.; Shimizi, Y.; Kanai, M., Copper-Catalyzed Oxyboration of Unactivated Alkenes. *Chem. Eur. J.,* **2015,** *21*, 15955 - 15959.

47. Chen, Z.; Liang, J.; Yin, J.; Yu, G.-A.; Liu, S. H., Alder-ene reaction of aryne with olefins. *Tet. Lett.,* **2013,** *54* (43), 5785-5787.

48. You, H.; Rideau, E.; Sidera, M.; Fletcher, S. P., Non-stabilized nucleophiles in Cu-catalysed dynamic kinetic asymmetric allylic alkylation. *Nature,* **2015,** *517* (7534), 351-5.

49. Meuer, L. H. P.; Johannes, C. G.; Niel, V.; K.Pandit, U., NADH model-19. *Tetrahedron,* **1984,** *40* (24), 5185-5195.

50. Rosa, D.; Orellana, A., Palladium-catalyzed cross-coupling of cyclopropanolderived ketone homoenolates with aryl bromides. *Chem., Commun.,* **2013,** *49* (47), 5420-5422.

51. Lee, D. Y.; Hong, B. S.; Cho, E. G.; Lee, H.; Jun, C. H., A hydroacylation-triggered carbon--carbon triple bond cleavage in alkynes via retro-Mannich type fragmentation. *J. Am. Chem. Soc.,* **2003,** *125* (21), 6372-3.

52. Padwa, A., *Aziridines and Azirines: Monocyclic*. 1st ed.; Elsevier Science: 2008; Vol. 1.

53. Ouyang, K.; Hao, W.; Zhang, W. X.; Xi, Z., Transition-Metal-Catalyzed Cleavage of C-N Single Bonds. *Chem. Rev.,* **2015,** *115* (21), 12045-90.

54. Ilardi, E. A.; Njardarson, J. T., Ring expansions of vinyloxiranes, -thiiranes, and -aziridines: synthetic approaches, challenges, and catalytic success stories. *J. Org. Chem.,* **2013,** *78* (19), 9533-40.

55. Mack, D. J.; Njardarson, J. T., New mechanistic insights into the copper catalyzed ring expansion of vinylaziridines: evidence in support of a copper(I) mediated pathway. *Chem. Sci.,* **2012,** (3), 3321.

56. Ohno, H., Synthesis and applications of vinylaziridines and ethynylaziridines. *Chem. Rev.,* **2014,** *114* (16), 7784-814.

57. Spears, G. W.; Nakanishi, K.; Ohfune, Y., Novel Entry to a 3,4-Disubstituted 2-Azetidinone Derivative via Palladium-Assisted Carbonylation of a 2-Substituted 3-Vinylaziridine. *Synlett.,* **1991,** *1991* (02), 91-92.

58. Fontana, F.; Tron, G. C.; Barbero, N.; Ferrini, S.; Thomas, S. P.; K., A. V., Stereoselective synthesis of trans-beta-lactams by palladium-catalysed carbonylation of vinyl aziridines. *Chem. Commun.,* **2010,** *46* (2), 267-9.

59. Heo, Y. M.; Paek, S. M., Ring expansion of vinylaziridines through the strain-release pericyclic reaction: recent developments and applications. *Molecules,* **2013,** *18* (8), 9650-62.

60. Khumtaveeporn, K.; Alper, H., Transition Metal Mediated Carbonylative Ring Expansion of Heterocyclic Compounds. *Acc. Chem. Res.,* **1995,** *28* (10), 414-422.

61. Tanner, D.; Somfai, P., Palladium-catalyzed transformation of a chiral vinylaziridine to a β-lactam. An enantioselective route to the carbapenem (+)-PS-5. *Bioorg. & Med. Chem.Lett.,* **1993,** *3* (11), 2415-2418.

62. Davoli, P.; Forni, A.; Moretti, I.; Prati, F.; Torre, G., On the effect of ring substituents in the carbonylation of aziridines. *Tetrahedron,* **2001,** *57* (9), 1801-1812.

63. Piotti, M. E.; Alper, H., Inversion of Stereochemistry in the Co2(CO)8-Catalyzed Carbonylation of Aziridines to β-Lactams. The First Synthesis of Highly Strainedtrans-Bicyclic β-Lactams. *J. Am. Chem. Soc.,* **1996,** *118* (1), 111-116.

64. Davoli, P.; Moretti, I.; Prati, F.; Alper, H., Carbonylation of Silylated Hydroxymethyl Aziridines to β-Lactams. *J. Org. Chem.,* **1999,** *64* (2), 518-521.

65. Minicone, F.; Rogers, W. J.; Green, J. F. J.; Khan, M.; Smith, G. M. T.; Bray, C. D., Direct conversion of epoxides into aziridines with N-arylphosphoramidates. *Tet. Lett.* **2014,** *55* (43), 5890-5891.

66. Dauth, A.; Love, J. A., Reactivity by design--metallaoxetanes as centerpieces in reaction development. *Chem. Rev.,* **2011,** *111* (3), 2010-47.

67. Wills, V. S.; Zhou, X.; Allen, C.; Holstein, S. A.; Wiemer, D. F., Stereocontrolled regeneration of olefins from epoxides. *Tet. Lett.,* **2016,** *57* (12), 1335-1337.

68. Wong, K.-T.; Yuan, T.-M.; Wang, M. C.; Tung, H.-H.; Luh, T.-Y., Chelation Assistance in the Activation of Csp3-S Bonds in Nickel-Catalyzed Cross-Coupling Reactions. *J. Am.Chem. Soc.,* **1994,** *116* (20), 8920-8929.

69. Evans, D. A.; Faul, M. M.; Bilodeau, M. T., Copper-catalyzed aziridination of olefins by (N-(p-toluenesulfonyl)imino)phenyliodinane. *J. Org. Chem.,* **1991,** *56* (24), 6744-6746.

70. Rogers, E.; Araki, H.; Batory, L. A.; McInnis, C. E.; Njardarson, J. T., Highly selective copper-catalyzed ring expansion of vinyl thiiranes: application to synthesis of biotin and the heterocyclic core of plavix. *J. Am. Chem. Soc.,* **2007,** *129* (10), 2768-9.

71. Jacob, J.; Espenson, J. H., Stereospecific rhenium catalyzed desulfurization of thiiranes. *Chem. Commun.,* **1999,** (11), 1003-1004.

72. Eisavi, R.; Zeynizadeh, B.; Baradarani, M. M., Zeolite Molecular Sieve 4Å: A Reusable Catalyst for Fast and Efficient Conversion of Epoxides to Thiiranes with Thiourea. *Phosphorus, Sulfur, and Silicon and the Related Elements* **2011,** *186* (9), 1902-1909.

73. Dong, J.; Xu, J., Facile synthesis of thietanes via ring expansion of thiiranes. *Org. Biomol. Chem.,* **2017,** *15* (4), 836-844.

74. Culvenor, C. C. J.; Davies, W.; Heath, N. S., 66. Reactions of ethylene oxides. Part II. Reactions with thioamides, thiols, and inorganic sulphur salts. *J. Chem. Soc. (Res.)* **1949**.

75. Hou, D.-R.; Hsieh, Y.-D.; Hsieh, Y.-W., New formation of 4,5,6,7-tetrahydroisoindoles. *Tet. Lett.,* **2005,** *46* (35), 5927-5929.

VITA

Heather Rounds (Schoonover) was born in Effingham, Illinois to Randy and Andrea Schoonover. She grew up in Herrick, IL and had two brothers, Nathan and Ethan. She attended Herrick Grade School, Cowden-Herrick Junior High School, and Cowden-Herrick High School. Heather was a big fan of sports and participated all through school. While in grade school she was a cheerleader and in junior high she participated in basketball, volleyball, cheerleading, and cross-country. In high school, she decided to pursue her favorite sport, volleyball and won multiple awards that included most valuable player (MVP).

She went on to Millikin University pursue a Bachelor of Science degree in Biology with a concentration in Pre-Medicine. While she was there, she participated in college volleyball where she played as a defensive specialist for two years. She decided to focus on studying for the MCAT and after taking the exam her junior year, she concluded that medical school was not the right path. She started undergraduate research with Dr. Anne Rammelsberg working in a biochemistry lab where she gathered plant samples native to the area and made extracts to test antimicrobial properties against *Escherichia coli*. After presenting her research at her senior seminar, she figured out that her real passion was for chemistry and started working in Dr. Paris Barnes' inorganic chemistry lab making iron oxide nanoparticles. This is when she added chemistry as a double major and started to pursue a career path to graduate school.

Heather was admitted to the graduate program at Eastern Illinois University where she worked under the supervision of Dr. Radu Semeniuc synthesizing rotaxanes. These rotaxanes were made from pyridine-based linkers and metallation with rhodium and ruthenium paddlewheel complexes. She gained a lot of experience with air-free synthetic techniques, chromatography, and crystallization. Still having a passion for helping others and enjoying the synthetic side of chemistry, she decided to pursue a Ph.D. in chemistry so she could work in the pharmaceutical industry.

Purdue University admitted Heather into their Ph.D. program where she started working under a newly hired professor, Dr. Christopher Uyeda. Dr. Uyeda's research centered around the discovery of new organometallic complexes and using these complexes for catalysis. Heather worked on strained ring activation with a dinuclear nickel complex and was able to study the mechanism of these reactions with trapped organometallic complexes and DFT calculations. While

working on the strained ring project, she discovered the ability of vinylaziridines to ring expand into β- or δ-lactams depending on the protecting group on the nitrogen. She also discovered the ability of the dinuclear complex to perform oxidative transfer reactions with heteroatom-containing strained rings.

In Heather's second year of graduate school at Purdue University she married Kyle Rounds after being engaged for five years. They married in the Dominican Republic and had a large reception where their family and friends attended. As Heather finished up her doctorate degree, she realized how blessed she was to have great friends, family, and colleagues. Without them she knew she would not have gotten this far in achieving her career goals.

PUBLICATION

ORGANOMETALLICS Article

Cite This: *Organometallics* 2018, 37, 545−550

Dinuclear Pathways for the Activation of Strained Three-Membered Rings

Heather R. Rounds, Matthias Zeller, and Christopher Uyeda*

Department of Chemistry, Purdue University, West Lafayette, Indiana 47907, United States

Supporting Information

ABSTRACT: Dinuclear, strain-induced ring-opening reactions of vinylaziridines and vinylcyclopropanes are described. The previously reported [NDI]$Ni_2(C_6H_6)$ complex (NDI = naphthyridine−diimine) reacts with *N*-tosyl-2-vinylaziridine via C−N oxidative addition to generate a dinickel metallacyclic product. On the basis of this stoichiometric reactivity, the [NDI]-$Ni_2(C_6H_6)$ complex is shown to be a highly active catalyst for the rearrangement of vinylcyclopropane to cyclopentene. Notably, 2-phenyl-1-vinylcyclopropane undergoes regioselective activation at the less hindered C−C bond in contrast to the noncatalytic thermal rearrangement. DFT calculations provide insight into the ability of the Ni−Ni bond to stabilize key intermediates and transition states along the catalytic pathway.

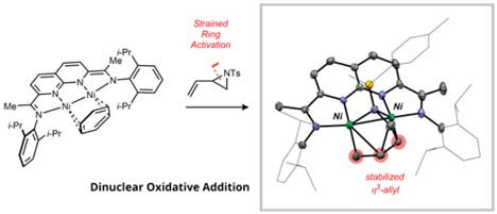

INTRODUCTION

Cyclopropanes, aziridines, and epoxides participate in a broad range of strain-induced ring-opening reactions mediated by transition metal catalysts.[1] A key step in many of these transformations is a carbon−carbon or carbon−heteroatom oxidative addition that activates the ring and generates a metallacyclic intermediate.[2] In order to facilitate this process, catalysts that are effective for ring-opening reactions commonly employ strongly donating and sterically encumbering ligands that support electron-rich metals with low coordination numbers (Figure 1).[3] For example, Louie demonstrated that $(NHC)_2Ni$ complexes are remarkably active catalysts for the rearrangement of vinylcyclopropanes to form cyclopentenes.[4] Computational models suggest that the catalytic intermediates are monoligated Ni species and that C−C oxidative addition is likely rate-determining.[5]

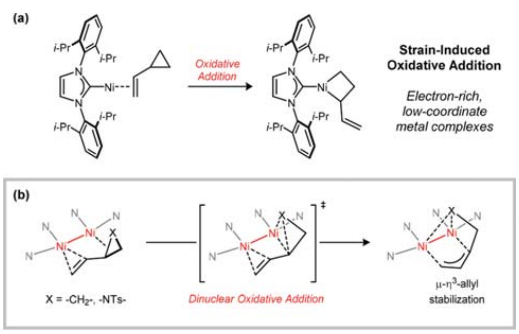

Figure 1. Design principles for strain-induced oxidative addition reactions of vinyl three-membered ring substrates. (a) C−C oxidative addition using electron-rich, low-coordinate metal complexes. (b) Oxidative addition driven by dinuclear stabilization of allyl groups (X = C and N).

Our group is interested in identifying alternative approaches to promoting bond activation reactions that exploit the cooperative function of multiple metal centers. In this context, we recently described a dinuclear [$^{i\text{-}Pr}$NDI]$Ni_2(C_6H_6)$ complex that effects the oxidative addition of allyl chloride to form a $Ni_2(\mu\text{-allyl})Cl$ product.[6] A notable feature of this reaction is its unusually low activation barrier (4.1 kcal/mol by DFT), which we attributed to the ability of the dinuclear system to form a stabilizing π-interaction with the incipient allyl system as the C−Cl bond is cleaved. This observation led us to question whether this activation mode could be generalized to other classes of substrates.[7] Here, we report a dinuclear mechanism for the stoichiometric and catalytic activation of strained three-membered ring substrates, including vinylaziridines and vinylcyclopropanes.

RESULTS AND DISCUSSION

Stoichiometric Aziridine Ring-Opening. In our initial studies, we examined a stoichiometric oxidative addition reaction of a model strained ring system. Accordingly, [$^{i\text{-}Pr}$NDI]$Ni_2(C_6H_6)$ complex **1**[8] reacts with *N*-tosyl-2-vinylaziridine over the course of 30 min at room temperature to provide the product of C−N oxidative addition (**2**) in 65% isolated yield as a diamagnetic, crystalline green solid (Figure 2a). In a similar fashion to the previously reported [$^{i\text{-}Pr}$NDI]-Ni_2(allyl)Cl complex, the solid-state structure features a μ-η^3-

Received: December 1, 2017
Published: February 6, 2018

 © 2018 American Chemical Society

DOI: 10.1021/acs.organomet.7b00862
Organometallics 2018, 37, 545−550

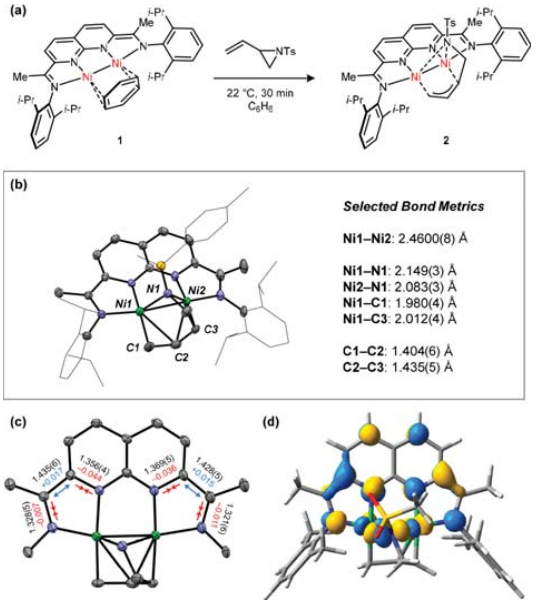

Figure 2. (a) Oxidative addition of *N*-tosyl-2-vinylaziridine using **1**. (b) Solid-state structure for **2** and select bond metrics. (c) Changes in bond metrics indicative of ligand-centered redox activities. Bond metrics for **2** (black) are shown in Å. Changes relative to complex **1** are shown in red and blue. (d) LUMO for **2**, which shows primarily ligand character.

coordination mode for the allyl fragment and a μ-NTs ligand that symmetrically bridges the two metals (Figure 2b). The Ni−Ni bond distance for **2** (2.4600(8) Å) is relatively unchanged from that observed for **1** (2.496(1) Å), suggesting that the electron pair required for the two-electron oxidative addition is being provided by the reduced ligand π-system rather than from the Ni−Ni bond. This description is supported by distortions in the NDI bond metrics that are characteristic of a change in the ligand charge state from dianionic to neutral (Figure 2c). DFT calculations are also consistent with an oxidative addition reaction that involves substantial electronic participation from the redox-active ligand. The calculated LUMO for **2** is predominantly associated with the delocalized NDI π-system with a minor fraction of Ni−Ni π^* character (Figure 2d). This orbital corresponds to the HOMO for $Ni_2(C_6H_6)$ complex **1**.

The [$^{i\text{-Pr}}$IP]Ni(COD) complex **3** bears a supporting ligand that approximates half of the $^{i\text{-Pr}}$NDI system and thus provided a suitable mononickel analog for **1**. Complex **3** similarly reacts with *N*-tosyl-2-vinylaziridine to yield blue diamagnetic metallacycle **4** in 66% yield (Figure 3a). The ^{1}H NMR resonances for complex **4** are broad at room temperature but sharpen and resolve at lower temperatures, suggestive of a fluxional process that occurs on the ^{1}H NMR chemical shift time scale. The most notable structural difference between the dinuclear and mononuclear oxidative addition products is the orientation of the coordinated allyl group (Figure 3b). In **2**, the allyl ligand spans the two Ni centers and is η^3-coordinated with C1−C2 and C2−C3 distances that are nearly equal. By contrast, the allyl ligand in **4** is η^1-coordinated, and the C2−C3 distance is

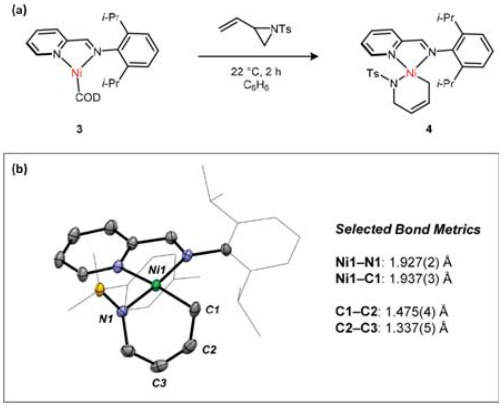

Figure 3. (a) Oxidative addition of *N*-tosyl-2-vinylaziridine using **3**. (b) Solid-state structure for **4** and select bond metrics.

relatively short at 1.337(5) Å, suggesting that it maintains significant double bond character.

Catalytic Rearrangement of Vinylcyclopropane. At 1 mol % loading, [$^{i\text{-Pr}}$NDI]$Ni_2(C_6H_6)$ complex **1** catalyzes the rearrangement of vinylcyclopropane to cyclopentene, reaching full conversion after 24 h at room temperature (Table 1). Complex **1** is the only observable catalyst resting state under the reaction conditions. Additionally, in stoichiometric

Table 1. Comparison of Nickel Catalysts for the Rearrangement of Vinylcyclopropane[a]

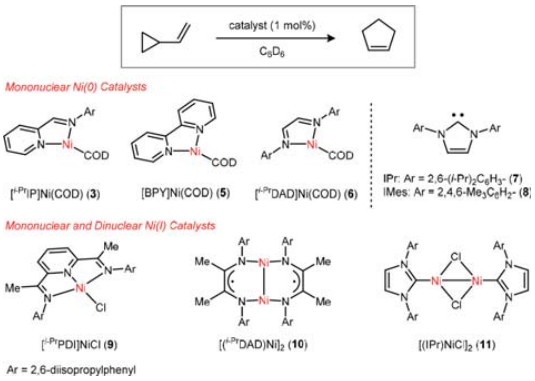

entry	catalyst	time/temp	yield
1	[$^{i\text{-Pr}}$NDI]$Ni_2(C_6H_6)$ (**1**)	24 h/22 °C	83%
2	[$^{i\text{-Pr}}$IP]Ni(COD) (**3**)	24 h/60 °C	<1%
3	[BPY]Ni(COD) (**5**)	24 h/60 °C	<1%
4	[$^{i\text{-Pr}}$DAD]Ni(COD) (**6**)	24 h/60 °C	<1%
5	$Ni(COD)_2$	24 h/60 °C	<1%
6	$Ni(COD)_2$ + IPr (**7**)[b]	24 h/60 °C	8%
7	$Ni(COD)_2$ + IMes (**8**)[b]	24 h/60 °C	5%
8	[$^{i\text{-Pr}}$PDI]Ni_2Cl (**9**)	24 h/60 °C	<1%
9	[($^{i\text{-Pr}}$DAD)Ni]$_2$ (**10**)	24 h/60 °C	<1%
10	[(IPr)NiCl]$_2$ (**11**)	24 h/22 °C	6%
11	[(IPr)NiCl]$_2$ (**11**)	24 h/60 °C	50%

[a]Reactions were conducted in a sealed NMR tube, and yields were determined by ^{1}H NMR integration against a mesitylene standard. [b]Conditions: 1 mol % $Ni(COD)_2$ and 2 mol % NHC.

DOI: 10.1021/acs.organomet.7b00862
Organometallics 2018, 37, 545−550

reactions between **1** and vinylcyclopropane (1.0 equiv), no intermediates are observed en route to cyclopentene, indicating that the catalytic intermediates are endothermic relative to the C_6H_6 adduct.

Mononickel complex **3**, shown above to activate *N*-tosyl-2-vinylaziridine, is not capable of mediating C−C oxidative addition with vinylcyclopropane, providing no detectable conversion of starting material even after 24 h of heating at 60 °C. Related [N,N]Ni(COD) complexes (**5** and **6**) were similarly unreactive under these conditions, as were the mononuclear and dinuclear Ni(I) complexes [$^{i\text{-Pr}}$PDI]Ni_2Cl (**9**)[9] and [($^{i\text{-Pr}}$DAD)Ni]$_2$ (**10**).[10] The [NHC]$_2$Ni catalysts, previously studied by Louie,[4] are active for the rearrangement of the parent vinylcyclopropane molecule but require elevated temperatures in order to achieve detectable levels of conversion. For example, an IPr/Ni(COD)$_2$ mixture provides 8% yield of cyclopentene after 24 h of heating at 60 °C. Dimeric [(IPr)NiCl]$_2$ complex **11**[11] is more active than its Ni(0) counterpart, though it is unclear whether **11** might disproportionate under the reaction conditions to generate an active Ni(0) species. It is noteworthy that while the [IPr]$_2$Ni catalyst is only modestly active for the rearrangement of vinylcyclopropane it is substantially more efficient for substrates bearing alkene substituents.[4] In contrast, Ni_2 catalyst **1** is only capable of activating substrates with unsubstituted vinyl groups, presumably due to its large steric profile.

For vinylcyclopropane derivatives bearing ring substitutions, the ratio of rearranged cyclopentene isomers is dictated by which of the two cyclopropane C−C bonds is cleaved. In the case of phenyl-substituted vinylcyclopropane **12**, the catalytic rearrangement with **1** selectively targets the less hindered C−C bond, providing **13** in 93% yield as a single isomer (Figure 4).

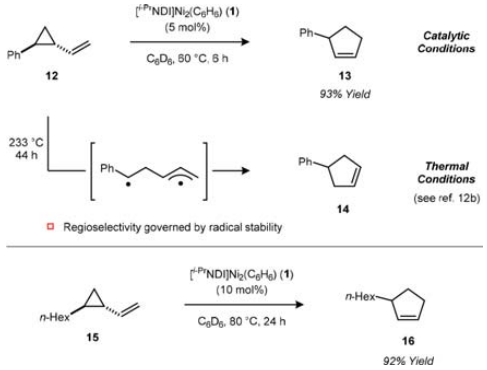

Figure 4. Catalytic rearrangements of vinylcyclopropanes bearing ring substitution.

A similar regioselectivity is observed using the alkyl-susbstituted vinylcyclopropane **15**, which forms **16** in 92% yield. It is noteworthy that the thermal rearrangement of **12** proceeds at >200 °C and provides only the alternative product isomer **14**.[12] This thermal rearrangement is proposed to occur by C−C bond homolysis to generate a biradical intermediate and is thus governed by the relative stabilities of the benzylic vs the primary radical.

Given the lack of observable intermediates in the Ni_2-catalyzed vinylcyclopropane rearrangement, we turned to DFT models to further probe the mechanism of this reaction (Figure 5). As expected based on our experimental results, the exchange of C_6H_6 for vinylcyclopropane is an endothermic process (+13.7 kcal/mol). The vinylcyclopropane adduct (**B**) exhibits a highly activated C−C bond (1.728 Å), likely due to a strong interaction with the bent C−C σ-bonding orbital of the cyclopropane. Notably, the oxidative addition from **B** is nearly barrierless (<0.1 kcal/mol), and the C−C distance in the transition state (**C**) is elongated by only 0.020 Å relative to **B**. The oxidative addition is highly exothermic and generates a Ni_2 metallacycle (**D**), which closely resembles the analogous structure that was characterized using *N*-tosyl-2-vinylaziridine (Figure 2). From **D**, reductive elimination is calculated to be rate-determining for the catalytic cycle and has an activation energy of 22.1 kcal/mol. Resulting cyclopentene adduct **F** is relatively unstable, and ligand exchange with C_6H_6 to generate the free product is favorable.

It is salient to compare the energetics of the key mechanistic steps using dinuclear catalyst **1** with those previously calculated for the mononuclear [NHC]Ni catalyst.[5] The most significant consequence of the dinuclear active site is that the oxidative addition transition state and resulting metallacycle intermediate are highly stabilized by the additional π-interactions formed with the second Ni center. The oxidative addition is calculated to be nearly barrierless using **1** but is the rate-determining step for the [NHC]Ni catalyst (approximately 15.6 kcal/mol activation energy).[5] Likewise, the conversion of the [NHC]Ni vinylcyclopropane adduct to the oxidative addition product is thermoneutral, whereas the analogous dinuclear oxidative addition from **B** to **D** is exothermic by 17.2 kcal/mol using **1**. In contrast to the oxidative addition steps, the C−C reductive elimination is calculated to be more facile for the [NHC]Ni catalyst (15.5 kcal/mol) as compared to that for **1** (22.1 kcal/mol). Overall, these results suggest that dinuclear systems may be particularly suited to accelerating challenging oxidative addition reactions of allylic bonds but do so at the expense of stabilizing the resulting metallacycles and slowing down subsequent reductive elimination.

Catalytic Rearrangements of Heteroatom-Containing Cyclopropanes. We next turned our attention to exploring activation reactions of cyclopropanes bearing pendant heteroatom-containing substituents. Cyclopropyl imine substrate **17** undergoes a catalytic rearrangement with **1** to form acyclic α,β-unsaturated product **18** (Figure 6).[13] This result suggests that following cyclopropane ring-opening, β-hydride elimination outcompetes the C−N reductive elimination that would lead to 2,5-dihydro-1*H*-pyrrole formation. Similarly, cyclopropylcarboxaldehyde **19** undergoes a catalytic rearrangement to form crotonaldehyde **20** in 80% yield.[14] Finally, cyclopropanol substrate **21** rearranges to ketone **22** in high yield.[15]

In summary, the dinuclear active site of the [NDI]Ni_2 platform provides a unique electronic environment for the activation of vinyl-substituted strained rings. The presence of an additional metal center enables precoordination of the alkene and provides stabilization to the allyl system that results from ring opening. Accordingly, oxidative addition reactions of substrates such as vinylaziridines and vinylcyclopropanes proceed with remarkably low activation barriers. Ongoing studies are aimed at exploiting these properties for the activation of other strained and unstrained molecules.

■ EXPERIMENTAL SECTION

General Information. All manipulations were carried out using standard Schlenk or glovebox techniques under an atmosphere of N_2.

DOI: 10.1021/acs.organomet.7b00862
Organometallics 2018, 37, 545−550

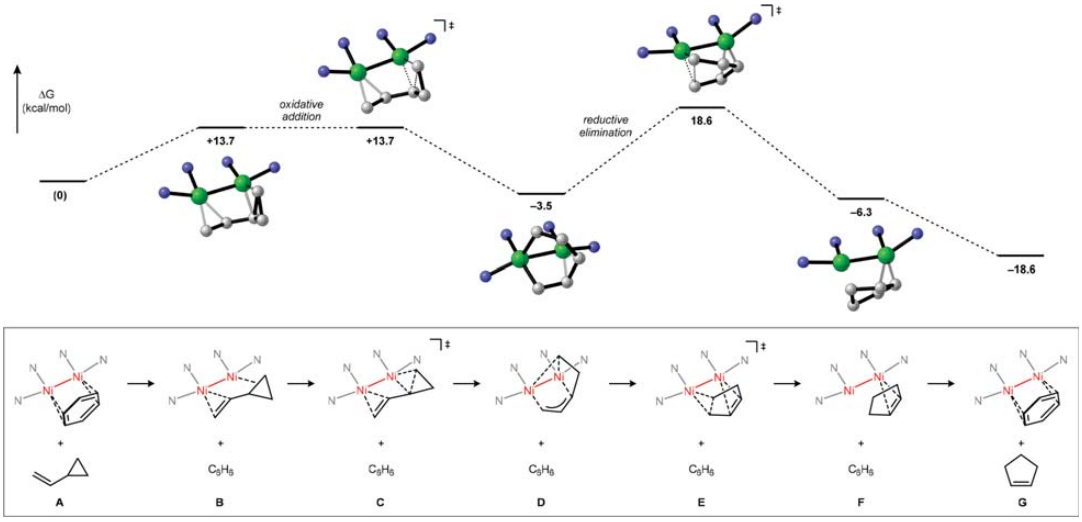

Figure 5. Calculated reaction coordinate for the Ni_2-catalyzed vinylcyclopropane rearrangement (M06*l*/6-31G(d,p) level of DFT). Free energies (ΔG) are in kcal/mol and are relative to that of **A**. In the model, the catalyst *i*-Pr groups are truncated to Me groups.

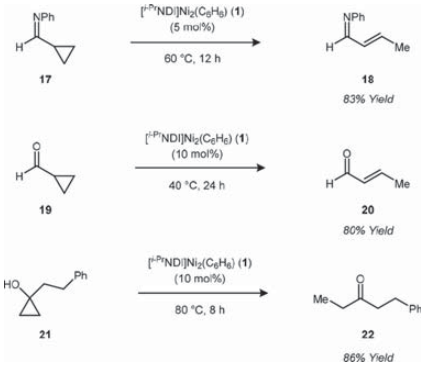

Figure 6. Catalytic rearrangements of cyclopropanes bearing heteroatom-containing substituents.

Solvents were dried and degassed by passing through a column of activated alumina and sparging with Ar gas. Starting materials for the rearrangement reactions were synthesized and purified according to reported procedures. All other reagents were purchased from commercial vendors and used without further purification unless otherwise noted. $[^{i\text{-Pr}}NDI]Ni_2(C_6H_6)$ complex **1** was prepared according to previously reported procedures.[8]

Complex 2. In a 20 mL vial, $[^{i\text{-Pr}}NDI]Ni_2(C_6H_6)$ (**1**) (30 mg, 0.041 mmol, 1.0 equiv) and 1-tosyl-2-vinylaziridine[16] (9.2 mg, 0.041 mmol, 1.0 equiv) were dissolved in C_6H_6 (5 mL). The solution was observed to undergo an immediate color change from red-brown to green. After stirring at ambient temperature for 30 min, the reaction mixture was filtered through a glass fiber pad, and the filtrate was concentrated to dryness under reduced pressure. The crude residue was washed with pentane (3 × 1 mL), then dried under reduced pressure to give **2** (21 mg, 65% yield) as a dark green powder. Single crystals suitable for XRD were obtained by cooling saturated solutions of **2** in Et_2O to −30 °C in a glovebox freezer. ^{1}H NMR (500 MHz, 295 K, C_6D_6) δ 8.79 (br s, 1H), 7.88 (d, J = 7.4 Hz, 2H, Ts H), 7.53 (d, J = 7.5 Hz, 1H, Ar H), 7.47 (d, J = 7.5 Hz, 1H, Ar H), 7.32 (d, J = 7.0 Hz, 1H, Ar H), 7.23 (t, J = 7.7 Hz, 1H, Ar H), 6.99 (m, 3H), 6.90 (m, 1H), 6.84 (d, J = 7.5 Hz, 2H, Ts H), 6.58 (d, J = 8.0 Hz, 1H), 6.27 (d, J = 7.9 Hz, 1H), 4.96 (d, J = 6.3 Hz, 1H), 4.38 (d, J = 7.5 Hz, 1H), 3.86 (sept, J = 11.0 Hz, 1H, $-CH(CH_3)_2$), 3.63 (sept, J = 7.0 Hz, 1H, $-CH(CH_3)_2$), 3.39 (br s, 1H), 3.35 (d, J = 11.0 Hz, 1H), 2.82 (sept, J = 6.7 Hz, 1H, $-CH(CH_3)_2$), 2.08 (s, 3H, Ts CH_3), 1.67 (s, 6H, imine CH_3), 1.38 (d, J = 6.6 Hz, 3H, $-CH(CH_3)_2$), 1.29 (d, J = 6.5 Hz, 3H, $-CH(CH_3)_2$), 1.14 (s, 6H, $-CH(CH_3)_2$), 1.03 (d, J = 6.5 Hz, 3H, $-CH(CH_3)_2$), 0.90 (d, J = 6.7 Hz, 3H, $-CH(CH_3)_2$), 0.68 (sept, J = 6.6 Hz, 1H, $-CH(CH_3)_2$), 0.48 (d, J = 6.7 Hz, 3H, $-CH(CH_3)_2$), 0.23 (d, J = 6.7 Hz, 3H, $-CH(CH_3)_2$). $^{13}C\{^1H\}$ NMR (126 MHz, 295 K, C_6D_6) δ 164.9, 164.4, 162.9, 152.9, 149.3, 147.6, 147.3, 147.3, 146.1, 145.9, 143.9, 141.4, 139.6, 128.8, 128.3, 127.9, 127.7, 127.5, 126.7, 125.9, 124.1, 124.0, 124.0, 123.5, 116.9, 112.4, 108.8, 49.3, 44.8, 29.9, 28.2, 28.0, 27.1, 25.6, 24.8, 24.8, 24.6, 24.3, 24.2, 24.0, 23.8, 21.0, 18.3, 14.5. UV−vis (THF) (λ) {ε, cm^{-1}, M^{-1}} 667 {4500}, 345 {17 000}, 275 {29 000}. Anal. Calcd for (**2**) ($C_{47}H_{57}N_5Ni_2O_2S$): C 64.63%, H 6.58%, N 8.02%. Found: C 64.85%, H 6.75%, N 7.76%.

Complex 4. In a 20 mL vial, $[^{i\text{-Pr}}IP]Ni(COD)$ (**3**)[17] (40 mg, 0.093 mmol, 1.0 equiv) and 1-tosyl-2-vinylaziridine (21 mg, 0.093 mmol, 1.0 equiv) were dissolved in THF (5 mL). The solution was observed to undergo a gradual color change from purple to blue. After 2 h, the reaction mixture was filtered through a glass fiber pad, and the filtrate was concentrated to dryness under reduced pressure. The crude residue was washed with pentane (3 × 1 mL), then dried under reduced pressure to give **4** (33.6 mg, 66%) as a dark blue powder. Single crystals suitable for XRD were obtained by cooling saturated solutions of **4** in Et_2O to −30 °C in a glovebox freezer. ^{1}H NMR (500 MHz, 233 K, toluene-d_8) δ 9.51 (s, 1H, C*H*NAr), 8.28 (d, 2H, Ar H), 7.61 (s, 1H, Ar H), 6.91 (m, 4H, Ar H), 6.06 (d, J = 8.5 Hz, 1H, C*H*═CH), 5.22 (d, J = 8.4 Hz, 1H, C*H*═CH), 4.21 (s, 1H, $-CH(CH_3)_2$), 3.80 (d, J = 16.6 Hz, 1H, $-CH(CH_3)_2$), 3.03−2.90 (m, 2H, $-CH(CH_3)_2$), 2.51 (d, J = 16.8 Hz, 1H, $-CH(CH_3)_2$), 2.22−2.11 (m, 1H), 1.96 (s, 3H, CH_3), 1.58 (d, J = 5.6 Hz, 3H, $CH(CH_3)_2$), 1.18−1.02 (m, 6H, $-CH(CH_3)_2$), 0.76 (d, J = 5.9 Hz, 3H, $-CH(CH_3)_2$). $^{13}C\{^1H\}$ NMR (126 MHz, 295 K, C_6H_6) δ 164.3, 152.2, 145.0, 145.6, 142.2, 140.6, 139.4, 137.2, 131.8, 128.8, 128.6, 128.3, 127.9, 127.7, 127.6, 123.9, 123.4, 47.2, 28.3, 24.5, 22.8, 20.8, 16.8. UV−vis (THF) (λ) {ε, cm^{-1}, M^{-1}} 329 {1800}, 273 {15 000}, 228 {33 000}. Anal. Calcd for (**4**) ($C_{29}H_{35}N_3NiO_2S$): C 63.52%, H 6.43%, N 7.66%. Found: C 63.48%, H 6.39%, N 7.66%.

General Procedure for the Catalytic Rearrangement of Vinylcyclopropane (Table 1). In an N_2-filled glovebox, vinylcyclopropane[18] (0.14 mmol), mesitylene (0.14 mmol), and the Ni

DOI: 10.1021/acs.organomet.7b00862
Organometallics 2018, 37, 545−550

catalyst (0.0014 mmol, 1 mol %) were dissolved in C_6D_6 (0.5 mL), and the solution was loaded into an NMR tube equipped with a J. Young valve. The reaction mixture was allowed to react at ambient temperature or 60 °C for 24 h, and the yield of cyclopentene was determined by ^{1}H NMR integration against the mesitylene standard.

Catalytic Rearrangement of 1-Phenyl-2-vinylcyclopropane (12). In an N_2-filled glovebox, 1-phenyl-2-vinylcyclopropane[19] (29 mg, 0.20 mmol), mesitylene (24 mg, 0.20 mmol), and [$^{i\text{-Pr}}$NDI]$Ni_2(C_6H_6)$ (7.3 mg, 0.01 mmol, 5 mol %) were dissolved in C_6D_6 (0.5 mL), and the solution was loaded into an NMR tube equipped with a J. Young valve. The reaction mixture was allowed to react at 60 °C for 6 h, and the yield of 3-phenylcyclopentene[20] was determined by ^{1}H NMR integration against the mesitylene standard (93% yield). The crude mixture was directly loaded on to an SiO_2 column for purification (mobile phase: pentane). 3-Phenylcyclopentene (**13**) was isolated in 52% yield (15 mg) as a colorless oil. ^{1}H NMR (500 MHz, 295 K, $CDCl_3$) δ 7.33−7.28 (m, 2H, Ar H), 7.23−7.18 (m, 3H, Ar H), 5.96 (dq, J = 5.7, 2.3 Hz, 1H, C*H*═CH), 5.80 (dq, J = 5.7, 2.1 Hz, 1H, C*H*═CH), 3.91 (m, 1H, CH), 2.58−2.47 (m, 1H, CH_2), 2.47−2.37 (m, 2H, CH_2), 1.79−1.69 (m, 1H, CH_2). ^{13}C{^{1}H} NMR (126 MHz, 295 K, $CDCl_3$) δ 146.5, 134.3, 131.9, 128.4, 127.2, 126.0, 51.4, 33.9, 32.5.

Catalytic Rearrangement of 1-Hexyl-2-vinylcyclopropane (15). In an N_2-filled glovebox, 1-hexyl-2-vinylcyclopropane (15.2 mg, 0.10 mmol), mesitylene (12 mg, 0.10 mmol), and [$^{i\text{-Pr}}$NDI]$Ni_2(C_6H_6)$ (7.3 mg, 0.01 mmol, 10 mol %) were dissolved in C_6D_6 (0.5 mL), and the solution was loaded into an NMR tube equipped with a J. Young valve. The reaction mixture was allowed to react at 80 °C for 24 h, and the yield of 3-hexylcyclopentene[21] was determined by ^{1}H NMR integration against the mesitylene standard (92% yield). The crude mixture was directly loaded on to a SiO_2 column for purification (mobile phase: pentane). 3-Hexylcyclopentene (**16**) was isolated in 58% yield (9 mg) as a colorless oil. ^{1}H NMR (500 MHz, 295 K, $CDCl_3$) δ 5.69 (m, 2H, CH═CH), 2.63 (br s, 1H), 2.30 (m, 2H), 2.03 (m, 1H), 1.35 (m, 11H, CH_2), 0.89 (t, J = 6.6 MHz, 3H, CH_3). ^{13}C{^{1}H} NMR (126 MHz, 295 K, C_6D_6) δ 135.5, 123.0, 45.6, 36.2, 32.0, 31.9, 29.9, 29.6, 28.0, 22.7, 14.1.

Catalytic Rearrangement of 17. In an N_2-filled glovebox, **17**[22] (8.0 mg, 0.054 mmol), mesitylene (6.6 mg, 0.054 mmol), and [$^{i\text{-Pr}}$NDI]$Ni_2(C_6H_6)$ (2 mg, 0.0027 mmol, 5 mol %) were dissolved in C_6D_6 (0.5 mL), and the solution was loaded into an NMR tube equipped with a J. Young valve. The reaction mixture was allowed to react at 60 °C for 12 h, and the yield of **18** was determined by ^{1}H NMR integration against the mesitylene standard (83% yield). ^{1}H NMR (300 MHz, 295 K, C_6D_6) δ 7.87 (d, J = 8.8 Hz, 1H, −C*H*NPh), 7.25−6.98 (m, 5H, Ar H), 6.64−6.45 (m, 1H, −CH═C*H*CH_3), 5.87 (m, 1H, −C*H*═$CHCH_3$), 1.49 (d, J = 6.8 Hz, 3H, CH_3).

Catalytic Rearrangement of 19. In an N_2-filled glovebox, cyclopropanecarboxaldehyde **19** (4.4 mg, 0.063 mmol), mesitylene (7.6 mg, 0.063 mmol), and [$^{i\text{-Pr}}$NDI]$Ni_2(C_6H_6)$ (5 mg, 0.0063 mmol, 10 mol %) were dissolved in C_6D_6 (0.5 mL), and the solution was loaded into an NMR tube equipped with a J. Young valve. The reaction mixture was allowed to react at 40 °C for 24 h, and the yield of **20** was determined by ^{1}H NMR integration against the mesitylene standard (80% yield). ^{1}H NMR (300 MHz, 295 K, $CDCl_3$) δ 9.27 (d, J = 6.7 Hz, 1H, −CHO), 6.03−5.77 (m, 2H, CH═CH), 1.30 (d, J = 5.4 Hz, 3H, CH_3).

Catalytic Rearrangement of 21. In an N_2-filled glovebox, 1-phenethylcyclopropan-1-ol[23] **21** (4.4 mg, 0.027 mmol), mesitylene (3.3 mg, 0.027 mmol), and [$^{i\text{-Pr}}$NDI]$Ni_2(C_6H_6)$ (2 mg, 0.0027 mmol, 10 mol %) were dissolved in C_6D_6 (0.5 mL), and the solution was loaded into an NMR tube equipped with a J. Young valve. The reaction mixture was allowed to react at 80 °C for 8 h, and the yield of **22**[24] was determined by ^{1}H NMR integration against the mesitylene standard (86% yield). ^{1}H NMR (400 MHz, 295 K, $CDCl_3$) δ 7.32−7.24 (m, 2H, Ar H), 7.19 (m, 3H, Ar H), 2.90 (t, J = 7.6 Hz, 2H, CH_2), 2.74 (t, J = 7.7 Hz, 2H, CH_2), 2.40 (q, J = 7.3 Hz, 2H, −C*H*$_2$$CH_3$), 1.04 (t, J = 7.3 Hz, 3H, −CH_2C*H*$_3$).

■ ASSOCIATED CONTENT

Supporting Information

The Supporting Information is available free of charge on the ACS Publications website at DOI: 10.1021/acs.organomet.7b00862.

Experimental details and characterization data (PDF)

Cartesian coordinates for calculated structures (XYZ)

Accession Codes

CCDC 1588576−1588577 contain the supplementary crystallographic data for this paper. These data can be obtained free of charge via www.ccdc.cam.ac.uk/data_request/cif, or by emailing data_request@ccdc.cam.ac.uk, or by contacting The Cambridge Crystallographic Data Centre, 12 Union Road, Cambridge CB2 1EZ, UK; fax: +44 1223 336033.

■ AUTHOR INFORMATION

Corresponding Author

*E-mail: cuyeda@purdue.edu.

ORCID

Christopher Uyeda: 0000-0001-9396-915X

Notes

The authors declare no competing financial interest.

■ ACKNOWLEDGMENTS

This research was supported by the NSF (CHE-1554787) and by Purdue University. C.U. is an Alfred P. Sloan Research Fellow. X-ray diffraction data were collected using instruments funded by the NSF (DMR-1337296).

■ REFERENCES

(1) Recent reviews of transition metal catalyzed epoxide, aziridine, and cyclopropane ring-opening reactions: (a) Jun, C.-H. *Chem. Soc. Rev.* **2004**, *33*, 610−618. (b) Lu, B.-L.; Dai, L.; Shi, M. *Chem. Soc. Rev.* **2012**, *41*, 3318−3339. (c) Gao, Y.; Fu, X.-F.; Yu, Z.-X. *Top. Curr. Chem.* **2014**, *346*, 195−232. (d) Tasker, S. Z.; Standley, E. A.; Jamison, T. F. *Nature* **2014**, *509*, 299−309. (e) Huang, C.-Y.; Doyle, A. G. *Chem. Rev.* **2014**, *114*, 8153−8198. (f) Chen, P.-H.; Billett, B. A.; Tsukamoto, T.; Dong, G. *ACS Catal.* **2017**, *7*, 1340−1360.

(2) (a) Rybtchinski, B.; Milstein, D. *Angew. Chem., Int. Ed.* **1999**, *38*, 870−883. (b) Souillart, L.; Cramer, N. *Chem. Rev.* **2015**, *115*, 9410−9464.

(3) (a) Tipper, C. F. H. *J. Chem. Soc.* **1955**, 2045−2046. (b) Adams, D. M.; Chatt, J.; Guy, R. G.; Sheppard, N. *J. Chem. Soc.* **1961**, *0*, 738−742. (c) Schlodder, R.; Ibers, J. A.; Lenarda, M.; Graziani, M. *J. Am. Chem. Soc.* **1974**, *96*, 6893−6900. (d) Lin, B. L.; Clough, C. R.; Hillhouse, G. L. *J. Am. Chem. Soc.* **2002**, *124*, 2890−2891. (e) Ney, J. E.; Wolfe, J. P. *J. Am. Chem. Soc.* **2006**, *128*, 15415−15422. (f) Desnoyer, A. N.; Bowes, E. G.; Patrick, B. O.; Love, J. A. *J. Am. Chem. Soc.* **2015**, *137*, 12748−12751.

(4) Zuo, G.; Louie, J. *Angew. Chem., Int. Ed.* **2004**, *43*, 2277−2279.

(5) Wang, S. C.; Troast, D. M.; Conda-Sheridan, M.; Zuo, G.; LaGarde, D.; Louie, J.; Tantillo, D. J. *J. Org. Chem.* **2009**, *74*, 7822−7833.

(6) Behlen, M. J.; Zhou, Y.-Y.; Steiman, T. J.; Pal, S.; Hartline, D. R.; Zeller, M.; Uyeda, C. *Dalton Trans.* **2017**, *46*, 5493−5497.

(7) Hartline, D. R.; Zeller, M.; Uyeda, C. *J. Am. Chem. Soc.* **2017**, *139*, 13672−13675.

(8) Zhou, Y.-Y.; Hartline, D. R.; Steiman, T. J.; Fanwick, P. E.; Uyeda, C. *Inorg. Chem.* **2014**, *53*, 11770−11777.

(9) Manuel, T. D.; Rohde, J.-U. *J. Am. Chem. Soc.* **2009**, *131*, 15582−15583.

(10) Dong, Q.; Yang, X.-J.; Gong, S.; Luo, Q.; Li, Q.-S.; Su, J.-H.; Zhao, Y.; Wu, B. *Chem. - Eur. J.* **2013**, *19*, 15240−15247.

DOI: 10.1021/acs.organomet.7b00862
Organometallics 2018, 37, 545−550

(11) Dible, B. R.; Sigman, M. S.; Arif, A. M. *Inorg. Chem.* **2005**, *44*, 3774−3776.
(12) (a) Marvell, E. N.; Lin, C. *J. Am. Chem. Soc.* **1978**, *100*, 877−883. (b) Baldwin, J. E.; Bonacorsi, S. J. *J. Am. Chem. Soc.* **1996**, *118*, 8258−8265.
(13) Kamitani, A.; Chatani, N.; Morimoto, T.; Murai, S. *J. Org. Chem.* **2000**, *65*, 9230−9233.
(14) (a) Ogoshi, S.; Nagata, M.; Kurosawa, H. *J. Am. Chem. Soc.* **2006**, *128*, 5350−5351. (b) Tamaki, T.; Nagata, M.; Ohashi, M.; Ogoshi, S. *Chem. - Eur. J.* **2009**, *15*, 10083−10091.
(15) (a) Ye, R.; Yuan, B.; Zhao, J.; Ralston, W. T.; Wu, C.-Y.; Unel Barin, E.; Toste, F. D.; Somorjai, G. A. *J. Am. Chem. Soc.* **2016**, *138*, 8533−8537. (b) Okumoto, H.; Jinnai, T.; Shimizu, H.; Harada, Y.; Mishima, H.; Suzuki, A. *Synlett* **2000**, *2000*, 0629−0630.
(16) Cunha, R. L. O. R.; Diego, D. G.; Simonelli, F.; Comasseto, J. V. *Tetrahedron Lett.* **2005**, *46*, 2539.
(17) Diercks, R.; Dieck tom, H. *Chem. Ber.* **1985**, *118*, 428−435.
(18) Fischetti, W.; Heck, R. F. *J. Organomet. Chem.* **1985**, *293*, 391−405.
(19) Itoh, T.; Matsueda, T.; Shimizu, Y.; Kanai, M. *Chem. - Eur. J.* **2015**, *21*, 15955−15959.
(20) Chen, Z.; Liang, J.; Yin, J.; Yu, G.-A.; Liu, S. H. *Tetrahedron Lett.* **2013**, *54*, 5785−5787.
(21) You, H.; Rideau, E.; Sidera, M.; Fletcher, S. P. *Nature* **2015**, *517*, 351.
(22) Meuer, L. H. P.; Johannes, C. G.; Niel, V.; Pandit, U. K. *Tetrahedron* **1984**, *40*, 5185−5195.
(23) Rosa, D.; Orellana, A. *Chem. Commun.* **2013**, *49*, 5420−5422.
(24) Lee, D.-Y.; Hong, B.-S.; Cho, E.-G.; Lee, H.; Jun, C.-H. *J. Am. Chem. Soc.* **2003**, *125*, 6372−6373.

DOI: 10.1021/acs.organomet.7b00862
Organometallics 2018, 37, 545−550

Reproduced with permission of copyright owner. Further reproduction prohibited without permission.